Development of Effective and Efficient Fault Diagnostic Methodologies and Tools for Planetary Gearboxes

BY

JAE MYUNG YOON
B.E., Kwangwoon University, 2006
M.S., University of Florida, 2012

THESIS

Submitted as partial fulfillment of the requirements for the degree of
Doctor of Philosophy in Industrial Engineering and Operations Research
In the Graduate College of the
University of Illinois at Chicago, 2015

Chicago, Illinois

Defense Committee:

David He, Chair and Advisor
Houshang Darabi, Mechanical and Industrial Engineering
Lin Li, Mechanical and Industrial Engineering
Michael Brown, Mechanical and Industrial Engineering
Eric Bechhoefer, GPMS LLC

To my wife, *Jungeun Park*, my son, *Andrew J. Yoon*, my parents, *Hyungsub Yoon* and *Heeja Yang*, my in-laws, *Wonrak Park* and *Younghee Bae*, and the rest of my family members for their unwavering support and constant encouragement.

ACKNOWLEDGMENTS

I would like to express the deepest appreciation to my Ph.D. advisor, Dr. David He, whose infinite motivation and inspiration carried me to the successful completion of my doctorate in Industrial Engineering and Operations Research degree. His constant guidance and the patience over the past years helped me mature academically, professionally, and personally.

I would also like to express my sense of gratitude to all my dissertation committee members, Dr. Houshang Darabi, Dr. Lin Li, Dr. Michael Brown, and Dr. Eric Bechhoefer for their time spent and valuable suggestions they provided.

In addition, a thank you to Dr. Eric Bechhoefer, Dr. Nicholas Propes, Dr. Ruoyu Li, and Dr. Yongzhi Qu who provided me great career opportunities in worldwide had lasting effect. Also, I thank all the past and current colleagues, Dr. Junda Zhu, Dr. Yongzhi Qu, Dr. Brandon Van Hecke, and Miao He, for their helpful discussions and time spent on my projects. It was my honor to be part of the team ISM&D and research with them. Finally, I would like to mention that the financial support on my research was provided by the University of Illinois at Chicago, Chicago, IL and the Renewable NRG systems.

CONTRIBUTION OF AUTHORS

Chapter I is an introduction to planetary gearbox fault diagnosis, research background, motivation, and scientific contribution. Chapter II is a literature review covering the state of the art machinery fault diagnostic techniques including signal processing and data mining based methods. Chapter III introduces the experimental test rig, fault seeded test, and fundamental of planetary gearbox. Chapter IV presents an unpublished research study of the vibration based planetary gearbox diagnostic methodology using spectral averaging. Chapter V presents a new planetary gearbox fault diagnostic method using an acoustic emission sensor. The majority of the content is composed of previously published work (Yoon, J. and He, D., 2015, "Planetary gearbox fault diagnostic method using acoustic emission sensors", *IET Science, Measurement, and Technology*, DOI: 10.1049/iet-smt.2014.0375.) for which I was the first author and perform the research. My advisor, Dr. David He supervised the research and edited the manuscripts. Chapter VI presents a new planetary gearbox fault diagnosis on the use a single piezoelectric strain sensor. The majority of the content is composed of previously published work (Yoon, J., He, D., and Van Hecke, B., 2015, "On the use a single piezoelectric strain sensor for wind turbine planetary gearbox fault diagnosis", *IEEE Transactions on Industrial Electronics*, DOI: 10.1109/TIE.2015.2442216.) for which I was the first author and perform the research. My advisor, Dr. David He supervised the research and edited the manuscripts and Dr. Brandon Van Hecke aided in collection of the data. Chapter VII also presents an unpublished comparative research study on the vibration, acoustic emission, piezoelectric strain analysis introduced in Chapter IV, V, and VI. Finally, Chapter VIII provides a synthesis of the research presented in this dissertation.

TABLE OF CONTENTS

CHAPTER PAGE

LISTS OF TABLES

TABLE PAGE

LIST OF FIGURES

FIGURE PAGE

LIST OF ABBREVIATIONS

AE	Acoustic emission
AM	Amplitude modulation
ANN	Artificial neural network
BP	Back propagation
CF	Crest factor
CI	Condition indicator
CMS	Condition monitoring system
CNS	Central nervous system
DAQ	Data acquisition
DAS	Data acquisition system
EMD	Empirical mode decomposition
Env	Enveloping
EO	Energy operator
EOL	End of life
FFT	Fast Fourier transform
FK	Fast kurtogram
FM	Frequency modulation
GDF	Gear distributed fault
HHT	Hilbert-Huang transform
IMF	Intrinsic mode function
KNN	K-nearest neighbor

KT	Kurtosis
LAMSTAR	Large memory storage and retrieval
LDC	Local data collector
NB	Narrow band-pass filter
NDE/T	Non-destructive evaluation / testing
NI	National Instruments
NREL	National renewable energy laboratory
PE	Piezoelectric
PGB	Planetary gearbox
PHM	Prognostics and health management
PSD	Power spectral density
P2P	Peak to peak
Res	Residual signal
RMS	Root mean square
RUL	Remaining useful life
RPM	Revolutions per minute
SA	Spectral averaging
SEnt	Shannon entropy
SK	Skewness
SOM	Self organizing map
SPC	Statistical process control
SVM	Support vector machine
TSA	Time synchronous average

TSR	Time synchronous resampling
Welch (W)	Welch windowed spectral averaging
Welch EO (WEO)	Energy operator of Welch

SUMMARY

Vibration analysis has been widely accepted in the field of machinery fault diagnosis. However, vibration signals theoretically have the amplitude modulation (AM) effect caused by time variant vibration transfer paths due to rotating planet gears and planet carrier around the sun gear. Their complex spectral structure makes it difficult to diagnose PGB faults via vibration analysis.

In this dissertation, new effective and efficient PGB diagnostic methodologies and tools using alternative sensors have been developed and validated with seeded fault tests with a PGB on a wind turbine simulator. Specifically, the following new effective and efficient PGB fault diagnostic methods are presented: a vibration based PGB diagnostic method, an acoustic emission (AE) based PGB diagnostic method, and a piezoelectric (PE) strain sensor based PGB diagnostic method.

The newly developed PGB fault diagnostic methods and tools have several significant advantages. First, a new vibration based PGB fault diagnostic method was developed using the Welch's spectral averaging. All localized PGB faults were isolable with this method while the conventional vibratory analyses of the time synchronous averaging (TSA), enveloping or the vibration separation (VS) techniques were not able to. Second, the heterodyning data acquisition (DAQ) system was applied to PGB in order to overcome the known challenge of the high sampling rate for AE analysis. Besides, with the AE based PGB fault diagnostic methods, not only it was isolating the location of the localized faults, but it is potentially capable of capturing incipient faults by using AE. Lastly, for the PE strain sensor based PGB diagnostic method, research reported in the literature has shown that strain sensor signals are closely related to torsional vibration, in which the only modulation effects are the AM and frequency modulation (FM) caused

by gear faults under constant input and output torque. Also, results from the PE strain sensor based condition indicators (CIs) were isolable for all localized faults and remain relatively stationary within the same loading condition regardless the change of the shaft speed. Those CIs could be utilized in establishing a threshold based condition monitoring system and is verifying that the measurements from a PE strain sensor are heavily affected by the torque change.

The research described in this dissertation was conducted in four stages: (1) developing an effective vibration based PGB diagnostic method with Welch's spectral averaging, (2) developing an effective AE based PGB diagnostic method using the heterodyning data acquisition (DAQ) system, (3) developing an effective PE strain sensor based PGB diagnostic method, and (4) a comparative study over all method developed in the stage of (1), (2) and (3). Different localized faults on sun gear, planet gear, and ring gear were seeded and tested. The comparative results have shown that the AE based PGB fault diagnostic method have shown that it is more desirable than the vibration based PGB fault diagnostic method with lower diagnostic error rates and higher reliability. On the other hand, the PE strain based fault diagnostic method could be the most desirable in that it didn't require a help of machine learning in PGB fault diagnostics.

I. INTRODUCTION

A. Background and Motivation

Planetary gearboxes (PGB) are desired for high power transmission applications as their unique design allows distributing the input torque in parallel and minimizing gearbox size. Thus, PGB is widely adopted in design of the following applications:

- Powertrain to convert wind power to electrical power in a wind turbine;
- Drivetrain to generate uplift force in a helicopter transmission system;
- Bucket wheel driving system to manage random varying load in the digging process of a surface mining excavator.

Especially, wind energy is one of the fastest growing energy source among various renewable energy options. Establishment of more proactive maintenance strategy is required before the recent massive industrial wind projects enter the wear-out failure zone. This will particularly be true for the off-shore wind farms, where not only the availability of the site for maintenance can be restricted but also the saline environment easily accelerates the mechanical and chemical failures. Recent papers have reported the fault diagnostic methods of a wide range of wind turbine components such bearing (Gong and Qiao, 2013), rotor (Vedreno-Santos *et al.*, 2014; Cusido *et al.*, 2008), electrical system (Freire *et al.*, 2013), generator (Yang *et al.*, 2010), energy conversion system (Karimi *et al.*, 2008), hydraulics, pitch adjustment, yaw system, lubricant (Zhu *et al.*, 2014), and etc. in order to extend the service time of wind turbine systems at their maximum rates. However, as reported in the technical reports from the US national renewable energy laboratory (NREL), the gearbox failure is the leading contributor to the total wind turbine downtime (Sheng *et al*., 2011). In the meantime, the statistics reported in Sheng (2014) have shown that 26% and 25% of all gearbox failures recorded in 2013 and 2014, respectively, were due to direct gear failure.

Similarly, according to Astridge (1989), 19.1% of all the helicopter transmission failures came from the gear failure. Therefore, developing an accurate and reliable PGB condition monitoring method for these assets is very desirable for improved availability while the cost of unscheduled maintenance is reduced. Representing examples of the PGB applications are provided in Figure 1.

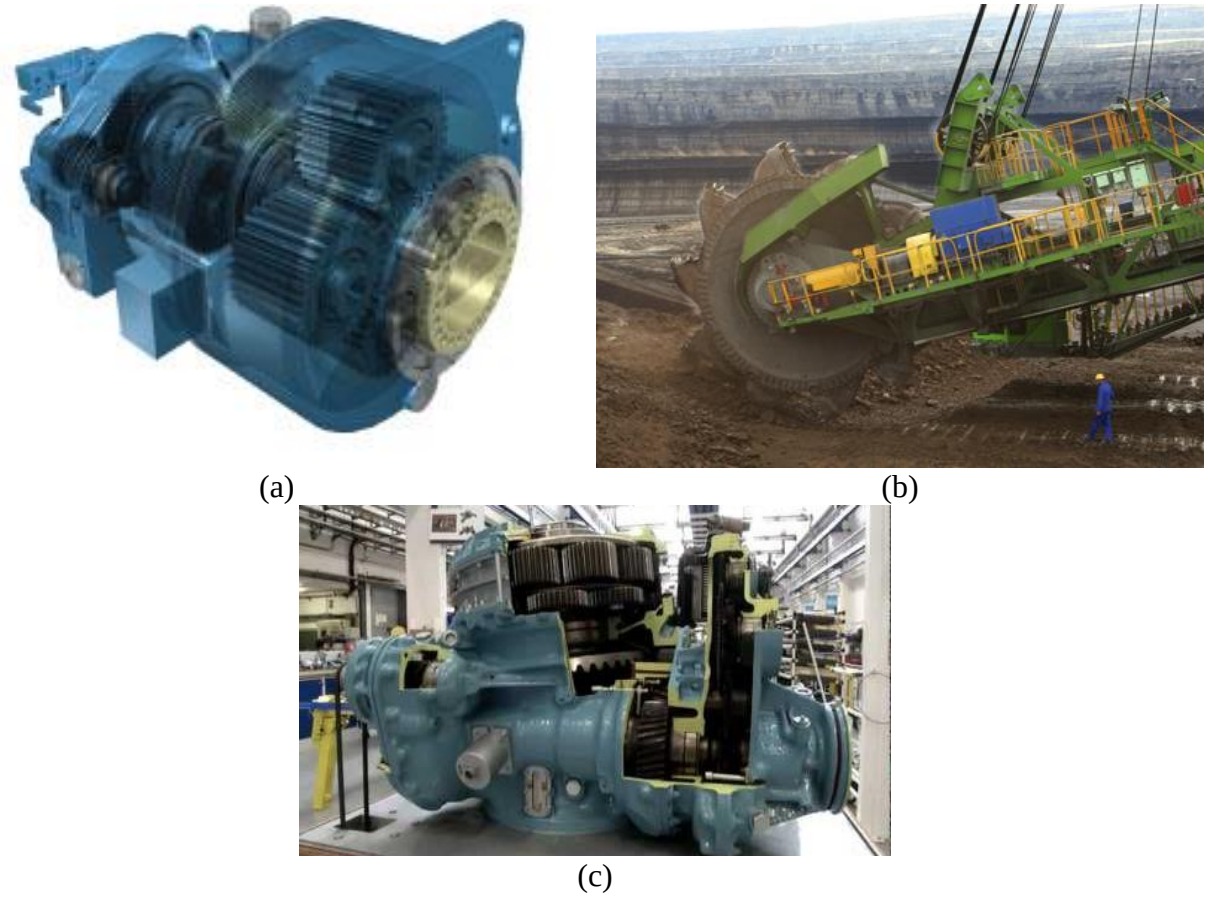

(a) (b)

(c)

Figure 1. PGB applications for (a) wind turbine (GE Drivetrain Technologies, 2015),(b) Bucket wheel excavator (FLSmidth, 2015), and (c) Rotorcraft transmission (Eurocopter, 2015).

When time variant disturbances and non-stationary operating conditions such as speed and loading changes are applied to a mechanical system, periodic or random oscillation occurs and it

defines vibration. Vibration analysis is carried for a machinery fault detection in an industrial or maintenance project to eliminate unnecessary costs and equipment downtime. To date, transverse vibration (generally known as 'vibration') analysis using accelerometer has been established as the industry standard for most of the machinery health condition monitoring. However, for the PGB application, transverse vibration signals theoretically have the amplitude modulation (AM) effect caused by time variant vibration transfer paths due to the unique dynamic structure of rotating planet gears. Provided in Figure 2, a pictorial example of the AM effect of PGB is displayed.

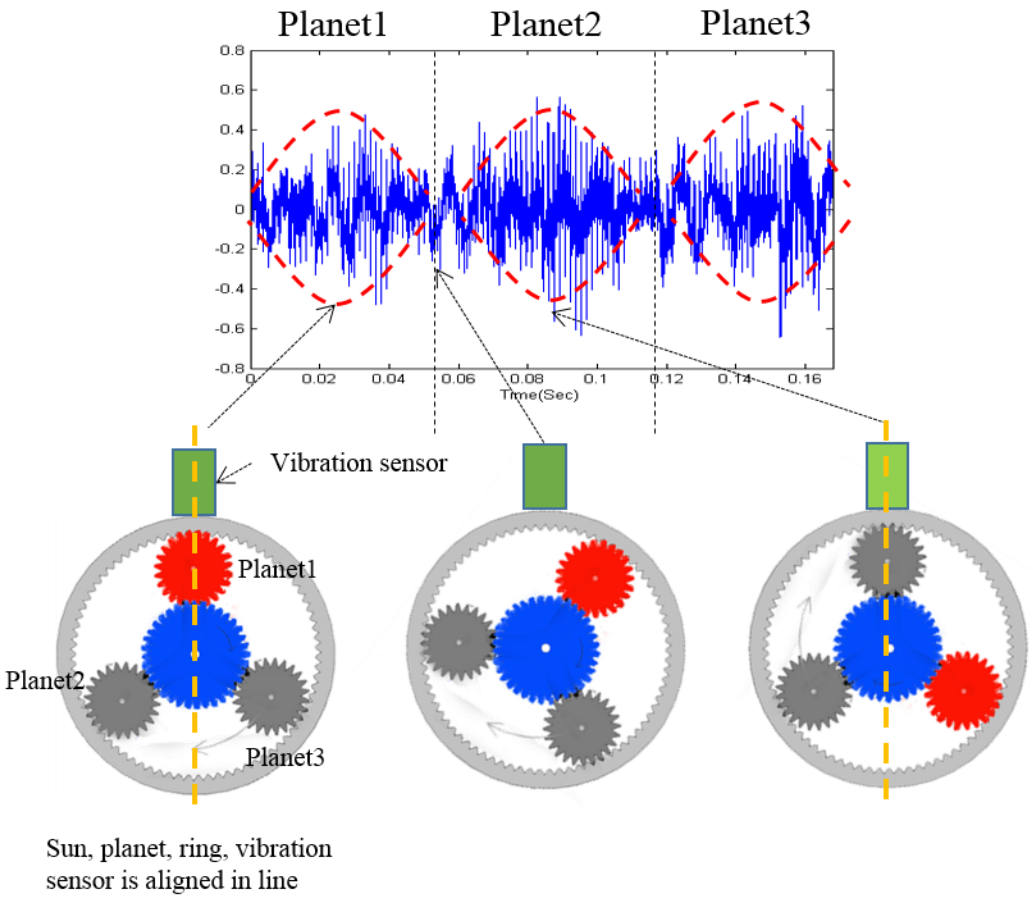

Figure 2. The AM effect of vibration signal on PGB.

Resultantly, it could be complicated to diagnose PGB faults via a vibration analysis such as time synchronous averaging (TSA, Braun, 1975), or vibration separation (VS, McFadden, 1991). Attractive solutions to this problem are either applying frequency/time-frequency vibration analysis methods or using alternative sensors that could be less sensitive to AM effect for PGB fault diagnosis. To overcome the above mentioned challenges, the following PGB fault diagnostic methodologies and tools will be developed: vibration analysis with Welch's spectral averaging; alternative sensors of AE and piezoelectric (PE) strain sensors.

First, Welch's spectral averaging method (Welch, 1967), recently reported for bearing fault diagnosis, by Bechhoefer *et al*., 2013a; Van Hecke *et al*., 2014a. Their methodology comprises the time synchronous resampling (TSR) technique with Welch's spectral averaging to obtain a power spectral density (PSD) estimate of the vibration signals. This PSD estimate will be utilized in search of an effective vibration based PGB fault diagnostic method. No similar research has reported in the literature for PGB fault diagnostic method.

Next, acoustic emission (AE) sensors in the machinery fault diagnostics area recently have captured growing acceptance.AE signals can be defined as the elastic stress waves generated inside a solid material (*e.g.* mechanical components made with metal) due to energy release. Thus, the AE sensor as failure analysis source could be beneficial to PGB fault diagnosis in that AE signals propagate from the wave source (*i.e.* faults) to sensing apparatus within mechanical components. Because of the fact that AE sensor can potentially be more sensitive to the incipient faults than vibration sensors, AE based machinery fault detection and diagnosis have attracted many research activities (Al-Balushi and Samanta, 2002; Loutas *et al*., 2011).Al-Ghamd and Mba (2006) have shown not only that AE offers an earlier fault detection than vibration, but also that AE provides

an indication of the fault level. Scheer *et al.* (2007) have shown that AE is effective to capture early stage of gear faults (*e.g.* tooth edge fracture and pitting) before they grow to change their vibration behavior. In Lucas (2012), AE is described as follows in comparison to vibration: (1) With AE, an early stage of defect including worn by usage and minor defects can be identified. In the meantime with vibration, damages must grow in a certain level to be represented by vibratory behaviors; (2) AE can pick up other faults such as a lack of lubrication, friction, and cracking, and (3) AE is considered as the next generation of vibration for condition monitoring. However, the high sampling rate requirement between 2 to 10 MHz has been one of the greatest obstacle for widespread and practical implementations of AE based fault diagnosis. Recent studies have shown that the high sampling rate issue of AE for fault diagnosis could be overcome by applying heterodyne based frequency reduction technique (Qu *et al.*, 2014; Bechhoefer *et al*., 2013b; Van Hecke *et al.*, 2014a; Yoon *et al.*, 2014). Until today, no effective AE based PGB fault diagnostic method has been developed using the heterodyne technique and no single method were reported to isolate different PGB fault locations of sun gear, planet gear, and ring gear.

Finally, one attractive solution is to utilize alternative sensors that have less sensitivity to the AM effect for PGB fault diagnosis and prognosis. In a recent paper, Feng and Zuo (2013) have shown the effectiveness of torsional vibration analysis for PGB fault diagnosis using a torque sensor. The frequency characteristics of torsional vibration were shown to be solely sensitive to the AM and FM effects caused by gear faults under constant torque on input and output shafts. Kiddy *et al.* (2011) used fiber optic strain signals for PGB fault diagnosis and showed a close relationship between strain measurement and torque changes. Although promising, the research reported in the literature on using less AM effect sensitive signals for PGB fault diagnosis has certain limitations. The torque sensors used by Feng and Zuo (2013) are more expensive than

vibration and strain sensors and require special installation. The fiber optic strain sensor array used by Kiddy *et al*. (2011) had to be embedded on the PGB components in order to be effective. Besides, those fiber optic strain sensors can only be sampled at a maximum sampling rate up to 1 kHz, which limits its coverage on shaft speed above 2060 rpm. Lastly, the strain signals were analyzed the same way as vibration signals. Fiber optic sensor signals were analyzed using the vibration separation technique after low frequency components were filtered out. No effective signal analysis techniques have been developed for strain signals. The PE strain sensor is desirable in having an improved strain resolution and applicability of a higher sampling rate in comparison with the conventional strain gauge sensors (Banaszak, 2001) or the fiber optic strain sensors (Jiang *et al.*, 2013). Until today, no effective PE strain signal based PGB fault diagnostic analysis techniques have been reported. Also, no PE strain analysis method were displayed to isolate different PGB fault locations of sun gear, planet gear, and ring gear. To overcome the above mentioned challenges and fulfill the diagnostic capability on PGB faults, a research investigation via PE strain sensor signal analysis has been conducted and is reported in this dissertation.

B. Dissertation Scope and Scientific Contribution

In this dissertation, new PGB diagnostic methodologies and tools will be developed using vibration, AE, and PE strain sensors. The potential contributions will include:

(1) New effective vibratory PGB fault diagnostic methods and tools developed using Welch's spectral averaging;

(2) New effective and computationally efficient PGB fault diagnostic methods and tools developed using AE sensor signal analysis techniques that are potentially less sensitive to the AM effect;

(3) New effective and computationally efficient PGB fault diagnostic methods and tools developed using PE strain sensor signal analysis techniques that are potentially less sensitive to the AM effect;

(4) A comparative study over all of PGB fault diagnostic methods developed in previous stages. There is no similar study available that is comparing the diagnostic performance of all three vibration, AE, and PE strain for PGB application;

(5) Validation of the developed diagnostic methods and tools using seeded fault tests on a PGB test rig in the laboratory.

C. Dissertation Outline

The proposal is outlined as following. CHAPTER II gives a literature review on current PGB fault diagnostic techniques. CHAPTER III introduces the experimental test rig and PGB fundamentals. CHAPTER IV explains the methodology details and validation results of the vibration based PGB fault diagnostics methodology using Welch's spectral averaging (SA). CHAPTER V depicts the methodology details and validation results for the new AE based PGB fault diagnostics methods. CHAPTER VI describes the development procedures details and validation results for the new PE strain sensor based PGB fault diagnostic method and tools. CHAPTER VII presents the comparative study for all those three vibration, AE, and PE strain methods and tools. CHAPTER VIII concludes the dissertation for the new PGB fault diagnostic methods.

II. LITERATURE REVIEW

(Parts of the literature review in this chapter were previously published as Yoon, J., He, D., and Van Hecke, B., 2015, "On the use a single piezoelectric strain sensor for wind turbine planetary gearbox fault diagnosis", *IEEE Transactions on Industrial Electronics*, DOI: 10.1109/TIE.2015.2442216. and Yoon, J. and He, D., 2014, "Planetary gearbox fault diagnostic method using acoustic emission sensors", *IET Science, Measurement, and Technology*, DOI: 10.1049/iet-smt.2014.0375.)

In this chapter, relevant literatures are reviewed. In particular, currently available PGB fault diagnosis techniques are reviewed intensively in Section A divided into two parts: vibration analysis and non-vibration analysis. Then, AE based machinery fault diagnostic methods and applications are reviewed in Section B. A brief review on the data mining based machinery fault diagnostic methods is followed in Section C.

A. PGB Fault Diagnostics

PGB fault diagnosis techniques could generally be split into two categories: vibration based and non-vibration analysis based. They are viewed in the next two sections.

1. Vibration Analysis

In general, vibration is the most widely researched condition parameter in the field of machinery health diagnostics (*e.g.* bearings, gears, shafts, and etc.). Common vibration measuring apparatus includes accelerometers, displacement sensors, and velocity sensors. In industrial applications, useful methodologies vary depending on their specific environment.

Likewise, a large portion of PGB diagnostic systems has been devoted to vibration analysis using accelerometers. Time synchronous averaging (TSA) is one of the most representing signal processing techniques for vibration analysis to extract a periodic waveform from noisy signals of rotating machines (Braun, 1975; McFadden, 1987). The underlying idea of TSA is to intensify a periodically repeated waveform by computing the ensemble average of successive periods of a waveform of interest. Although TSA has been widely accepted to the fixed axes gear applications, literature to date barely finds TSA based PGB fault diagnosis. As reported in the literature, PGB fault diagnosis is very complicated for the following two reasons: (1) the complexity in dynamic rolling structures does not allow for direct attachment of sensors within the rotating elements for example, the sun and planet gears (Samuel *et al.,* 2004); (2) PGB includes multiple and complicated gear meshes; dynamic rotating planets and it load sharing introduces complex gear mesh excitations (Luo *et al.,* 2014).

In a recent review study, Lei *et al.,* (2014) summarized the PGB condition monitoring and fault diagnosis and prognosis methodologies in a review study. A vibration analysis technique specialized in PGB application, namely "vibration separation (VS)" was introduced by McFadden (1991) and McFadden and Howard (1990). Vibration separation enables to decompose a raw vibration signal into individual PGB component (*e.g.* sun gear or planet gears) oriented vibration signals by taking windowed vibration signals only when the vibration sensor, ring gear, planet gear, and sun gear are aligned inline. The windowed vibration signals are recombined specifically for the targeted gear component by utilizing the geometric properties of corresponding PGB. A pictorial description of the vibration separation technique is provided in Figure 3 and Figure 4. In the Figure 3, assume that the planet gear #1, which is marked in red, is the gear component of interest. In the first place, vibration separation is initiated when all of sun gear, planet gear #1, and

ring gear are placed in line with a vibration sensor; perpendicularly aligned in this example (see Figure 3(a)). From the moment, the vibration sensor collects a windowed vibration signal for tooth hunting. Until the planet gear #1 becomes available perpendicularly again, the sun gear and other planet gears operates as designed (see Figure 3(b) through Figure 3(e)). When the planet gear #1 forms the next perpendicular alignment (see Figure 3(f)), the vibration sensor collects another windowed vibration signal. This procedure is repeated until the number of collected vibration windows and the number of planet gear teeth becomes the same. Then, the windowed vibration samples are decomposed upon the particular planetary gear geometry. Provided in Figure 4, vibration decomposition procedure is pictorially explained. Each windowed vibration signals are relocated by their tooth order and combined in time domain.

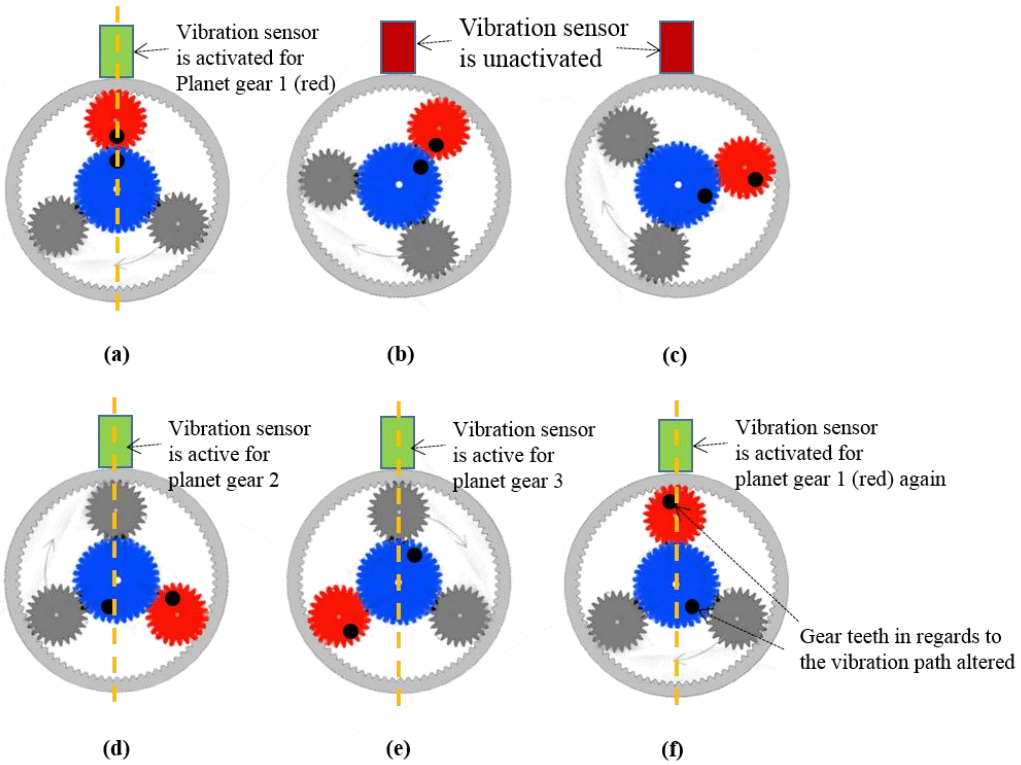

Figure 3. Graphical representation of vibration separation technique.

Subsequent studies by Howard (1990), McFadden (1994), Samuel *et al*. (2004), and Lewicki *et al.* (2011) validated this research with slightly modified versions of the technique. However, the fundamental idea of vibration separation remains unchanged.

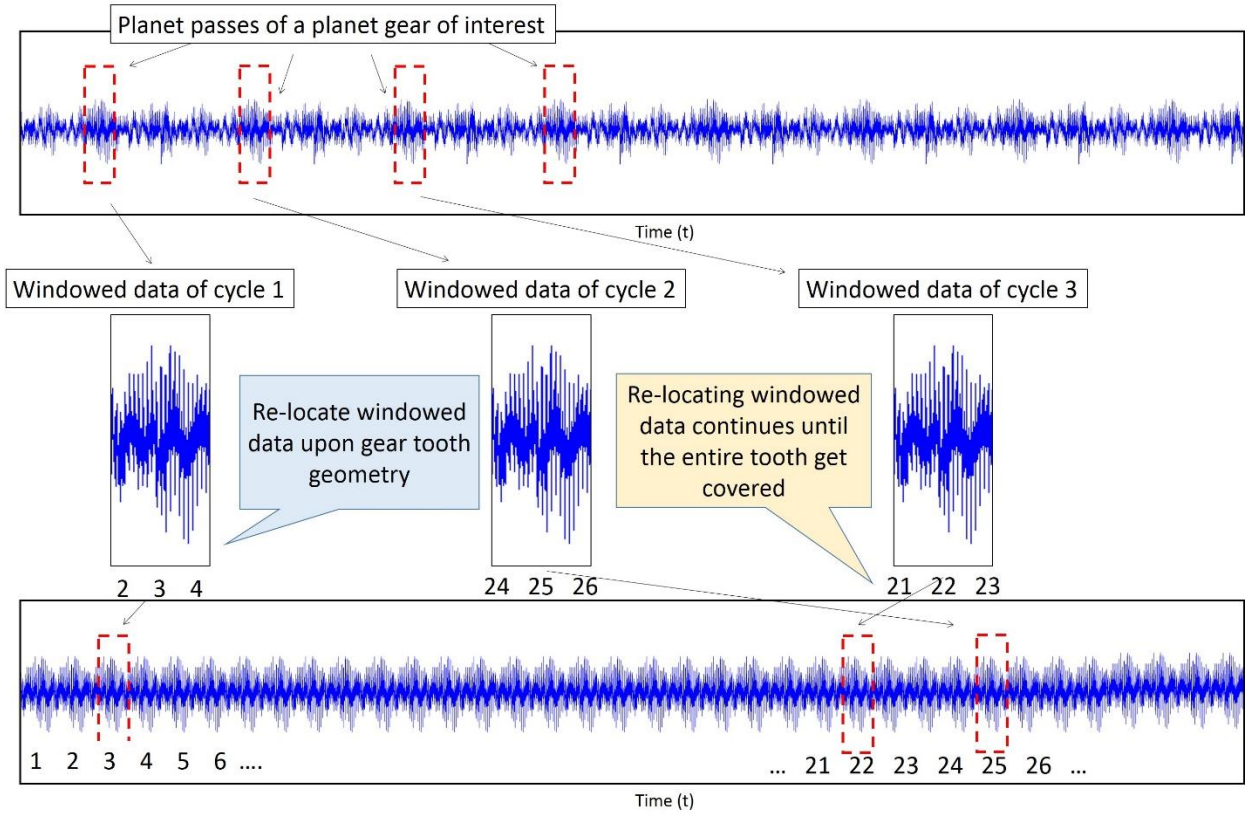

Figure 4. Vibration separation decomposition procedure.

Other researches on PGB fault diagnostic methods associated with vibration sensor could be found in the literature. Bartelmus and Zimroz (2009a) showed that the spectral characteristics of vibration signal obtained from planetary gear help not only fault detection but gear fault location. They further proposed a linear relation between the operating conditions and the signal amplitude based diagnostic feature for PGB condition monitoring with a time-varying load (Bartelmus and

Zimroz, 2009b). Then, Zimroz and Batkowiak (2013) suggested using data vectors based principal component analysis and canonical discriminant analysis to reduce data dimensions and increase diagnostic accuracy under non-stationary circumstances. Feng and Zuo (2012) derived mathematical models of a faulty planetary gear for detecting and locating a fault by considering the characteristic frequency of AM and frequency modulation (FM) effects. Feng and Liang (2014a) showed that an adaptive optimal kernel based method performs well to extract the time-varying characteristic frequencies of PGB under non-stationary conditions. Feng *et al.,* (2015) suggested that the iterative generalized demodulation can be used to improve the time-frequency readability of synchrosqueezing transform. Additionally, Feng *et al.*(2013) proposed the local mean decomposition based joint amplitude and frequency demodulation analysis for PGB fault diagnosis. To address the weak feature extraction in PGB fault diagnosis, Lei *et al.* (2013) presented an adaptive stochastic resonance method to strengthen the characteristic frequencies. Feng and Liang (2014b) introduced a Fourier dictionary into an iterative atomic decomposition thresholding method to enhance the gear fault characteristic frequency. Wu *et al*. (2004) have shown the detectability of a planet carrier crack in a planetary gearbox. In their study, raw vibration data and TSA data were transferred to the frequency domain and wavelet domain to obtain differentiable features. In a paper by Patrick *et al*. (2007), a vibration data based framework for on-board fault diagnosis and failure prognosis of helicopter transmission component was presented. In their study, TSA preprocessed vibration data and particle filter based diagnostic and prognostic models were used. Barszcza and Randall (2009) applied spectral kurtosis method for PGB fault detection of gear tooth crack in wind turbine application. Hilbert-Huang transform (HHT, Huang *et al.*, 1998) analysis also has been recently applied to vibration analysis of rotational machinery fault detection (Liu *et al.*, 2006 and Yan *et al., 2006*). However, the fundamental issue of the AM

effect of PGB has not been resolved. Thus, one attractive solution to this problem could be using alternative sensor signals that have less sensitivity to AM effect for PGB fault diagnosis and prognosis.

2. Non-vibration Analysis

Non-vibration based PGB fault diagnostic techniques are reviewed in this section. Two types of sensor analysis techniques are reported in the literature. One is torsional vibration analysis using torque sensor and the other one is strain analysis using fiber optic sensor. As pointed out, vibration signals theoretically have the AM effect caused by time variant vibration transfer paths due to the unique dynamic structure of rotating planet gears. First, in Feng and Zuo (2013), the effectiveness of torsional vibration analysis for PGB fault diagnosis was shown by using a torque sensor. The frequency characteristics of torsional vibration were displayed to be solely sensitive to the AM and FM effects caused by gear faults under constant torque on input and output shafts.

Then, Kiddy *et al.* (2011) used fiber optic strain signals for PGB fault diagnosis and showed a close relationship between strain measurement and torque changes. In this study, fiber optic strain signals were divided into two parts based on their frequency: low frequency part and high frequency components. Actual damage detection was performed by using vibration separation technique by analyzing the high frequency component only. Although promising, the research reported in the literature on using less AM effect sensitive signals for PGB fault diagnosis has certain limitations. The torque sensors used by Feng and Zuo (2013) are more expensive than vibration and strain sensors and require special installation. The fiber optic strain sensor array used by Kiddy *et al.* (2011) had to be embedded in the PGB in order to be effective. The strain signals of fiber optic strain sensor can only be sampled at a maximum sampling rate up to 1 kHz, which limits its coverage on shaft speed above 2060 rpm.

B. AE Based Machinery Fault Diagnostic Methods

AE is commonly defined as transient elastic waves within a material, caused by the release of localized stress energy (Mathews, 1983). AE was originally developed for non-destructive evaluation / testing (NDE/T) of static structures, however, those sudden internal stress redistributions are assumed to be related to failure on mechanical components such as crack initiation and growth, crack opening and closure, pitting on various monolithic materials, or composite materials. While vibration analysis is relatively well established, AE analysis is still immature not only for PGB fault diagnostics but for the entire machinery fault diagnostics field.

An early endeavor to explain an AE based fault detection technique could be found in the literature. For gears, Tomoya *et al*. (1994) analyzed the fatigue crack growth in a carburized gear tooth by AE. In their paper, it was shown that AE energy rate increased proportionally to the stress intensity factor and crack growth rate. Tandon and Mata (1999) applied AE to spur gears test rig with jet oil lubrication system to investigate the detectability gear pitting damages. Simulated pitting has constant depth (500μm) but variable diameter (250/350/450/550/1100 and 2200μm). Their investigation has shown the advantage of AE over vibration for early detection of defects in gears by observing that the AE data displayed a sharp increase in the parameters when the defect size was around 500μm while vibration data displayed a comparable increase when the defect size was more than 1000μm. For bearings, Yoshioka and Fujiwara (1982; 1984) have shown that AE parameters were able to identify bearing defects before their appearance in the vibration range. This led to an investigation that used the AE technique for the detection of subsurface cracks resulting from rolling contact fatigue (Yoshioka, 1992). The method provided the ability to determine the position of sub-surface fatigue cracks by relating the crack positions to the location of the AE signal source. The conclusions of Yoshioka and Fujiwara (1982; 1984) were later

validated by Hawman and Galinaitisin (1988) in a study that also made the observation that AE techniques are able to detect bearing faults earlier than vibration analysis methods.

More recently, machinery fault diagnostic capability using AE analysis have captured growing acceptance due to the fact that AE sensor can potentially be more sensitive to the incipient faults than vibration sensors. In Al-Balushi and Samanta (2002), energy-based features were extracted from the time domain AE to construct energy index. Their method was further test for early fault diagnostic ability compared to other AE methods and vibration methods. In Al-Ghamd and Mba (2006), an experimental investigation on AE technique was provided in order to detect the presence of mechanical defect on a radially loaded bearing and its size. In their study, it has shown not only that AE offer an earlier fault detection than vibration, but also that AE provides an indication of the fault level. Scheer *et al.* (2007) have shown that AE is effective to capture early stage of gear faults (*e.g.* tooth edge fracture and pitting) before they grow to change their vibration behavior. In a study by Eftekharnejad *et al.* (2011) in comparing the applicability of AE and vibration technologies for the monitoring of rolling bearing degradation, it was shown that AE was more sensitive for incipient fault detection when compared to vibration. In Lucas (2012), AE is described as follows in comparison to vibration: (1) With AE, an early stage of defect including worn by usage and minor defects can be identified. In the meantime with vibration, damages must grow in a certain level to be represented by vibratory behaviors; (2) AE can pick up other faults such as a lack of lubrication, friction, and cracking, and (3) AE is considered as the next generation of vibration for condition monitoring.

Despite the fact that AE has been studied a while and its feasibility is well proven, AE for machine fault diagnosis has not been widely applied yet in industrial applications because of the high computational cost and difficulties in AE analysis. AE is distinguishable from acoustic signals

in that acoustic signals generally lie on the audible range of human (*e.g.* 20 Hz ~ 20 kHz). On the contrary, AE signals lie on a higher frequency range (*e.g.* 1 kHz ~ 1 MHz). Thus a high sampling rate between 2 to 10 MHz has been a typical choice of sampling rate for AE data collection. Other issues may arise including a high data volume and complicated feature of AE signals, which make the AE data processing challenging. Recent studies indicate that the fundamental issue of high sampling rate could be overcome by applying frequency reduction technique so called heterodyne technique. Bechhoefer *et al*. (2013) and Qu *et al*. (2013a; 2014) have shown the effectiveness AE based fault detection and diagnosis using heterodyne technique with a split torque type gearbox.

Other researches in regards to AE sensor could be found in the literature. Empirical mode decomposition (EMD, Huang *et al.*, 1998) based analysis technique has been recently applied to AE analysis of full ceramic bearing fault diagnostic methods (He *et al.*, 2011; Yoon *et al.*, 2013). Welch's spectral averaging based steel bearing fault diagnostic methods were developed in Van Hecke*et al.*, 2014b. In the preceding papers, EMD was utilized in pre-processing before AE features were extracted. Then AE features were utilized in training supervised learning algorithms.

C. Data Mining Based Machinery Fault Diagnostic Methods

Machine fault diagnostics is a mapping procedure of a combinatorial information of features ($\mathbf{F}^{\boldsymbol{l}}$) and measurements ($\mathbf{M}^{m}$) toward fault types ($\mathbf{T}^{n}$). That is $\mathbf{F}^{l} \times \mathbf{M}^{m} \rightarrow \mathbf{T}^{n}$, where $l, m,$ and n stands for dimensions of feature space ($\mathbf{F}$), measurement space($\mathbf{M}$), and fault type space($\mathbf{T}$), respectively. Previously, this mapping was performed manually by experienced experts. Recently, data mining based diagnostics approaches were successfully applied to this mapping and the approaches could be classified: statistical approach and machine learning approaches.

Machine learning approaches utilize computational algorithms to "learn" information directly from given data without predetermined model equations. Those algorithms adaptively

evolve through learning process and samples. Specifically, supervised learning for classification is a popular choice in data mining based diagnostics approaches. The diagnostic system obtains availability to classify the machine status into different classes (*e.g.* healthy, faulty, or identification of probable failure mode) based on input data (or signal) as a result of learning process. Supervised learning for classification (Mathworks, 2015) includes 1) support vector machine (SVM), 2) artificial neural network (ANN), 3) Naïve Bayes, 4) decision tree, 5) k-nearest neighbor (KNN), etc. In this dissertation, two types of ANN – the back propagation (BP) and the large memory storage and retrieval (LAMSTAR) – and KNN will be mainly utilized.

ANN is a computational model that mimics a biological (human or animal) central nervous system (CNS). It comprises a layered network of simple processing elements (also called as neurons) such that this network enables to simulate a complex non-linear function or model. The decision making principles in the most of ANN approaches are alike. If the '*n*'inputs denoted as $\{x_{ij}; i = 1,2, \dots, n\}$ are fed into j^{th} neuron, output 'y_j' satisfies as:

$$y_j = \mathrm{f_N}\left[\sum_{i=1}^{n} w_{ij} x_{ij}\right] \tag{1}$$

where$\mathrm{f_N}(\cdot)$ represents nonlinear activation function. BP network (Rumelhart *et al.*, 1986) is the most representing ANN methodology which performs weight adjustment back and forth using gradient descent. A graphical structure of the BP network is provided in Figure 5.

BP training process could be described in the following three steps and repeated until a desired error criteria is met (Rojas 1996):

(1) *Feed-forward computation*: The summation of output signal from each neuron at the former layer are computed and saved. Also the evaluated derivatives of the activation functions are saved. In this step sigmoid function could be used as excitation.

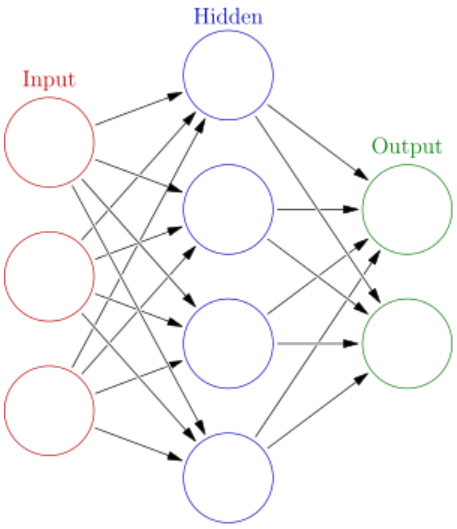

Figure 5. A graphical structure of the BP network.

(2) *Back propagation from output layer to hidden layer and input layer*: Back propagated error δ of each layer is computed and saved at each neuron. Now the partial derivatives of error with respect weight propagation are saved.

(3) *Weight updating*: after computing errors in partial derivative forms, the neuronal weights are adjusted in the negative gradient direction. Herein, the learning constant of γ defines the range of the correction.

The BP network based classification approach has been one of the most popular amongst the entire ANN algorithms. However, BP networks have the potential danger of being captured by local minima (Rojas 1996, Graupe, 2013). Also, in comparison to other machine learning methods, the BP network takes far more processing time. Therefore, in this dissertation, another ANN technique of LAMSTAR is presented for a machinery fault classifier. Unlike the other supervised learning algorithms, LAMSTAR network has barely been reported in the prognostics and health management (PHM) field. However, the LAMSTAR network was introduced in biomedical,

financial, and image processing fields due to its rapid processing capability. The LAMSTAR network was previously a United States patented (Graupe, 1999) ANN but currently is in the public domain (Google Patents, 2015). As opposed to the BP NN, the LAMSTAR network is claimed to be less sensitive to local minima phenomena (Graupe and Kordylewski, 1998). Besides, it is shown Its unique reward/punishment structure promises that the LAMSTAR network circumvents the local minima and converges to the desired output. In addition to that, LAMSTAR is faster than the BP network by as much as 30%, faster than SVM by as much as 55% (Graupe, 2013). Kohonen's self-organizing map (SOM, Kohonen 1984) modules enable a LAMSTAR network to handle a huge amount of data in a short time. In an extreme cases, LAMSTAR network was shown to be almost one thousand times faster than BP network while a similar level of classification accuracy was achieved (Kordylewski *et al.* 2001).

The LAMSTAR produces a winning decision '*v*' from the *J* output neurons in the decision SOM module by considering the sum of link weights that connect the winning neuron *w*, in each *k* of the *K* input SOM modules.

$$E(j) = \sum_{k \in K} L_{i,j}^{k,m}, \forall j \in J \tag{2}$$

$$E(v) \geq E(j), \forall j \in J. \tag{3}$$

where $L_{i,j}^{k,m}$ represents the links between neuron *i* in k^{th} module and neuron *j* in m^{th} module. When feedback as to the correct decision becomes available, the LAMSTAR updates the link weight values associated with the decision making process as follows:

$$L_{i,j}^{k,m}(t+1) = L_{i,j}^{k,m}(t) + \Delta L \tag{4}$$

$$L_{i,j}^{k,m}(t+1) = L_{i,j}^{k,m}(t) - \Delta M \tag{5}$$

$$L(0) = 0 \tag{6}$$

whereΔL and ΔM are pre-specified reward and punishment values, respectively. The details of LAMSTAR network implementation could be found in (Graupe, 2013).

In Yoon *et al*. (2013), LAMSTAR network is explored for the first time in the PHM field to develop a full ceramic bearing fault diagnostic system. In this study, LAMSTAR network has shown to be effective and efficient tool as a machinery fault classifier. In TABLE I, a brief summary on all three fault classifiers are provided.

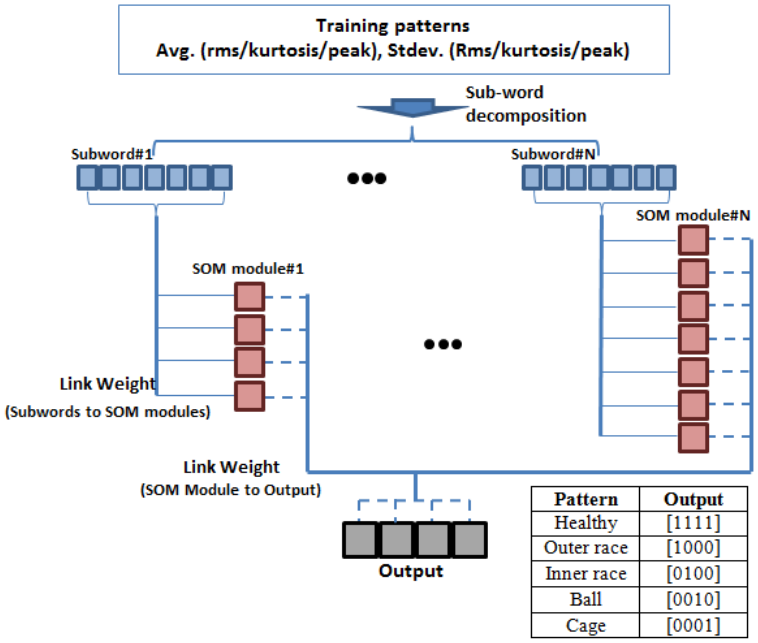

Figure 6. A graphical structure of the LAMSTAR network (Yoon *et al.*, 2013)

TABLE I.

THE THREE SUPERVISED LEARNING ALGORITHMS

Algorithm	Description
KNN (Altman, 1992)	- One of the simplest supervised learning algorithm - An object is classified by a majority vote of its neighbors
BP network (Rumelhart *et al.*, 1986)	- One of the most popular ANN methodology which mimics the biological CNS - Neural structure is optimized by back and forth propagated errors - BP network could potentially be captured by a local minima - The convergence of BP learning is slow
LAMSTAR (Graupe and Kordylewski, 1998)	- SOM based ANN which claims to be less sensitive to a local minima and faster in training than BP - Unique link-weight system attempts to imitate the efficient storage and retrieval capabilities in big data applications - Inherent transparency by link-weight system provides a forgetting capability in time-varying applications - United States patented (#US5920852) but is open for research and is in public domain.

III. EXPERIMENTAL TEST RIG

(The majority of the content in this chapter is composed of previously published work as Yoon, J., He, D., and Van Hecke, B., 2015, "On the use a single piezoelectric strain sensor for wind turbine planetary gearbox fault diagnosis", *IEEE Transactions on Industrial Electronics*, DOI: 10.1109/TIE.2015.2442216. and Yoon, J. and He, D., 2014, "Planetary gearbox fault diagnostic method using acoustic emission sensors", *IET Science, Measurement, and Technology*, DOI: 10.1049/iet-smt.2014.0375.)

This chapter introduces the experimental test rig used to validate the PGB fault diagnostic methods presented later on.

A. Introduction of the PGB Test Rig

Provided in Figure 7 displays the front view of the PGB test rig used in data collection the under different gear health and operating conditions.

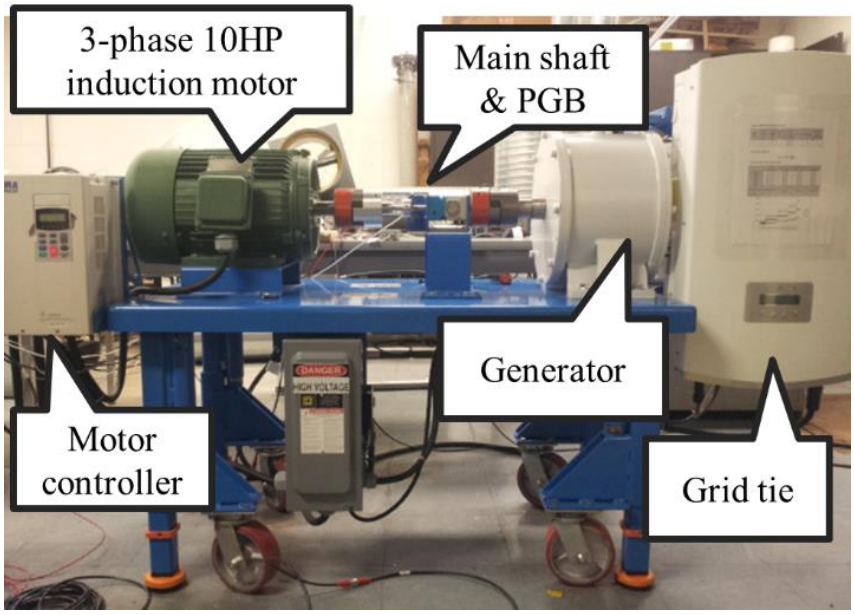

Figure 7. The front view of the PGB test rig.

The PGB test rig composes four main parts: (1) the DAQ systems, (2) the driving part, (3) the PGB gearbox, (4) the load generator. The DAQ systems will be introduced in each chapter by introducing their sensors and design purposes. A Hall effect sensor and a toothed wheel mounted on the motor shaft were paired to records the real-time shaft rotating remarks. The driving motor is a 3-phase 10 HP induction motor with a motor controller. The output shaft of the gearbox is connected to an electricity generator and a grid tie to serve as a load generator. The structure of the PGB test rig is similar to those used in a residential wind turbine.

B. Fundamental of PGB

In this dissertation, a commercially available single stage PGB with a 5:1 speed reduction ratio was used. Amongst the three different PGB operational types, a specific PGB with the fixed ring gear was utilized. Provided in Figure 8, a notional sketch of the PGB structure with the fixed ring gear could be found.

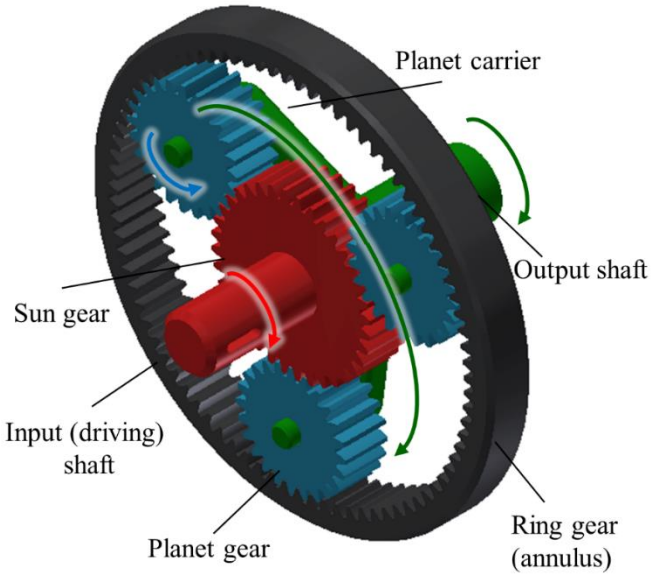

Figure 8. Notional sketch of a PGB structure.

For this type of PGB, the number of teeth is linear to the radius of each gears pitch circle. This indicates that the input to output velocity ratio is also related to the angular velocity (ω) of the gears. The gear ratio can be defined as:

$$\begin{aligned} R &= \frac{\omega_1}{\omega_A} \\ &= 1 + \frac{z_3}{z_1} \end{aligned} \tag{7}$$

where ω_{i} is the angular velocities on i^{th} gear component; z_{i} is the number of teeth on i^{th} gear component; the gear component index subscript 1, 2, 3, and *A* correspond sun, planet, ring, and planet carrier, respectively. The planet carrier rotation speed (*i.e.* output speed) in frequency could be obtained as:

$$f_a = \frac{f_1}{R} \tag{8}$$

where f_i is the rotation speed in frequency at i^{th} gear component. Also, a meshing characteristic frequency of PGB can be obtained as:

$$f_{12} = f_{23} = \frac{f_1 z_1 z_3}{(z_1 + z_3)} = \frac{f_1 \cdot z_3}{R} \tag{9}$$

where f_{ij} is the relative rotation speed in frequency between i^{th} and j^{th} gear component. The most common three failure modes of the PGB is the sun gear fault, planet gear fault, and ring gear fault. The corresponding fault frequencies are represented as follows:

$$f_{f,1} = s \cdot (f_1 - f_a) = \frac{f_1 z_3 s}{(z_1 + z_3)} \tag{10}$$

$$f_{f,2} = 2(f_2 + f_a) = \frac{4 n_1 z_1 z_3}{(z_3^2 - z_1^2)} \tag{11}$$

$$f_{f,3} = s \cdot f_a = \frac{f_1 z_1 s}{(z_1 + z_3)} \tag{12}$$

where $f_{f,i}$ indicates the fault frequency at ith gear component; $s$represents the number of planet gears in the gearbox. For more details, see Bartelmus and Zimroz (2011). TABLE II and TABLE III present the structural information and characteristic frequencies of the PGB used in this dissertation.

TABLE II

THE PARAMETERS OF THE PGB.

Parameter	Number of teeth on sun gear (z_1)	Number of teeth on planet gear (z_2)	Number of teeth on ring gear (z_3)	Number of planet gears (s)
Value	27	41	108	3

TABLE III

CHARACTERISTIC FREQUENCIES OF THE PGB AT VARIED INPUT SHAFT SPEED.

Input Shaft Speed in Frequency (f_1)	Output Shaft Speed in Frequency (f_a)	Meshing Frequency ($f_{12} = f_{23}$)	Sun Fault Frequency ($f_{f,1}$)	Planet Fault Frequency ($f_{f,2}$)	Ring Fault Frequency ($f_{f,3}$)
10	2	216	24	10.67	6
20	4	432	48	21.33	12
30	6	648	72	32.00	18
40	8	864	96	42.67	24
50	10	1080	120	53.33	30

* All the values are in unit of Hz.

IV. VIBRATION BASED PLANETARY GEARBOX DIAGNOSIS USING SPECTRAL AVERAGING

The wind energy industry currently utilizes vibratory analysis as a standard method for PGB condition monitoring. Amongst them, the vibration separation (VS) is considered as one of the well-established vibratory analysis techniques. However, the drawbacks of the VS technique as reported in the literature include: potential sun gear fault diagnosis limitation, multiple sensors and large data requirement, and vulnerability to external noise. This paper presents a new method using a single vibration sensor for PGB fault diagnosis. It combines the techniques of enveloping, Welch's spectral averaging, and data mining based fault classifiers. Using the presented approach, vibration fault features for wind turbine PGB are extracted as condition indicators (CIs) for fault diagnosis and CIs are used as inputs to fault classifiers for PGB fault diagnosis. The presented methodology is validated using a set of seeded fault tests performed on a PGB test rig in a laboratory. The results have shown a promising PGB fault diagnosis performance with the presented method.

The remainder of the Chapter is organized as follows. Section A gives a detailed explanation of the proposed methodology. In Section B, the details of the PGB test rig, seeded fault tests in a laboratory, and the experimental setup for validating the proposed methodology. Section C presents the PGB fault diagnostic results from the seeded fault tests. Finally, Section D concludes the Chapter.

A. Methodology

The framework of the methodology for wind turbine PGB fault diagnosis is provided in Figure 9. The methodology will be explained in two sections. Section A.1 approach for processing the PGB vibration signals followed by computation of CIs in Section A.2. Then, the CIs are further input into machine learning algorithms for PGB fault diagnosis.

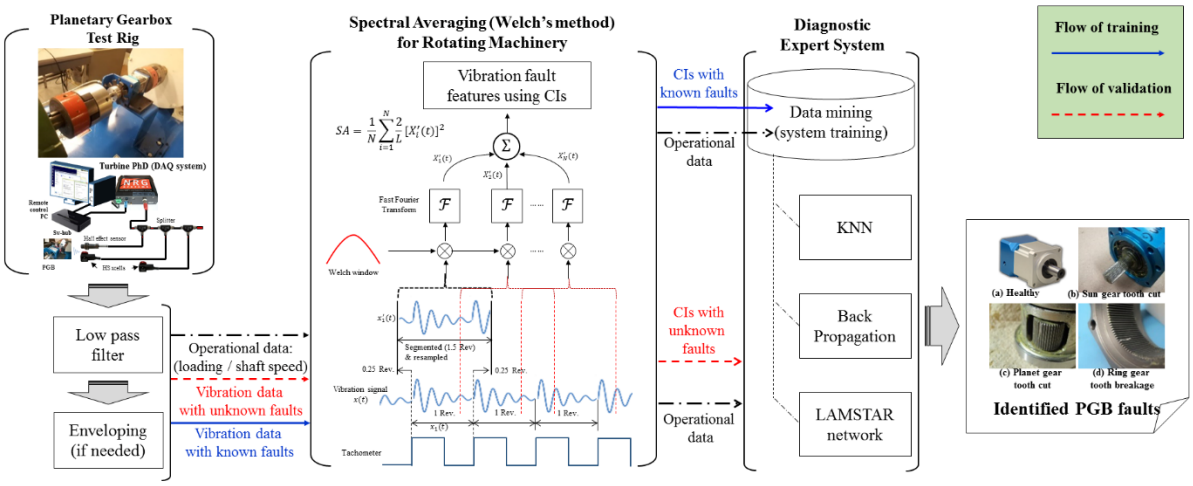

Figure 9. The framework of the methodology for PGB fault diagnosis.

1. Spectral Averaging Based Machinery Fault Diagnosis

Welch (1967) expressed the theoretical background of this approch by letting $Z(j)$, for $j = 0, \dots N-1$ be a sample from a stationary, stochastic sequence whose expected value of $E(Z) = 0$ and letting $Z(j)$ have spectral density $P(f)$, $|f| \leq \frac{1}{2}$, where f is the normalized frequency. Then if one takes several possibly overlapping segments of length L with starting points of the segments M units apart and letting $\mathrm{Z}_1(j), j = 0, \dots, L-1$ be the first segment. Then,

$$Z_1(j) = Z(j), \qquad \text{for } j = 1, \dots, L-1 \tag{13}$$

Likewise,

$$Z_2(j) = Z(j + M), \qquad \text{for } j = 1, \dots, L-1 \tag{14}$$

And finally,

$$\mathrm{Z}_k(j) = Z(j + (K-1)M), \qquad \text{for } j = 1, \dots, L-1 \tag{15}$$

The result comprises K segments (*i.e.*$Z_1(j), \dots, Z_k(j)$) covering the entire sample of interest such that $(k-1)M + L = N$. Then, from each modified segment of length L, a periodogram is obtained. In other words, a proper windowing function can be applied for fourier transforms of segments. This can be expressed in mathematical form as:

$$F_k(n) = \frac{1}{L}\sum_{j=0}^{L-1} Z_k(j)W(k)e^{-i(2kjn/L)} \tag{16}$$

where i stands for the imaginary unit. The periodograms correspond to the K number of segments can be obtained as:

$$B_k(f_n) = \frac{L}{S}|F_k(n)|^2, \qquad \text{for } k = 1,2, \dots, K \tag{17}$$

where $f_n = \frac{n}{L}$, for n $= 0, \dots, \frac{L}{2}$; S $= \frac{1}{L}\sum_{j=0}^{L-1} W^2(j)$. Finally, the Welch's PSD estimate, $\hat{P}(f_n)$, is obtained by averaging Eq (5) as:

$$\hat{P}(f_n) = \frac{1}{K}\sum_{k=1}^{K} B_k(f_n) \tag{18}$$

Figure 10 displays a graphical representation of the SA for rotating machinery fault diagnosis shown in Van Hecke *et al.* (2014b). To implement the SA for machinery fault diagnosis, the sensor signals must be segmented by a particular size. The shaft revolutionary information is first obtaind by using the tachometer's zero-crossing. The data points in each revulution is interpolated and resampled into equally sized revolutions by applying the time synchronized resampling (TSR,

Bechhoefer *et al.*, 2013a). Then the duration between shaft revolutions with two overlaps before and after is utilized as the segments to apply SA. The SA based vibration fault features were obtained from the time domain signal as below:

$$x_{SA} = |\mathcal{F}^{-1}(|\mathcal{F}(x)|^2)| \tag{19}$$

where $\mathcal{F}$ and $\mathcal{F}^{-1}$ represent Fourier transform and inverse Fourier transform, respectively; $|\mathcal{F}(x)|^2$ originally refers to the PSD of the signal x but is replaced with the PSD estimate with Welch's method in this study. The terminology "Welch" indicates the CIs from x_{SA}, hereafter.

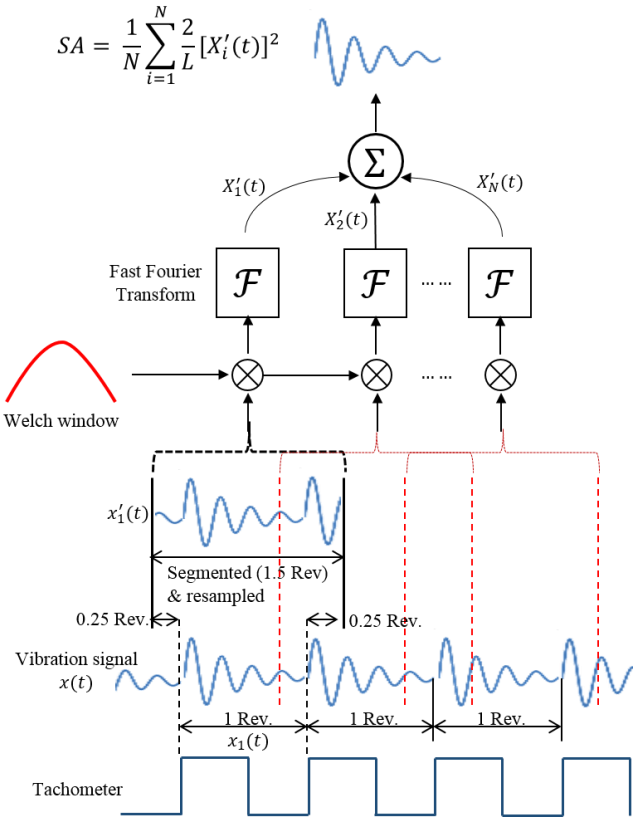

Figure 10. Welch's method for machinery fault diagnosis.

2. Vibration Based Fault Feature Extraction

In this Chapter, the CIs reported effective for gear fault diagnosis using vibration signals for wind turbine applications will be computed as reported in Sheng (2012). The five basis CIs were selected: root mean square (*RMS*), peak to peak (*P2P*), skewness (*SK*), kurtosis (*KT*), and crest factor (*CF*). Each type of CI can be computed using different input signals. Other types of input signals were generated by pre-processing: residual, energy operator (EO), narrow band (NB), amplitude modulation (AM), frequency modulation (FM), The residual is a time domain signal with the primary meshing and shaft components removed from the input signal. Gear distributed fault (GDF) is used as an effective CI for distributed gear faults wear and multiple tooth cracks. GDF is calculated from the formula below:

$$GDF = \frac{\text{StdDev(residual signal)}}{\text{StdDev(original signal)}} \tag{20}$$

The EO introduced by Teager (1992) is defined as the residual of the autocorrelation function as following:

$$x_{EO,i} = x_{IN,i}^2 - x_{IN,i-1} \cdot x_{IN,i+1}, (\text{for } i = 2, 3, \dots, N-1) \tag{21}$$

where$x_{EO,i}$ is the i^{th} element of EO data; $x_{IN,i}$ is the i^{th} element of the input datax_{IN}. The NB filtered signal, x_{NB}, could be obtained by filtering out all tones except those of the gear mesh and the characteristic frequencies. In this Chapter, the characteristic frequencies are the sun gear fault frequency, planet gear fault frequency, and ring gear fault frequency, respectively. AM and FM CIs are obtained by AM analysis and FM analysis of x_{NB}. AM and FM signals are the absolute value and the derivative of the angle of the Hilbert transform of x_{NB}, respectively. For more details of NB, AM, and FM, please see Sheng (2012). Finally, Welch's method is further processed to

TABLE IV

THE DEFINITIONS OF THE CIS FOR THE VIBRATION BASED PGB DIAGNOSIS

		Input Signal (x_{IN})						
		Raw	EO	NB	AM	FM	Welch	Welch EO
Basis CI	Fomula	Time synchronous averaged and raw signal (x_{TSA}/x_{raw})	A residual of the autocorrelation function (x_{EO})	Narrow band pass filtered (x_{NB})	Amplitude modulation of NB filtered signal [$AM(x_{NB})$]	Frequency modulation of NB filtered signal [$FM(x_{NB})$]	Welch windowed spectral averaging (x_{SA})	Energy operator of Welch [$(x_{SA})_{EO}$]
Root mean square (*RMS*)	$RMS(x_{IN}) = \sqrt{\frac{1}{N}\sum_{i=1}^{N} x_i^2}$	$RMS(x_{IN})$:measures the energy evolution of the input signal.						
Peak to peak (*P2P*)	$P2P(x_{IN}) = \frac{[\max_{1\le i\le N}(x_i) - \min_{1\le i\le N}(x_i)]}{2}$	$P2P(x_{IN})$:measures the maximum difference within the input signal.						
Skewness (*SK*)	$SK(x_{IN}) = \frac{\frac{1}{N}\sum_{i=1}^{N}(x_i-\bar{x})^3}{\left[\sqrt{\frac{1}{N}\sum_{i=1}^{N}(x_i-\bar{x})^2}\right]^3}$	$SK(x_{IN})$:measures the asymmetry of the input signal about its mean value. A negative *SK* value and positive *SK* value imply the data has a longer or fatter left tail and the data has a longer or fatter right tail, respectively.						
Kurtosis (*KT*)	$KT(x_{IN}) = \frac{N\sum_{i=1}^{N}(x_i-\bar{x})^4}{\left[\sum_{i=1}^{N}(x_i-\bar{x})^2\right]^2}$	$KT(x_{IN})$:measures the peakedness, smoothness, and the heaviness of tail in the input signal.						
Crest factor (*CF*)	$CF(x_{IN}) = \frac{P2P(x_{IN})}{RMS(x_{IN})}$	$CF(x_{IN})$:measures the ratio between $P2P(x_{IN})$ and $RMS(x_{IN})$ to describe how extreme the peaks are in the input signal.						

Note: x_i is i^{th} element of the input datax_{IN}; N is the length of the input datax_{IN}; max(·) returns the maximal element of input datax_{IN}; min(·) returns the minimal element ofinput datax_{IN}; $\bar{x}$ is a mean value of the input datax_{IN} defined as $\sum_{i=1}^{N} x_i /N$; NB, AM, and FM refers to a narrow band, amplitude modulation, and frequency modulation, respectively.

obtain Welch CIs and Welch EO CIs. TABLE IV provides the definitions of the CIs investigated for PGB fault diagnosis.

B. Experimental Setup

This section covers the experimental setup used to validate the presented vibration based PGB fault diagnostic method. First, The DAQ system for vibration based PGB fault diagnosis is briefly introduce in section B.1. Then, seeded gear fault test procedure and DAQ plan will be shown in section B.2.

1. The DAQ System for Vibration Sensors

Figure 11displays the PGB test rig used in vibration data collection the under different gear health and operating conditions. The DAQ system includes a local data collector (LDC, model: turbine PhD by Renewable NRG systems), two high speed accelerometers, and tachometer. A Hall effect sensor and a toothed wheel mounted on the motor shaft were paired to records the real-time shaft rotating remarks. The detail settings for the DAQ system are provided in TABLE V.

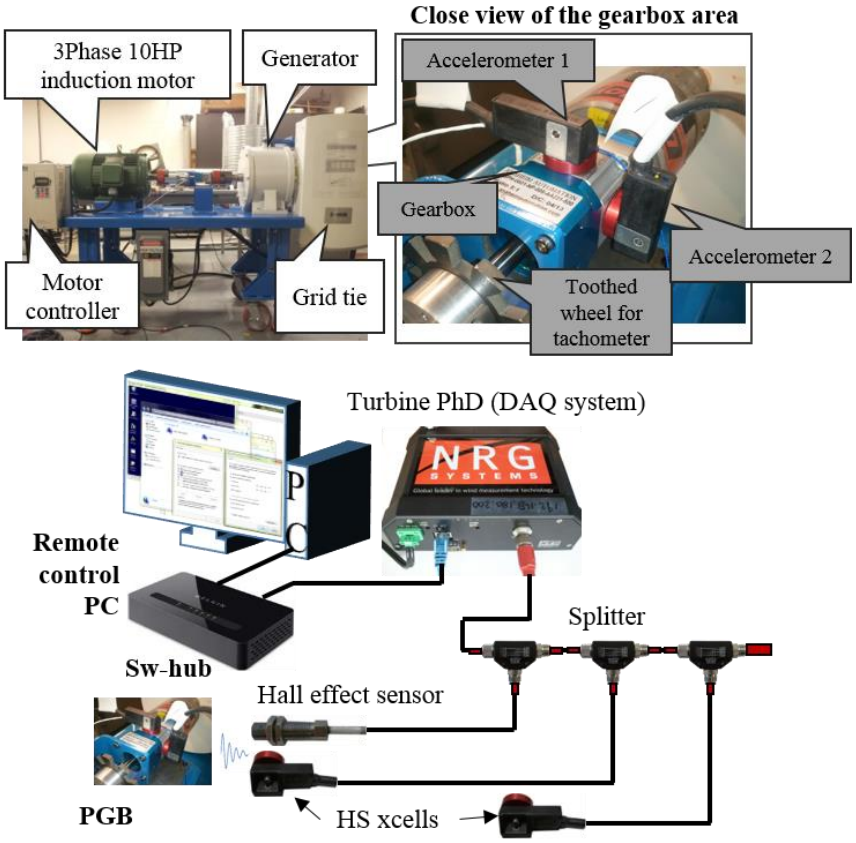

Figure 11. The PGB test rig for wind turbine simulator.

TABLE V

VIBRATION DAQ SETTING PARAMETERS.

	Vibration sensor 1	Vibration sensor 2	Tachometer
Sensor	High speed accelerometer	High speed accelerometer	Hall effect sensor
Manufacturer	NRG systems	NRG systems	Sensoronix
Sampling rate	6104 (Hz)	24414 (Hz)	1000 (Hz)
Sample recoding time for TSA	40 (sec)×5 samples	20 (sec) ×5 samples	-
Sample recording time for SA	4 (sec) ×50 samples	2 (sec) ×50 samples	-

2. Seeded Gear Faults

Three types of PGB faults were created: sun gear partial tooth cut, planet gear partial tooth cut, and ring gear tooth breakage. Each type of gear fault was artificially created by damaging a tooth on a sun gear, planet gear, and ring gear as shown in Figure 12. Both healthy and faulty gearboxes were tested under 20 combinational conditions of four varying loading conditions: 0% loading, 25% loading, 50% loading, and 75% loading out of the rated torque of the PGB, and five varying shaft speeds: 10 Hz, 20 Hz, 30 Hz, 40 Hz, and 50 Hz. After switching one gearbox to another, vibration sensors were mounted in the same location on the PGB to preserve the experimental consistency.

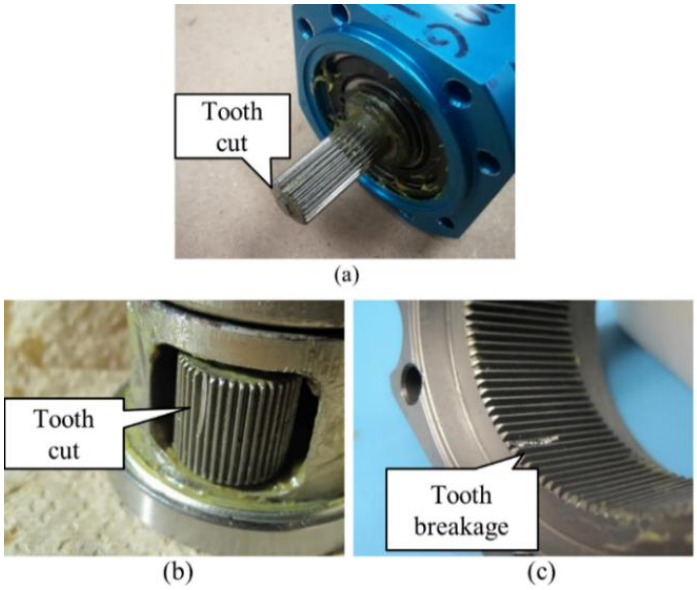

Figure 12. Seeded faults: (a) sun gear fault, (b) planet gear fault, (c) ring gear fault.

C. Validation Results

Figure 13 provides an overview of the experimental procedures including the proposed methodology.

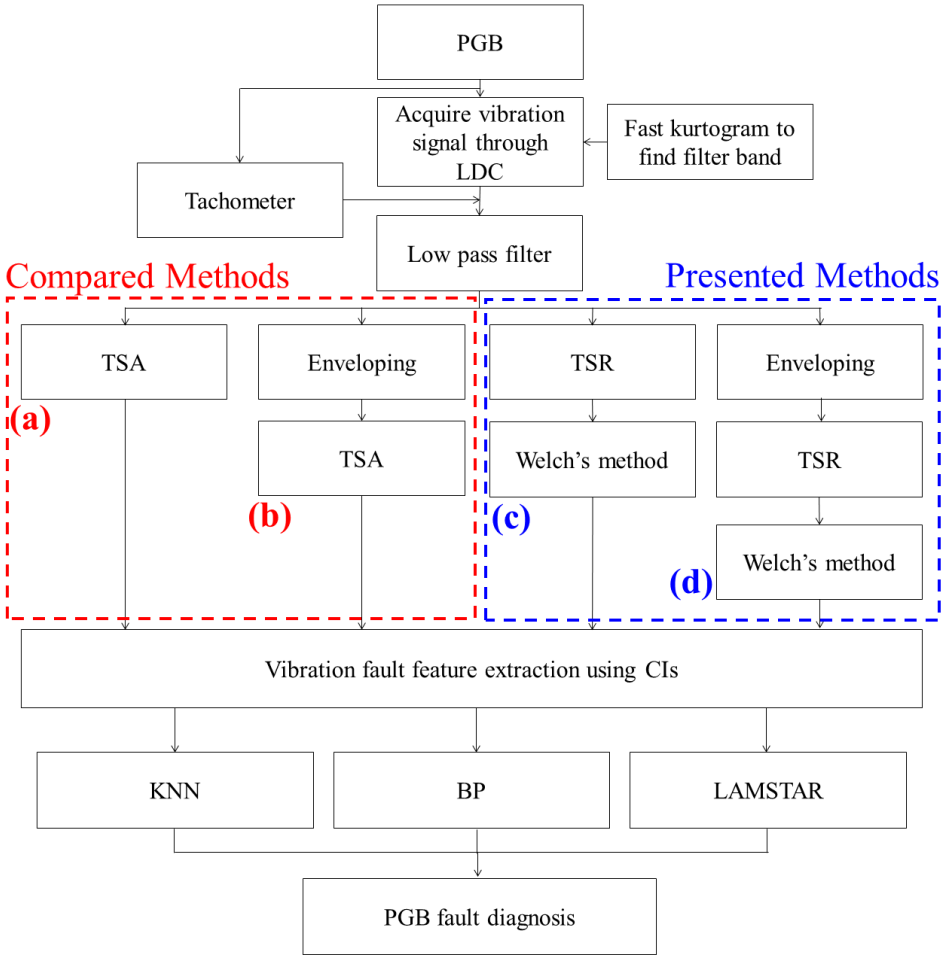

Figure 13. Overview of the experiment procedure for PGB fault diagnosis.

During the experiment, vibration data were processed with the following four different methods: (a) TSA, (b) enveloping then TSA. The presented methods are the proposed solution in this paper and include: (c) Welch's method (*i.e.* SA), (d) enveloping then Welch's method. After each processing technique was applied, the CIs were computed. First, low pass filtering was performed before each vibration processing technique as shown in Figure 13. Fast kurtogram, as reported in Antoni (2007), was applied to find universal filter bands for each vibration sensor. Statistics of the impulsivity locations over varied input shaft speed suggests that the accelerometer

1 and 2 have impulsivity located below 3 kHz and 12 kHz; thus, 3 kHz and 12 kHz were chosen for the cutoff frequencies in the low pass filters for accelerometer 1 and 2, respectively.

TABLE VI, gives a summary on the percentage separation of faulty gears from the healthy one using CIs generated by each of the four methods.

TABLE VI

STATISTICAL SEPARATION OF EACH CIS FOR PGB FAULT ISOLATION.

		Accelerometer 1 (*fs* = 6104)		
		Sun fault	**Planet fault**	**Ring**
Method	(a) TSA	-	≥80%: P2P	-
	(b) Env-TSA	-	≥80%: P2P	≥80%: RMS, P2P
	(c) Welch	≥80%: Res RMS, Res P2P, WEO P2P	≥ **90**%: RMS, Res RMS ≥80%: P2P, Res P2P, EO P2P, W RMS, WEO P2P	≥80%: Res RMS, Res CF, EO P2P, W RMS, W KT, WEO RMS
	(d) Env-Welch	≥80%: Res RMS, EO RMS, WEO P2P	≥80%: P2P, Res RMS, EO RMS, EO P2P, W P2P, WEO P2P	≥80%: Res RMS, EO RMS, WEO RMS, WEO P2P
		Accelerometer 2 (*fs* = 24414)		
		Sun	Planet	Ring
Method	(a) TSA	≥80%: Res RMS, Res P2P, GDF	-	≥90%: GDF
	(b) Env-TSA	≥80%: Res RMS, Res P2P, GDF	≥80%: RMS, Res RMS, Res P2P	-
	(c) Welch	≥ **90**%: FM0 ≥80%: Res RMS, Res KT, GDF	≥**100%**: Res RMS, WEO RMS ≥**90%**: P2P, Res P2P, EO RMS, EO P2P, W P2P, WEO P2P ≥80%: RMS, W KT, W SK	≥**100%**: GDF ≥**90%**: FM0, W RMS, WEO KT, WEO SK ≥80%: W KT, W CF, W SK, WEO RMS
	(d) Env-Welch	≥80%: Res RMS, EO RMS, WEO P2P	≥80%: P2P, Res RMS, EO RMS, EO P2P, W P2P, WEO P2P	≥80%: Res RMS, EO RMS, WEO RMS, WEO P2P

* Note: "Res" stands for the residual signal.

The percentage separation is defined as the percentage of the data samples that show a statistically significant difference between the CIs of the fault gear and healthy gear. From TABLE VI, one can see that the conventional signal processing techniques, method (a) and (b), barely differentiate the faulty PGBs from the healthy ones. On the other hand, the proposed method (c) and method (d) generated multiple CIs displaying PGB fault isolating performance. Also from TABLE VI, one can see that the most effective CIs were obtained when vibration signals of

accelerometer 2 were processed with method (c). These CIs include FM0 achieving 90% separation for the sun gear fault, Res RMS and WEO RMS achieving 100% separation for the planet gear fault, and GDF achieving 100% for the ring gear fault.

Figure 14 graphically shows the separation of the fault gear from the healthy gear achieved by above mentioned CIs. Each point and the vertical bar at each point represent the averaged CI value and the 95% confidence interval.

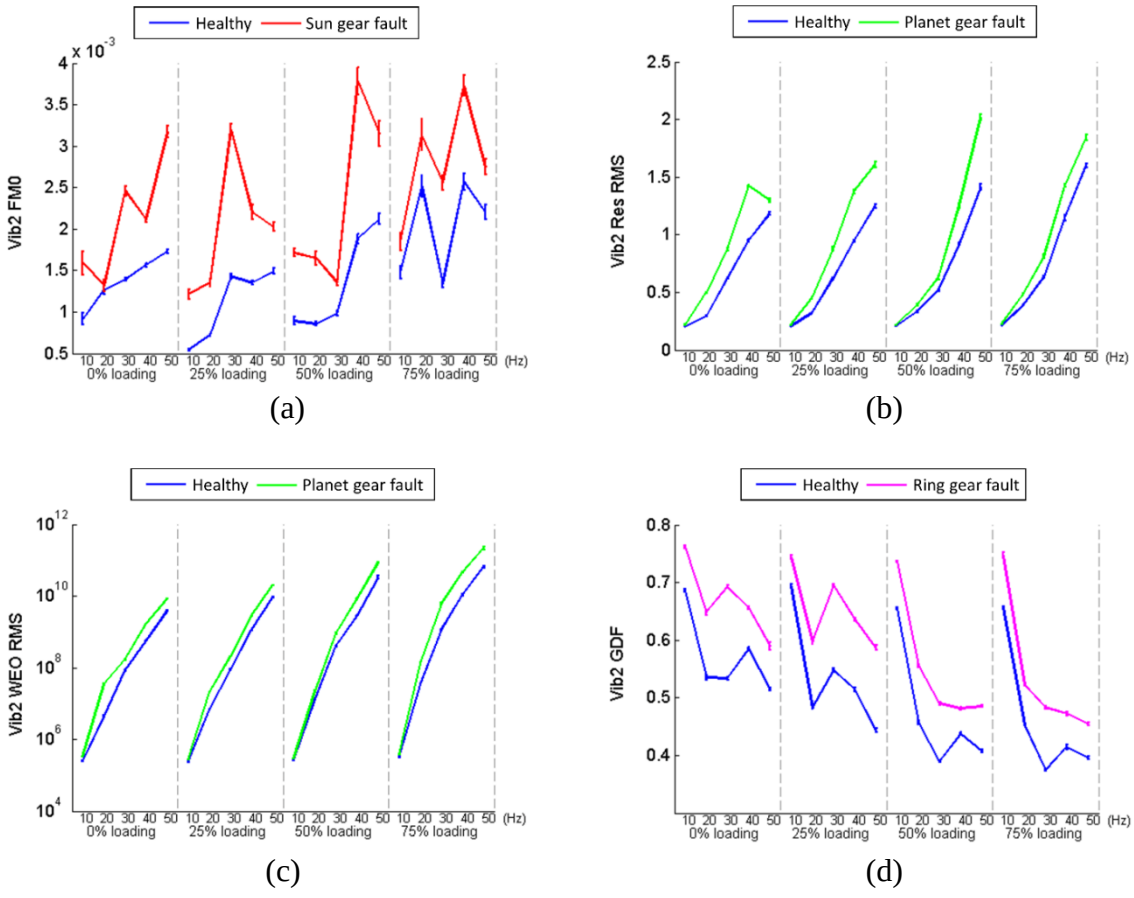

Figure 14. Effective CIs (a) FM0: healthy vs. Sun gear fault, (b) Residual RMS: healthy vs. planet gear fault, (c) WEO RMS: healthy vs. planet gear fault, (d) GDF: healthy vs. ring gear fault.

Effective CIs in TABLE VI were further utilized to isolate the fault locations (*e.g.* sun, planet, ring, or healthy) using three fault classifiers: KNN, BP, and LAMSTAR. In TABLE VII and

, the PGB fault diagnostic results using those fault classifiers are presented with the individual CIs and combinations of CIs. PGB operational parameters such as loading and shaft speed were included.

TABLE VII

PGB FAULT DIAGNOSTIC RESULTS USING INDIVIDUAL CI

CI: FM0						
Classifier	KNN (*k*=15)		BP (*N*=40)		LAMSTAR	
Type of fault	Mean error (μ)	Std dev. (σ)	Mean error (μ)	Std dev. (σ)	Mean error (μ)	Std dev. (σ)
Healthy	24.56	2.94	47.79	20.27	62.97	7.95
Sun	39.48	3.04	47.08	26.97	73.11	6.70
Planet	38.66	3.24	51.04	21.41	66.65	10.87
Ring	49.03	2.89	43.33	31.43	78.25	6.49
Overall	37.94	1.31	47.24	12.38	70.24	1.56
CI: Res RMS						
Classifier	KNN (*k*=15)		BP (*N*=30)		LAMSTAR	
Type of fault	Mean error (μ)	Std dev. (σ)	Mean error (μ)	Std dev. (σ)	Mean error (μ)	Std dev. (σ)
Healthy	20.50	2.37	43.97	21.75	34.67	3.83
Sun	38.04	2.94	32.63	25.79	42.58	3.38
Planet	19.21	2.42	54.16	22.01	33.39	3.45
Ring	34.07	2.80	29.47	20.32	47.43	3.36
Overall	27.95	1.03	40.32	13.18	39.47	1.14
CI: GDF						
Classifier	KNN (*k*=15)		BP (*N*=30)		LAMSTAR	
Type of fault	Mean error (μ)	Std dev. (σ)	Mean error (μ)	Std dev. (σ)	Mean error (μ)	Std dev. (σ)
Healthy	12.30	2.01	24.30	11.80	12.7	1.98
Sun	25.11	2.59	45.45	32.60	28.12	2.94
Planet	22.14	2.39	31.81	12.96	26.13	2.62
Ring	15.13	1.85	15.89	15.70	16.01	1.65
Overall	18.67	0.87	29.64	12.86	20.74	1.07
CI: WEO RMS						
Classifier	KNN (*k*=15)		BP (*N*=40)		LAMSTAR	
Type of fault	Mean error (μ)	Std dev. (σ)	Mean error (μ)	Std dev. (σ)	Mean error (μ)	Std dev. (σ)
Healthy	77.20	2.28	62.37	25.16	73.50	7.72
Sun	70.79	2.47	73.67	12.83	78.67	6.76
Planet	73.65	2.39	80.26	13.13	77.91	8.06
Ring	70.24	2.23	84.54	12.87	75.27	7.08
Overall	72.97	1.03	75.20	0.97	76.34	0.95

* Note: *k* is the search radius for a majority vote of its neighbors in KNN; *N* is the number of neurons in the hidden layer in BP network.

TABLE VIII

PGB DIAGNOSTIC RESULTS USING CI COMBINATION

1st CI combination: FM0, Res RMS, WEO RMS, GDF						
Classifier	**KNN (*k*=3)**		**BP (*N*=40)**		**LAMSTAR**	
Type of fault	Mean error (μ)	Std dev. (σ)	Mean error (μ)	Std dev. (σ)	Mean error (μ)	Std dev. (σ)
Healthy	1.52	0.88	4.56	13.64	1.99	0.73
Sun	6.38	1.44	9.24	18.49	6.67	1.50
Planet	4.33	1.30	14.13	21.60	4.43	1.11
Ring	2.27	1.01	7.96	22.77	2.81	0.87
Overall	3.63	0.56	8.94	12.71	3.98	0.54
2nd CI combination: P2P, FM0, Res RMS, Res KT, Res P2P, GDF, EO RMS, EO P2P, W RMS, W P2P, WEO RMS, WEO P2P, WEO KT, WEO SK.						
Classifier	**KNN (*k*=4)**		**BP (*N*=40)**		**LAMSTAR**	
Type of fault	Mean error (μ)	Std dev. (σ)	Mean error (μ)	Std dev. (σ)	Mean error (μ)	Std dev. (σ)
Healthy	28.73	2.47	14.33	18.19	29.15	2.67
Sun	23.11	2.65	22.42	22.76	22.29	2.38
Planet	21.24	2.38	14.06	13.03	19.31	2.00
Ring	29.73	2.68	11.44	18.02	30.04	2.40
Overall	25.71	1.20	15.51	12.44	25.20	1.22

* Note: *k* is the search radius for KNN; *N* is the number of neurons in the hidden layer in BP network

Out of 2000 samples, 70% of the data were randomly chosen and utilized for training and the remaining 30% of data were used for validation. In order to measure the statistical fault diagnostic performance, all classifiers were run 50 times in a random sampling manner. The average error rates (% of error) and its standard deviation were presented. The error rate is defined as the percentage of misclassified samples in validation. For KNN, the search radius of k was investigated within $k = 3{\sim}15$ range and the minimal error rate is shown on each table. Also, for the BP network, the neuronal structures in the hidden layer were investigated for N = 10, 20, 30, 40, and 50 and the one showing the minimal error is provided.

As one can see from TABLE VII, none of the single CI provides acceptable diagnostic performance for all three fault classifiers although each CI can detect faults from at least one or more PGB fault types. Thus, two combinations of CIs were generated. In the first CI combination, the CIs showing the highest statistical separation (*i.e.*≥90% for sun gear fault, 100% for planet

gear and ring gear faults) were grouped. In the second CI combination, the CIs with the second highest statistical separation (*i.e.*≥ 80% for sun gear fault, ≥ 90% for planet gear and ring gear faults) were included. The fault diagnostic results with both CIs combinations are provided in

. KNN achieved the overall best error rate of 3.63% when the first CI combination were used. When the local minima convergence is ignored, BP network achieved less than 5% overall diagnostic error rate. However, the final error rate drastically dropped down when the local minima convergence is considered. It should be noted that the occurrence of local minima convergence was approximately 12~16% over 50 runs and it is well reflected on the standard deviation of the error rate. Lastly, LAMSTAR network achieved the similar diagnostic error rate of 3.98% as it is claimed to be insensitive to the local minima issue unlike BP network. However, LAMSTAR network achieved the minimal standard deviation and it is desired aspect from the reliability perspective.

D. Conclusions

In this Chapter, a new method using a single vibration sensor for PGB fault diagnosis was presented. It combines the techniques of enveloping, Welch's spectral averaging, and data mining based fault classifiers. Using the presented approach, vibration fault features for wind turbine PGB are extracted as CIs and CIs are used as inputs to fault classifiers for PGB fault diagnosis. The presented method was validated with a set of seeded fault tests performed on a PGB test rig in a laboratory. First, the digitized accelerometer signals were processed by SA technique to extract PGB fault features and to compute CIs. The effective CIs were grouped into two combination sets according to the level of statistical separation followed by training three machine learning algorithms as fault classifiers: KNN, BP network, and LAMSTAR network. Each fault classifier was run 50 times to obtain the statistical results. The validation results have shown: (1) the minimal

error rate of 3.63% was achieved using KNN when the first set of CI combination was used; (2) an average diagnostic error rate of 8.94% was achieved using the BP algorithm. The local minima convergence was observed at a rate of 12~16% out of 50 runs; (3) LAMSTAR network displayed less sensitivity to the local minima issue and achieved a similar level of diagnostic error rate of 3.98% compared to KNN when the first set of CI combination was used. Also, LAMSTAR network resulted in the minimal standard deviation which is a desirable measurement from the reliability perspective. In summary, the proposed method effectively differentiated the localized faults on all gears: sun gear, planetary gear, and ring gear, which has not been presented in the literature.

V. A NEW PLANETARY GEARBOX FAULT DIAGNOSTIC METHOD USING AN ACOUSTIC EMISSION SENSOR

In this Chapter, a new AE sensor based planetary gearbox (PGB) fault diagnostic method is presented. It is sometimes painful to identify the vibration directions if the sources are complex and combinative. Hence, applying an AE sensor analysis could be beneficial to PGB fault diagnosis in that AE signals propagate from the wave source (*i.e.* faults) to sensing apparatus within mechanical components. The method includes a heterodyne based AE data acquisition system, empirical mode decomposition (EMD) based AE signal analysis method, and computation of condition indicators (CIs) for PGB fault diagnosis. The heterodyne technique is hardware-implemented to downshift the sampling frequency of AE signals at a rate compatible to vibration analysis. The sampled AE signals are processed using EMD to extract PGB fault features and compute the CIs. The CIs are input into supervised learning algorithms for PGB fault diagnosis. The method is validated on a set of seeded localized faults on all gears: sun gear, planetary gear, and ring gear. The validation results have shown a promising PGB fault diagnostic performance using the presented method.

The main contribution of the chapter is the development of the new PGB fault diagnosis method using AE sensors and the validation of the method using seeded gear tooth cut and breakage faults on all PGB gears: sun gear, planetary gear, and ring gear. Even though some of the

components of the presented method have been used for a long time, integrating AE sensor with them for PGB fault diagnosis and validating the method with real seeded fault tests on a PGB test rig has never been reported in the literature.

The remainder of the Chapter is organized as follows. Section A gives a detailed explanation of the presented methodology. In Section B, the experiments setup to validate the presented methodology and the seeded fault tests on a laboratory PGB test rig are explained. Section C presents the PGB fault diagnostic results from the seeded fault tests. Finally, Section D concludes the Chapter by showing a promising PGB fault diagnostic performance using the presented method.

A. Methodology

An overview of the proposed AE based PGB fault diagnostic methodology is provided in Figure 15. The heterodyne technique is hardware-implemented to sample AE signals at a rate of 100 kHz which is compatible to vibration analysis. The sampled AE signals are then processed using EMD to extract PGB fault features and compute CIs. The CIs are further input into fault classifiers.

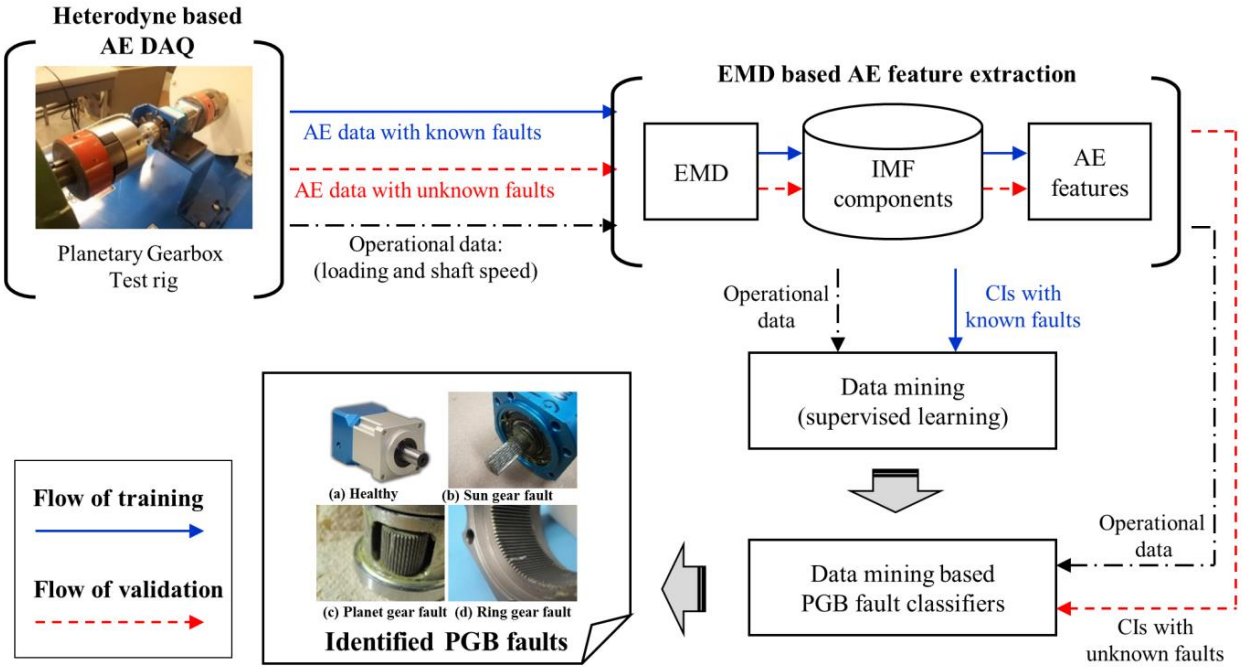

Figure 15. Overview of the proposed PGB fault diagnostic method with AE sensor.

1. AE Sampling Rate Reduction Using Heterodyne Technique

The theoretical foundation of heterodyne technique for AE sensor will be reviewed in this section. To apply AE based machine fault diagnosis, one technical challenge is to deal with the data storage and processing burden caused by the high sampling rate of an AE sensor. To meet the challenge, heterodyne technique (Fessenden, 1902) was hardware implemented to build up the AE DAQ system. Heterodyning is a radio signal processing technique which downshifts the frequency of the AE signals so that its sampling rate be comparable to that of vibration signals. Qu *et al.* (2013b) has shown that heterodyne based AE DAQ could be effective at a sampling rate as low as to 20 kHz for a split torque type gearbox.

The AE demodulating technique implemented in this Chapter works like a radio quadrature demodulator: shifting the carrier frequency to baseband, followed by low pass filtering. For two

signals with different frequencies f_1 and f_2, respectively, their product could be written by trigonometric identities as:

$$\sin(2\pi f_1 t)\sin(2\pi f_2 t) = \frac{1}{2}\cos[2\pi(f_1 - f_2)t] - \frac{1}{2}\cos[2\pi(f_1 + f_2)t] \quad (22)$$

where f_1 is the AE carrier frequency and f_2 is the demodulator's reference signal frequency. Technically, the heterodyning technique is aimed especially at demodulating the amplitude modulated signals. Although, frequency and phase modulation are potentially existent, they are considered trivial and will not be discussed herein. The amplitude modulation process can be mathematically expressed as:

$$U_a = (U_m + mx)\cos\omega_c t \quad (23)$$

where, U_a is the amplitude modulated signal, U_m is the carrier signal amplitude, m is the modulation coefficient, x is the signal of interest, and ω_c is the carrier signal frequency. By introducing an amplitude and frequency for x by X_m and Ω, respectively, the signal of interest x can be represented as:

$$x = X_m cos\Omega t \quad (24)$$

Note that it is assumed that Ω is much smaller than ω_c. Then, with the heterodyne technique, the modulated signal will be multiplied by a unit amplitude reference signal $\cos(\omega_c t)$. Then the resulting U_o can be written as:

$$U_o = (U_m + mx)\cos(\omega_c t)\cos(\omega_c t) = (U_m + mx)\left[\frac{1}{2} + \frac{1}{2}\cos(2\omega_c t)\right] \quad (25)$$

Substituting Equation (24) into Equation (25) yields:

$$U_o = \frac{1}{2}U_m + \frac{1}{2}mX_m cos\Omega t + \frac{1}{2}U_m cos(2\omega_c t) \quad (26)$$

$$+\frac{1}{4}mX_m[cos(2\omega_c+\Omega)t+cos(2\omega_c-\Omega)t]$$

Because U_m is assumed not to contain any useful information related to the modulated signal, it could be cancelled out. From Equation (26), it can be concluded that only the second term $\frac{1}{2}mX_m cos\Omega t$ will remain after applying low pass filter, while the high frequency components around frequency $2\omega_c$ will be removed. In the final heterodyning demodulation step, the signal frequency can be reduced to 10s of kHz. The resulting frequency range for AE signals becomes comparable to that of typical vibration signals. Thus, a lower sampling rate in an AE DAQ system can be used.

Finding a proper carrier signal is critical to the successful implementation of the heterodyne technique in AE DAQ. Since each AE sensor product from varying manufacturers has a unique frequency characteristic, the optimization process is necessary. The details of the optimization process are described in (Qu *et al.*, 2014).

2. EMD Based AE Feature Extraction

EMD has been proven to be an effective method in analyzing non-stationary signals for rotational machinery fault detection. It has been shown in (He et al., 2011; 2013) that the EMD method was effective in processing AE signals and extracting AE features for bearing fault diagnosis applications. Therefore, in this paper, the EMD method is utilized to extract AE features from heterodyned AE signals for PGB fault diagnosis. One of the advantages of using EMD based AE feature extraction is that it does not require pre-specified basis functions or filters. Instead, it decomposes an input signal by direct extraction of the local energy associated signals (*i.e.* IMFs). The pseudo-code of the EMD based AE feature extraction is provided in TABLE IX.

TABLE IX

PSEUDO-CODE OF EMD FOR AE FEATURE EXTRACTION PROCEDURE

[$C_i(t), for\ i = 1 \ldots N$] = EMD[$f(t)$]

1. **Calculate** the local maxima and local minima of $f(t)$.
2. **Calculate** the lower and upper envelopes of $f(t)$ using cubic spline.
3. **Calculate** mean values $m(t)$ by averaging the lower envelope and the upper envelope.
4. Subtract the $m(t)$ from the $f(t)$ to produce the IMF candidate component:

$$h_I\ (t)\ =\ f(t)\ -\ m(t)$$

   A. **IF** $h_I\ (t)$ is the true IMF, go to the next step and save the IMF component as $C_i(t)\ =\ h_m(t)$.

   B. **ELSE**, go back to Step 1 until the below stop condition is met.

$$SD \geq \sum_{t=1}^{T} \frac{[h_{m-1}(t) - h_m(t)]^2}{h_{m-1}^2(t)}$$

where $h_{m-1}(t)$ and $h_m(t)$ denote the IMF candidates of the m − l and m iterations, respectively. SD is typically chosen between 0.2 and 0.3.

5. **Calculate** the residual component by subtracting IMF component from the $f(t)$ as:

$$res_i(t) = f(t) - C_i(t)$$

6. **Repeat** Steps 1-5 until the last residual component ($res_i(t)$)becomes a monotonic function and no more IMF component can be extracted or the envelopes becomes smaller than a pre-determined value.
7. **Pick** the best *k* number of IMFs from the energy significance perspectives.
8. **Accumulate** IMFs to obtain AE based PGB fault features using (27).

After IMF components $\{c_i(t),\ for\ i = 1,2, \ldots, N\}$ are extracted from $f(t)$, a certain number (*e.g.* $k(k \leq N)$) of $c_i(t)$ are accumulated from the energy significance perspective as follows:

$$x_{EMD} = \sum_{i=1}^{k} c_i(t). \tag{27}$$

Using (6) the CIs will be further computed for PGB fault diagnosis.

3. AE Sensor Based Fault Feature Extraction

The five basis measurements were chosen: root mean square (*RMS*), peak to peak (*P2P*), skewness (*SK*), kurtosis (*KT*), and crest factor (*CF*). CIs were computed using those basis measurements over varied input signals: Raw AE signals, energy operator (EO), narrow band (NB), amplitude modulation (AM), frequency modulation (FM), spectral averaging (SA) via Welch's method (Welch), and EO of the Welch. FM0 is obtained as an effective CI for distributed gear faults wear and multiple tooth cracks. FM0 is calculated from the formula below:

$$FM0 = \frac{P2P}{\sum A_k} \tag{28}$$

where A_k is the sum of the gear mesh harmonics.

The EO in Teager (1992) is defined as the residual of the autocorrelation function as following:

$$x_{EO,i} = x_{IN,i}^2 - x_{IN,i-1} \cdot x_{IN,i+1}, \quad (\text{for } i = 2, 3, \dots, N-1) \tag{29}$$

where $x_{EO,i}$ is the i^{th} element of EO data; $x_{IN,i}$ is the i^{th} element of the input datax_{IN}. The NB filtered signal, x_{NB}, could be obtained by filtering out all tones except those of the gear mesh and the characteristic frequencies. In this Chapter, the characteristic frequencies are the sun gear fault frequency, planet gear fault frequency, and ring gear fault frequency, respectively. Finally, AM and FM CIs are obtained by AM analysis and FM analysis ofx_{NB}. AM and FM signals are the absolute value and the derivative of the angle of the Hilbert transform of x_{NB}, respectively.

The SA based CIs were obtained as below:

$$x_{Welch} = |\mathcal{F}^{-1}(|\mathcal{F}(x)|^2)| \tag{30}$$

where $\mathcal{F}$ and $\mathcal{F}^{-1}$ represent Fourier transform and inverse Fourier transform, respectively; $|\mathcal{F}(x)|^2$ originally refers to the power spectral density (PSD) of x and is replaced with the PSD estimate with Welch's method. The terminology "Welch" refers to the SA obtained by the Welch's PSD estimate hereafter. TABLE X provides the definitions of the CIs investigated for PGB fault diagnosis. Once the CIs are computed, they will be used train the PGB fault classifiers using three supervised learning algorithms.

TABLE X
THE DEFINITIONS OF THE CIS FOR THE AE BASED PGB DIAGNOSIS

		Input Signal (x_{IN})						
		Raw:	EO:	NB:	AM:	FM:	Welch:	Welch EO:
CI	Formula	Raw input signal (x_{raw})	A residual of the autocorrelation function (x_{EO})	Narrow band pass filtered (x_{NB})	Amplitude modulation of NB filtered signal [$AM(x_{NB})$]	Frequency modulation of NB filtered signal [$FM(x_{NB})$]	Welch windowed spectral averaging (x_{Welch})	Energy operator of Welch [$(x_{Welch})_{EO}$]
Root mean square (*RMS*)	$RMS(x_{IN}) = \sqrt{\frac{1}{N}\sum_{i=1}^{N} x_i^2}$	$RMS(x_{IN})$: measures the energy evolution of a signal.						
Peak to peak (*P2P*)	$P2P(x_{IN}) = \frac{[\max_{1\le i\le N}(x_i) - \min_{1\le i\le N}(x_i$	$P2P(x_{IN})$: measures the maximum difference within the data range.						
Skewness (*SK*)	$SK(x_{IN}) = \frac{\frac{1}{N}\sum_{i=1}^{N}(x_i-\bar{x})^3}{\left[\sqrt{\frac{1}{N}\sum_{i=1}^{N}(x_i-\bar{x})^2}\right]^3}$	$SK(x_{IN})$: measures the asymmetry of the data about its mean value. A negative *SK* value and positive *SK* value imply the data has a longer or fatter left tail and the data has a longer or fatter right tail, respectively.						
Kurtosis (*KT*)	$KT(x_{IN}) = \frac{N\sum_{i=1}^{N}(x_i-\bar{x})^4}{\left[\sum_{i=1}^{N}(x_i-\bar{x})^2\right]^2}$	$KT(x_{IN})$: measures the peakedness, smoothness, and the heaviness of tail in a data set.						
Crest factor (*CF*)	$CF(x_{IN}) = \frac{P2P(x_{IN})}{RMS(x_{IN})}$	$CF(x_{IN})$: measures the ratio between $P2P(x_{IN})$ and $RMS(x_{IN})$ to describe how extreme the peaks are in a waveform.						

Note: x_i is i^{th} element of the input datax_{IN}; N is the length of the input datax_{IN}; max(·) returns the maximal element of input datax_{IN}; min(·) returns the minimal element ofinput datax_{IN}; $\bar{x}$ is a mean value of the input datax_{IN} defined as $\sum_{i=1}^{N} x_i / N$; NB, AM, and FM refers to a narrow band, amplitude modulation, and frequency modulation, respectively.

B. Experimental Setup

This section covers the experimental setup used to evaluate the presented AE sensor based PGB fault diagnostic methodology. Figure 16 displays the AE PGB test rig with AE DAQ setting used to conduct the PGB seeded fault tests.

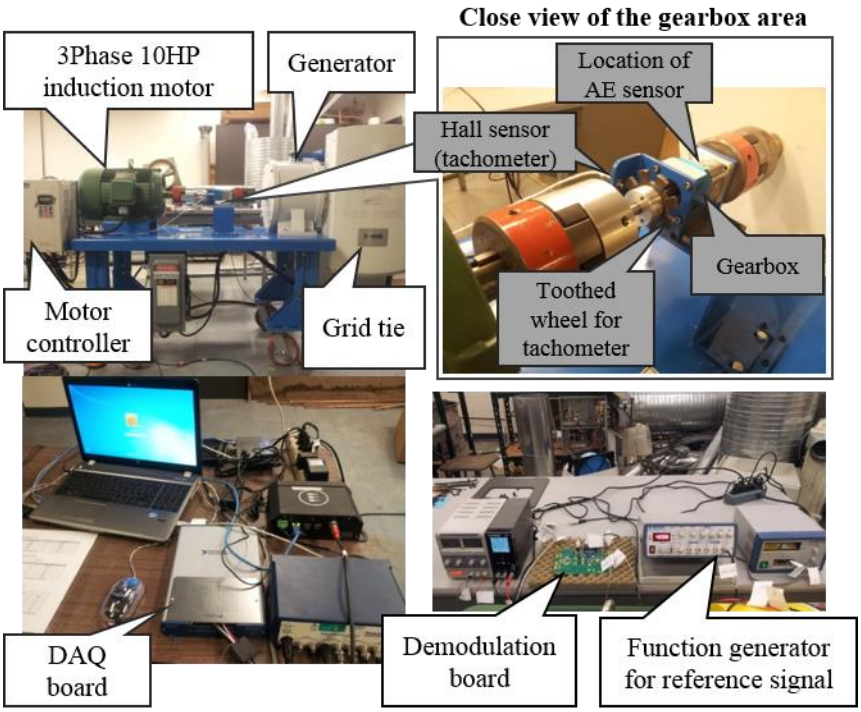

Figure 16. The PGB test rig with AE DAQ setting.

1. The AE DAQ System Using the Heterodyne Technique

The DAQ system includes a National Instruments (NI)'s DAQ board with a maximum analog input sampling rate of 1.25MHz, a wideband differential AE sensor, a pre-amplifier (20/40/60 db), a demodulation board, and a carrier frequency generator. A Hall effect sensor was used as the tachometer paired with a toothed wheel mounted on the motor shaft. Provided in Figure 17 and is the AE based DAQ system using the heterodyne technique

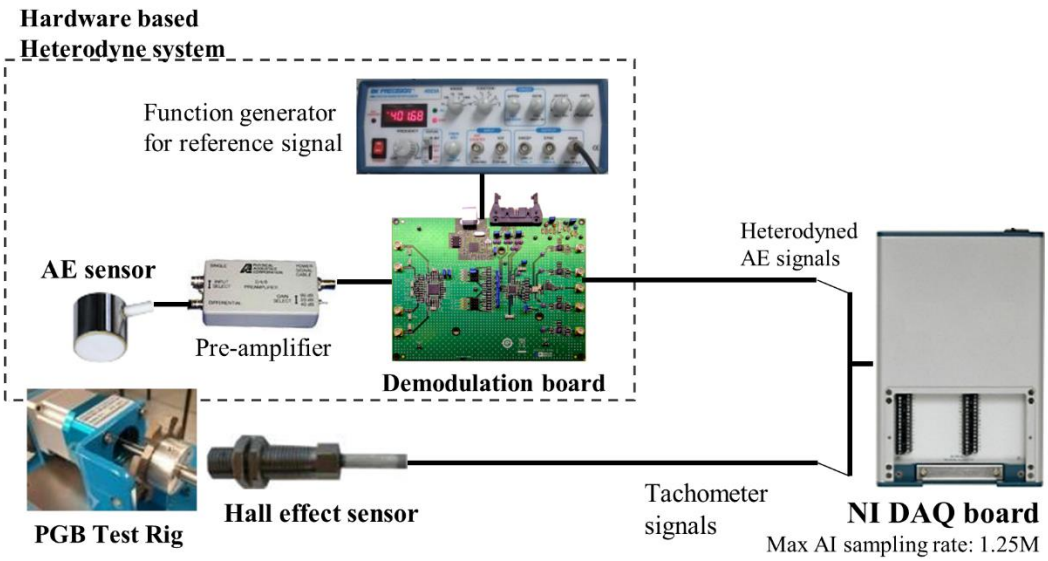

Figure 17. The AE based DAQ system using the Heterodyne technique.

TABLE XI

AE DAQ SETTING PARAMETERS.

	AE sensor	Tachometer
Sensor	Wideband differential sensor	Hall effect sensor
Manufacturer	Physical Acoustics	Sensoronix
Pre-amplifier	40db	-
Sampling rate	100k (Hz)	-
Sample recording time	2 (sec)	Used only for getting shaft speed only.

2. The Seeded Gear Faults

Three types of PGB faults were created: sun gear partial tooth cut, planet gear partial tooth cut, and ring gear tooth breakage. Each type of gear fault was created by artificially damaging a tooth on a sun gear, planet gear, and ring gear, respectively (see Figure 18).

During the seeded fault tests, AE signals were collected with a sampling rate of 100 kHz. The tachometer signals were recorded to get revolution stamps. Both the healthy gearbox and the gearboxes with seeded faults were tested at five different input shaft speeds: 10 Hz, 20 Hz, 30 Hz,

40 Hz, and 50 Hz. In addition to the shaft speed variation, varying loading conditions were added at the output shaft of the gearbox: 0%, 25%, 50%, and 75% of the maximum torque of the PGB. From each fault seeded PGBs, a total of 1,840 samples of one second AE data were collected (overall 7,360 samples for all fault types). After switching one gearbox to another, AE sensors were mounted in the same location on the PGB to preserve the experimental consistency.

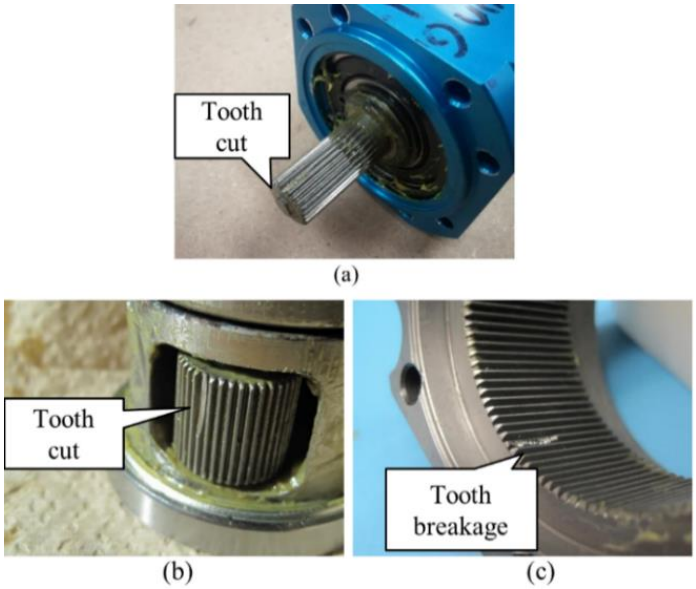

Figure 18. Seeded faults (a) sun gear fault, (b) planet gear fault, and (c) ring gear fault.

C. Validation Results

Upon examining the frequency spectrums of AE signals, the fundamental fault frequencies could not be identified. All of the AE signals were acquired using heterodyne based DAQ and processed using EMD. The first four IMF components were then summed using Equation (27) to compute the CIs. Among all of the CIs, FM0 showed 95% statistical separation for the sun gear fault, RMS displayed 100% statistical separation for the planet gear fault, and Welch CF, Welch EO KT, and Welch EO SK showed 100% statistical separation for the ring gear fault, respectively. Provided in Table VII is the summary of the statistically separable CIs. In addition to the result

from the proposed method, the conventional vibratory analysis results using TSA and enveloping in (Yoon *et. al.*, 2015) are provided for a comparison purpose. Note that the vibratory analysis results in this paper were obtained using the same PGB test rig and a commercially available wind turbine DAQ system. From Table VII, one can see that the AE based methods provide better fault separation performance than the vibration based methods.

TABLE XII

STATISTICAL SEPARATION OF EACH CIS FOR PGB FAULT ISOLATION

	Sun fault	**Planet fault**	**Ring**
Vibration Sensor 1 (sampling rate: 6104 Hz; sampling time: 40 sec)			
TSA	-	≥80%: P2P	-
Enveloping-TSA	-	≥80%: P2P	≥80%: RMS and P2P
Vibration Sensor 2 (sampling rate: 24414 Hz; sampling time: 20 sec)			
TSA	≥80%: Res RMS, Res P2P, GDF	-	≥90%: GDF
Enveloping-TSA	≥80%: Res RMS, Res P2P, GDF	≥80%: RMS, Res RMS, Res P2P	-
AE analysis w/ the proposed method (sampling fate: 100kHz; sampling time 1 sec)			
Heterodyned AE - EMD	≥90%: FM0	100%: RMS	100%: Welch CF, Welch EO KT, and Welch EO SK
	≥80%: KT, CF,EO P2P, EO KT, EO SK, and Welch CF	≥90%: FM0, NB RMS, NB P2P, Welch EO RMS, and Welch EO P2P	≥90%: Welch RMS, Welch KT, and Welch SK
		≥80%: KT, AM RMS, AM P2P, Welch RMS, Welch KT, Welch P2P, Welch CF, and Welch SK	≥80%: P2P, Welch EO RMS, Welch EO P2P, and Welch EO CF

Figure 19 to Figure 21 present the CIs that could effectively separate the healthy gear from the sun, planet, and ring gear faults with error bars (averaged CI values with 95% confidence intervals) under 4 loading conditions: 0% loading, 25% loading, 50% loading, and 75% loading. Under each loading condition, CI values for the following 4 shaft speed are displayed: 10 Hz, 20 Hz, 30 Hz, 40 Hz, and 50 Hz.

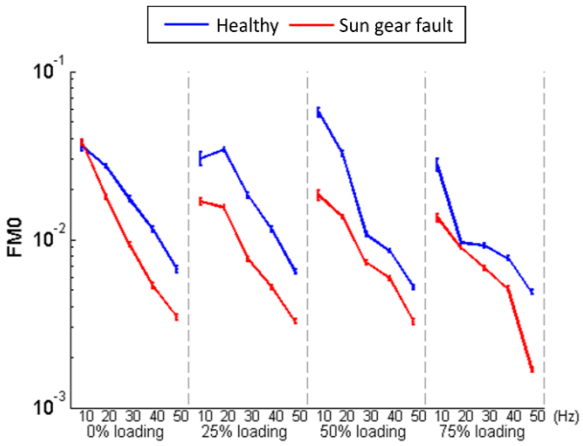

Figure 19. Sun gear fault detecting CI: FM0.

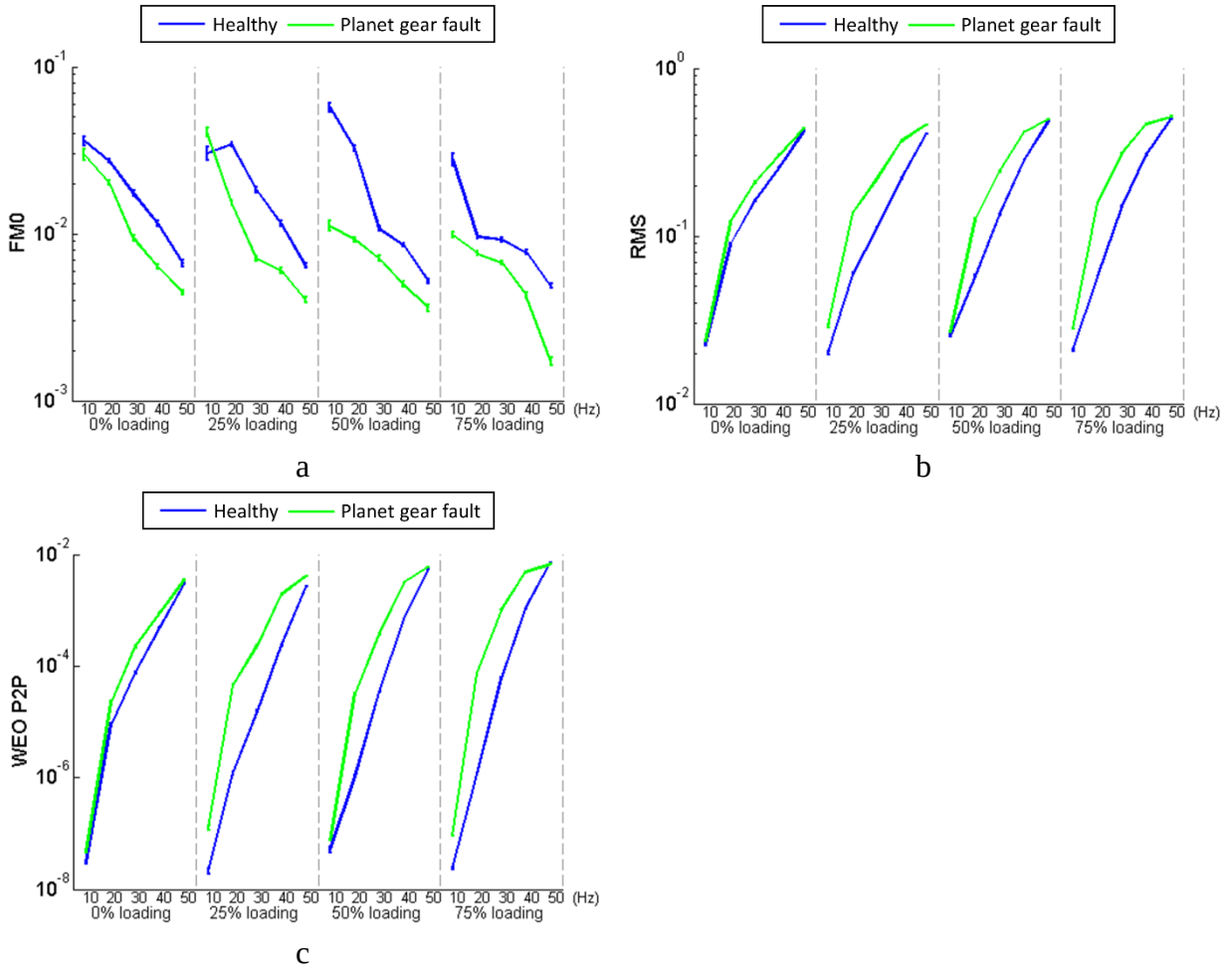

Figure 20. Planet gear fault detecting CIs: (a) FM0, (b) RMS, and (c) WEO P2P.

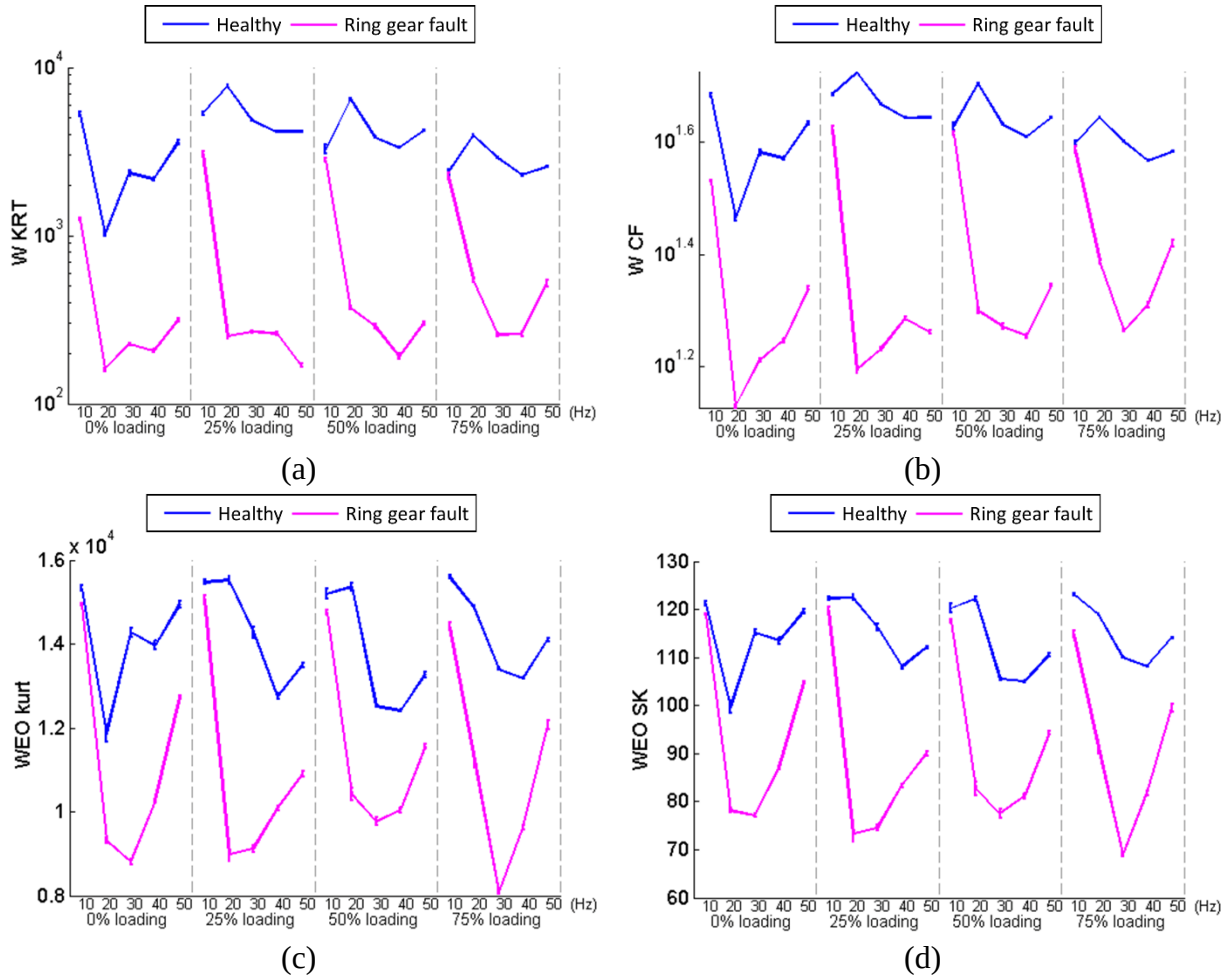

Figure 21. Ring gear fault detecting CIs: (a) Welch KT, (b) Welch CF, (c) Welch EO KT, and (d) Welch EO SK.

CIs were further utilized to classify the faults (*e.g.* sun, planet, ring, or healthy) using three classifiers: KNN, BP, and LAMSTAR. In TABLE XIII through TABLE XIV, the diagnostic results using the three classifiers with both the single CIs and combination of CIs are presented. For any single CIs and CI combinations, the operational parameter of loading condition and shaft rotating speed were included. Out of 7360 samples, 70% of the data were randomly chosen and utilized for training and the remaining 30% of data were used for validation. In order to provide fault diagnostic performance statistically, all classifiers were run 50 times with random sampling

and the average error rates (% of error) were computed. The error rate is defined as the percentage of misclassified samples in validation.

The fault diagnostic results using the three classifiers with individual CIs as inputs are provided in TABLE XIII.

TABLE XIII

PGB FAULT DIAGNOSTIC RESULTS USING INDIVIDUAL CIS

	CI: FM0			**CI: RMS**		
Classifier	KNN (*k*=15)	BP (*N*=40)	LAMSTAR	KNN (*k*=15)	BP (*N*=40)	LAMSTAR
Healthy	33.45	31.78	41.93	20.46	38.7	25.18
Sun gear fault	44.84	52.88	60.68	9.62	29.2	21.25
Planet gear fault	43.14	40.04	54.45	6.28	3.32	26.49
Ring gear fault	35.70	36.88	49.22	13.35	29.62	30.16
Overall	39.28	40.48	51.57	12.43	25.24	25.77
	CI: Welch CF			**CI: Welch EO KT**		
Classifier	KNN (*k*=15)	BP (*N*=40)	LAMSTAR	KNN (*k*=4)	BP (*N*=40)	LAMSTAR
Healthy	9.21	10.98	16.81	38.63	18.76	17.59
Sun gear fault	5.63	7.62	14.47	21.83	13.86	16.97
Planet gear fault	8.91	7.32	15.67	43.64	23.64	25.97
Ring gear fault	7.43	24.04	13.27	16.79	23.28	25.75
Overall	7.79	12.54	15.06	30.22	19.9	21.57
	CI: Welch EO SK					
Classifier	KNN (*k*=15)	BP (*N*=40)	LAMSTAR			
Healthy	17.09	16.58	15.88			
Sun gear fault	10.01	10.86	24.18			
Planet gear fault	18.02	21.12	26.60			
Ring gear fault	11.27	23.12	22.14			
Overall	14.10	17.92	22.20			

* Note: *k* is the search radius for a majority vote of its neighbors in KNN; *N* is the number of neurons in the hidden layer in BP network

As shown, for all three classifiers, none of the single CIs provides an acceptable level of diagnostic performance although each CIs display statistical separation capability for a particular fault type as shown in Table VII. Thus, two combinations of CIs were generated. In the first CI combination, the CIs showing the highest statistical separation (*i.e.* ≥90% for sun gear fault, 100% for planet gear and ring gear faults) were grouped. In the second CI combination, the CIs showing over 80% statistical separation were added to the first combination (*i.e.* ≥ 80% for sun gear fault,

≥ 90% for planet gear and ring gear faults). The fault diagnostic results using those generated CI combinations are provided in TABLE XIV.

TABLE XIV

PGB DIAGNOSTIC RESULTS USING CI COMBINATION

1st CI combination: FM0, RMS, W CF, WEO KT, and WEO SK			
Classifier	KNN (*k*=4)	BP (*N*=40)	LAMSTAR
Healthy	17.25	5.96	0.29
Sun gear fault	16.16	5.92	0.27
Planet gear fault	24.84	5.85	0.51
Ring gear fault	10.74	6.37	0.58
Overall	17.25	6.04	0.41
2nd CI combination: KT, CF, FM0, RMS, EO P2P, EO KT, EO SK, NB RMS, NB P2P, W RMS, W KT, W CF, W SK, WEO RMS, WEO P2P, WEO KT, and WEO SK			
Type of fault	KNN (*k*=4)	BP (*N*=40)	LAMSTAR
Healthy	6.41	6.59	4.6
Sun gear fault	7.19	6.63	6.52
Planet gear fault	8.59	6.64	6.11
Ring gear fault	5.62	7.17	8.66
Overall	6.95	6.78	6.47

* Note: *k* is the search radius for a majority vote of its neighbors in KNN; *N* is the number of neurons in the hidden layer in BP network

Seen from TABLE XIV, KNN achieved 7% error rate when the 2nd CI combination was used. The search radius of k was investigated for $k = 3{\sim}15$ range and the minimal classification error rate of 7% was achieved when $k = 4$. For BP network, different numbers of hidden neurons (N) were investigated and the best performance was achieved when the BP network with $N = 40$ was used. Although BP network achieved less than 1% overall diagnostic error rate when the local minima convergence is ignored, it should be noted that the occurrence of local minima convergence was around 12~16% out of 50 total runs. When BP network was converged to a local minima, the error rate in diagnostics drastically increases up to 25~75%. Thus, taking the local minima cases into consideration, the average diagnostic error rate increases to 7% and is similar to that of KNN achieved with the second CI combination. As described in Section 2.4, LAMSTAR network is not sensitive to the local minima issue and achieved the lowest diagnostic error rate of

≤1%. It is, however, noted that LAMSTAR network achieved the best diagnostic result when a minimal but carefully selected CI combination with the highest statistical separation was used.

D. Conclusions

In this Chapter, a new PGB fault diagnostic method using AE sensors was presented. The presented method combines a heterodyne based AE DAQ system, EMD based AE signal analysis method, computation of CIs, and data mining based PGB fault diagnosis. The heterodyne technique was hardware implemented to sample AE signals at a rate comparable to vibration based methodologies. The presented method is considered the first reported effort in using AE sensor for PGB fault diagnosis and has been validated using seeded gear tooth cut and breakage faults on all PGB gears: sun gear, planetary gear, and ring gear, which has not been presented in the literature. First, the sampled AE signals were processed using EMD to extract PGB fault features and compute CIs. The CIs were grouped into two combination sets according to the level of statistical separation followed by training three supervised learning algorithms (*i.e.* classifier): KNN, BP, and LAMSTAR. Each classifier was run 50 times to obtain the results. The validation results have shown: (1) An error rate of 7% was achieved using KNN when the second set of CI combination was used; (2) An average diagnostic error rate of 7% was achieved using the BP algorithm. However, a local minima convergence was observed at a rate of 12~16% out of 50 runs; (3) The LAMSTAR network displayed less sensitivity to the local minima issue. The best overall diagnostic error rate of about 0.5% was achieved using the LAMSTAR network when the first CI combination set was used.

VI. ON THE USE A SINGLE PIEZOELECTRIC STRAIN SENSOR FOR WIND TURBINE PLANETARY GEARBOX FAULT DIAGNOSIS

Planetary gearboxes are widely used in the drivetrain of wind turbines. Any planetary gearbox failure could lead to breakdown of the whole drivetrain and major loss of wind turbines. Therefore, planetary gearbox fault diagnosis is important to reducing the downtime and maintenance cost and improving the reliability and lifespan of wind turbines. Planetary gearbox fault diagnosis has been done mostly through vibration analysis over the past years.

In a recent paper, Feng and Zuo (2013) pointed out that vibration signals theoretically have the amplitude modulation effect caused by time variant vibration transfer paths due to the unique dynamic structure of rotating planet gears. One attractive solution to this problem is to use alternative sensor signals that have less sensitivity to the AM effect for PGB fault diagnosis and prognosis. They have shown the effectiveness of torsional vibration analysis for PGB fault diagnosis using a torque sensor. The frequency characteristics of torsional vibration were shown to be solely sensitive to the AM and FM effects caused by gear faults under constant torque on input and output shafts. Kiddy *et al.* (2011) used fiber optic strain signals for PGB fault diagnosis and showed a close relationship between strain measurement and torque changes. Although promising, the research reported in the literature on using less AM effect sensitive signals for PGB fault diagnosis has certain limitations. The torque sensors used by Feng and Zuo (2013) are more expensive than vibration and strain sensors and require special installation. In another paper, a

fiber optic strain sensor array used by Kiddy *et al*. (2011) had to be embedded in the PGB in order to be effective. In their study, fiber optic strain sensors could only be sampled at a maximum sampling rate up to 1 kHz, which limits its coverage on shaft speed above 2060 rpm. Also, the strain signals were analyzed the same way as vibration signals. Fiber optic sensor signals were analyzed using the vibration separation technique after low frequency components were filtered out.

To overcome the above mentioned challenges in developing effective PGB fault diagnosis capability, a research investigation on wind turbine planetary gearbox fault diagnosis via strain sensor signal analysis has been conducted and is reported in this Chapter. The PE strain sensor based planetary gearbox fault diagnosis method can be considered as an attractive alternative to traditional vibration analysis based approaches because the PE strain sensor signals are closely correlated to torsional vibration, which is less sensitive to the amplitude modulation effect caused by rotating vibration transfer path. Also, compared to the conventional strain gauge sensors and accelerometers, the PE strain sensors have certain advantages that could be summarized as follows: (1) ability to measure the first derivative of physical deformation, (2) high linearity and sensitivity from their superior noise immunity as compared to differentiated sensing performance of conventional strain sensors (Banaszak (2001); Lee and O'Sullivan (1991)), (3) high frequency range (Jiang *et al.*(2013)), (4) space-efficiency without a structural change on the measuring target (Kon *et al*. (2007)), and (5) negligible high temperature effect on the measurement output (Jiang *et al.*(2013), and Sirohi and Chopra (2000)). The aforementioned benefits allow for PE strain sensors to potentially have greater sensing resolution and accuracy. Thus, it is potentially easy and effective to diagnose planetary gearbox faults via stain sensor signal analysis. In this Chapter, a new method using a single piezoelectric strain sensor for planetary gearbox fault diagnosis is

presented. The method is validated on a set of seeded localized faults on all gears: sun gear, planetary gear, and ring gear. The validation results have showed a satisfactory planetary gearbox fault diagnostic performance using strain sensor signal analysis.

The remainder of the Chapter is organized as follows. Section A gives a detailed explanation of the presented methodology. In Section B, the experiments setup to validate the presented methodology and the seeded fault tests on a laboratory PGB test rig are explained. Section C presents the PGB fault diagnostic results from the seeded fault tests. Finally, Section D concludes the Chapter.

A. Methodology

An overview of the proposed methodology is provided in Figure 22. First, the PE strain sensor signals and tachometer signals are digitized simultaneously. Then, the low-pass filter is applied to the raw PE strain signal. As reported in Wachel and Szenasi (1993), after considering the torsional natural frequency and its higher harmonics at varied shaft speeds, it was concluded that the response range of torsional vibration is less than 1 kHz and doesn't exceed that of radial vibration. Also, in vibration analysis, a universal low-pass filter with a cutoff frequency of 20 kHz or less is commonly used to attenuate the signal of interest. Thus, a low-pass filter with a cut-off frequency of 20 kHz was used in this Chapter since there is no similar research previously available. Using the tachometer signals, the TSA signal, residual signals, and other input signals are computed. Lastly, the CIs are computed.

This Chapter will focus on the localized gear faults, while neglecting the faults of any other components such as shafts or bearings. The major components of the methodology are explained in the following two sections. Section 1 provides a brief review of TSA and the computation of CIs used for planetary gearbox fault diagnosis is explained in Section 2.

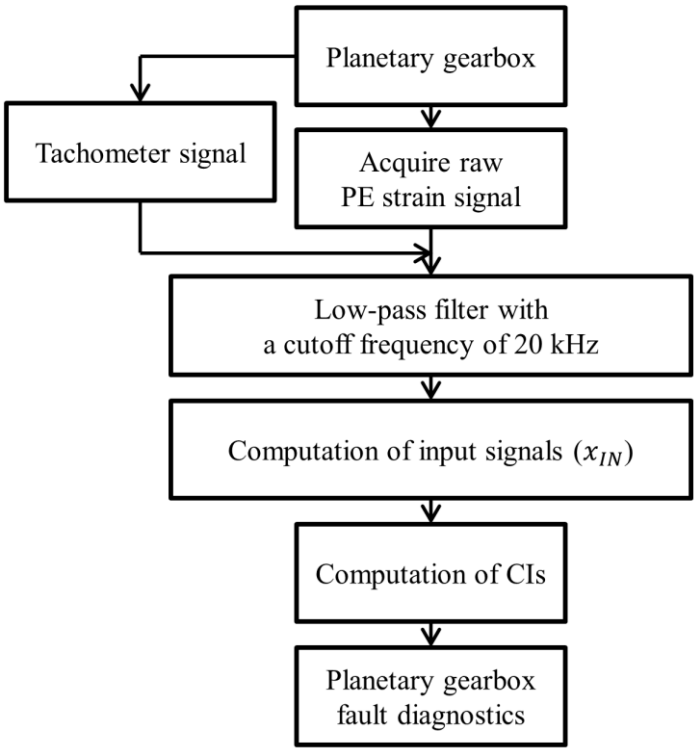

Figure 22.Overview of the methodology.

1. Time Synchronous Average

TSA is one of the most widely utilized signal processing techniques to extract a periodic waveform from noisy signals of rotating machines. The underlying idea of TSA is to obtain a periodically repeated waveform of interest over N number of revolutions. Theoretically, when a rotating machine is running at a constant speed, the periodic waveform is intensified while any noises are suppressed with a noise reduction rate of $\frac{1}{\sqrt{N}}$. Consider a signal $x(t)$ composed of a periodic signal $y(t)$ with known period T_R and additive noise$e(t)$:

$$x(t) = y(t) + e(t) \tag{31}$$

Assuming the total number of N observed periods, the TSA of $x(t)$ can be expressed as:

$$x_{TSA} = \frac{1}{N}\sum_{r=0}^{N-1} x(t - rT_R) \tag{32}$$

As $N \to \infty$, the TSA signal x_{TSA} approaches to $y(t)$. More details about TSA could be found in (Braun, 1975; McFadden, 1987; and Bechhoefer and Kingsley, 2009).

Basically, TSA chops up the raw sensor signal into multiple single revolution signals. Then, each of the revolution signals are resampled (via stretching or shrinking) to have the same number of sample points in one revolution. Then, the final periodic signal is obtained by averaging the resampled signals. After TSA is computed, any kind of fault diagnostic condition indicators can be evaluated. Even though successful TSA applications to other sensor analysis such as AE signals (Qu *et al.*, 2013a; 2014), application of TSA to PE strain signal processing for PGB fault diagnosis has not yet been reported.

2. PE Strain Sensor Based Fault Feature Extraction

CIs computed using vibration signals have been used effectively for gear fault diagnosis in real applications such as condition monitoring systems installed in helicopters and wind turbines (Sheng, 2012). In this Chapter, the CIs reported effective for gear fault diagnosis using vibration signals for wind turbine applications will be computed using the PE strain sensor signals. TABLE XV provides the definitions of the CIs investigated for PGB fault diagnosis.

The CIs can be defined into five general types: root mean square (*RMS*), peak to peak (*P2P*), skewness (*SK*), kurtosis (*KT*), and crest factor (*CF*). Each type of CI can be computed using different input signals. In addition to TSA signals, other types of input signals can be generated: residual, narrow band (NB), AM, and FM. Residual is a TSA signal with the primary meshing and shaft components being removed. The energy operator (EO) (Teager, 1992) is defined as the residual of the autocorrelation function as following:

$$x_{EO,i-1} = x_{TSA,i}^2 - \left(x_{TSA,i-1} \cdot x_{TSA,i+1}\right), \qquad for\ i = 2, 3, \dots, N-1 \tag{33}$$

where$x_{EO,i}$ is the i^{th} element of EO data; $x_{TSA,i}$ is the i^{th} element of x_{TSA}.The NB filtered signal, x_{NB}, could be obtained by filtering out all tones except those of the gear mesh and the characteristic frequencies. In this Chapter, the characteristic frequencies are the sun gear fault frequency, planet gear fault frequency, and ring gear fault frequency, respectively. Finally, AM and FM CIs are obtained by AM analysis and FM analysis of x_{NB}. AM and FM signals are the absolute value and the derivative of the angle of the Hilbert transform of x_{NB}, respectively. For more details of NB, AM, and FM, please see (Sheng, 2012).

TABLE XV

THE DEFINITIONS OF THE CIS FOR THE PE STRAIN BASED PGB DIAGNOSIS

		Input Signal (x_{IN})					
CI	Formula	TSA: Time synchronous averaged signal (x_{TSA})	Residual: TSA signal with the primary meshing and shaft components removed (x_{RES})	EO: residual of the autocorrelation function (x_{EO})	NB: Narrow band pass filtered (x_{NB})	AM: Amplitude modulation of NB filtered signal $(AM(x_{NB}))$	FM: Frequency modulation of NB filtered signal $(FM(x_{NB}))$
Root mean square (*RMS*)	$RMS(x_{IN}) = \sqrt{1/N \sum_{i=1}^{N} x_i^2}$	$RMS(x_{IN})$: measures the energy evolution of a signal.					
Peak to peak (*P2P*)	$P2P(x_{IN}) = \frac{(\max_{1\le i\le N}(x_i) - \min_{1\le i\le N}(x_i))}{2}$	$P2P(x_{IN})$: measures the maximum difference within the data range.					
Skewness (*SK*)	$SK(x_{IN}) = \frac{1/N \sum_{i=1}^{N}(x_i - \bar{x})^3}{\left[\sqrt{1/N \sum_{i=1}^{N}(x_i - \bar{x})^2}\right]^3}$	$SK(x_{IN})$: measures the asymmetry of the data about its mean value. A negative *SK* value and positive *SK* value imply the data have a longer or fatter left tail and the data have a longer or fatter right tail, respectively.					
Kurtosis (*KT*)	$KT(x_{IN}) = \frac{N \sum_{i=1}^{N}(x_i - \bar{x})^4}{\left[\sum_{i=1}^{N}(x_i - \bar{x})^2\right]^2}$	$KT(x_{IN})$: measures the peakedness, smoothness, and the heaviness of tail in a data set.					
Crest factor (*CF*)	$CF(x_{IN}) = \frac{P2P(x_{IN})}{RMS(x_{IN})}$	$CF(x_{IN})$: measures the ratio between $P2P(x_{IN})$ and $RMS(x_{IN})$ to describe how extreme the peaks are in a waveform.					

Note: x_i is i^{th} element of the input datax_{IN}; N is the length of the input datax_{IN}; max(·) returns the maximal element of input datax_{IN}; min(·) returns the minimal element of input datax_{IN}; $\bar{x}$ is a mean value of the input datax_{IN} defined as $\sum_{i=1}^{N} x_i / N$.

B. Experimental Setup

This section covers the experimental setup used to validate the PE strain sensor based planetary gearbox fault diagnostic technique.

1. The DAQ System for the PE Strain Sensor

Figure 23displays the PGB test rig used to collect the PE strain sensor data under varying gear health and operating conditions. The DAQ system includes a National Instruments (NI)' DAQ board with a maximum analog input sampling rate of 1.25 MHz, a PE strain sensor, and a signal conditioner with an unity gain from PCB Piezotronics. A Hall effect sensor was used as the tachometer paired with a toothed wheel mounted on the motor shaft. The PE strain sensor was glued on the housing of the ring gear as shown in Figure 23(c).

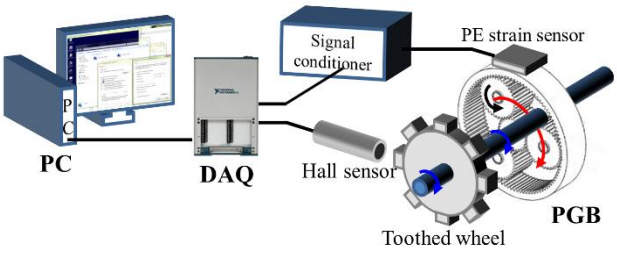

(a)

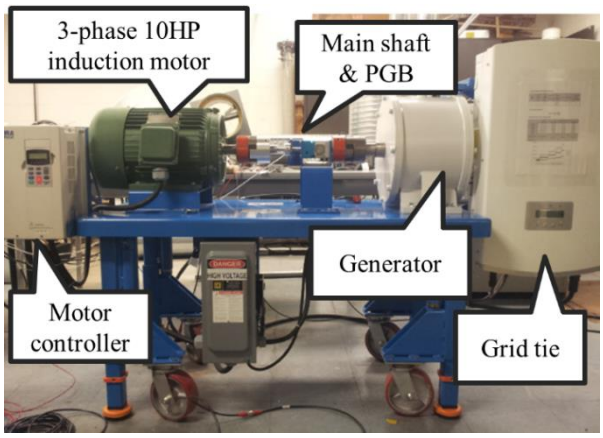

(b)

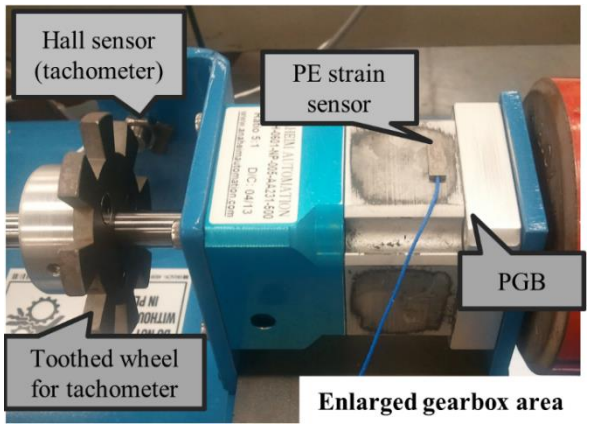

(c)

Figure 23. The PGB test rig for wind turbine simulator: (a) DAQ system connection, (b) the front view of the PGB test rig, (c) the enlarged view on the input shaft and sensor location.

2. Seeded Gear Fault Tests

This section covers the experimental setup used to validate the PE strain sensor based PGB fault diagnostic technique. Three types of PGB faults were created: sun gear tooth fault, planet gear tooth fault, and ring gear tooth fault. Each type of the gear fault was created by artificially damaging a tooth on a sun gear, planetary gear, and ring gear, respectively (see Figure 24).

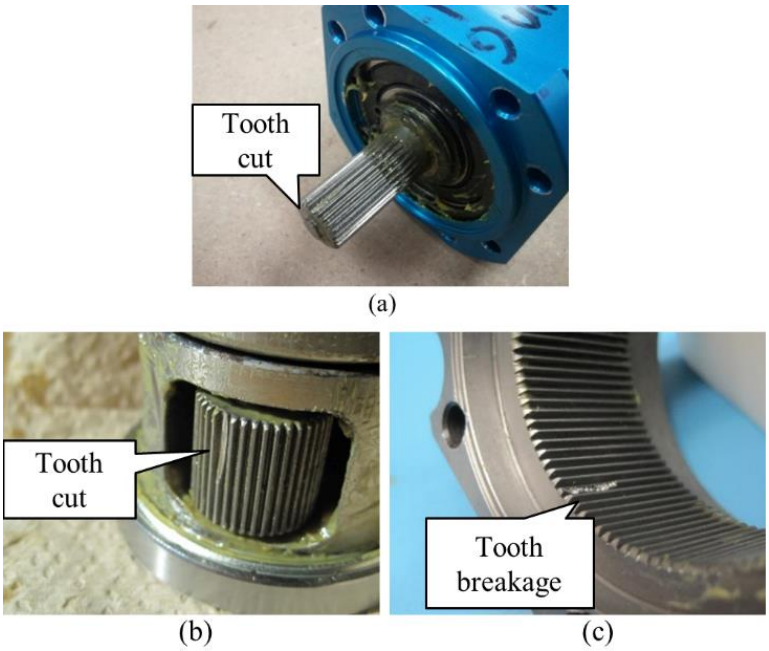

Figure 24. Seeded faults: (a) sun gear fault, (b) planet gear fault, (c) ring gear fault.

During the seeded fault tests, PE strain sensor signals were collected with a sampling rate of 100 kHz. The tachometer signals were simultaneously recorded along with the PE strain signals to get revolution stamps. Both the healthy gearbox and the gearboxes with seeded faults were tested at five different input shaft speeds: 10 Hz, 20 Hz, 30 Hz, 40 Hz, and 50 Hz. At each speed, five samples were collected. In addition to the shaft speed variation, varying loading conditions were applied at the output shaft of the gearbox: 0%, 25%, 50%, and 75% of the maximum torque of the planetary gearbox. At each loading condition, 25 samples (five samples per shaft speed for

five varying speeds) were taken. In addition, the PE strain sensors were carefully mounted at the same location of the gearbox for each data collection.

TABLE XVI

PE STRAIN SENSOR DAQ SETTING PARAMETERS.

	PE strain sensor	Tachometer
Sensor	ICP Piezoelectric strain sensor with titanium housing	Hall effect sensor
Manufacturer	PCB Piezotronics	Sensoronix
Signal conditioner	Unity gain	-
Sampling rate	100k (Hz)	100k (Hz)
Sample recording time	10 Hz – 30 sec 20 Hz – 24 sec 30 Hz – 16 sec 40 Hz – 12 sec 50 Hz – 10 sec	-

C. Validation Results

The validation results for the seeded fault tests conducted on the planetary gearbox test rig are provided in this section. Samples of the raw PE strain signals and their spectra are provided in Figure 25. Upon examining the frequency spectrums, the fundamental fault frequencies could not be identified. Thus, the calculated fault frequencies shown in TABLE III could not be used as the basis for band pass filter selection. Following the filter band optimization procedure in Van Hecke (2014a), Shannon entropy was computed on the healthy PGB signals after the implementation of different filter bands. Figure 26 shows an example of this technique applied to a healthy PGB signal at shaft speed of 50Hz. The highest level of entropy was observed with the use of a 0 ~ 20 kHz for all the filter bands. Therefore, a low-pass filter with a cutoff frequency of 20 kHz was selected and utilized for the results presented in this Chapter.

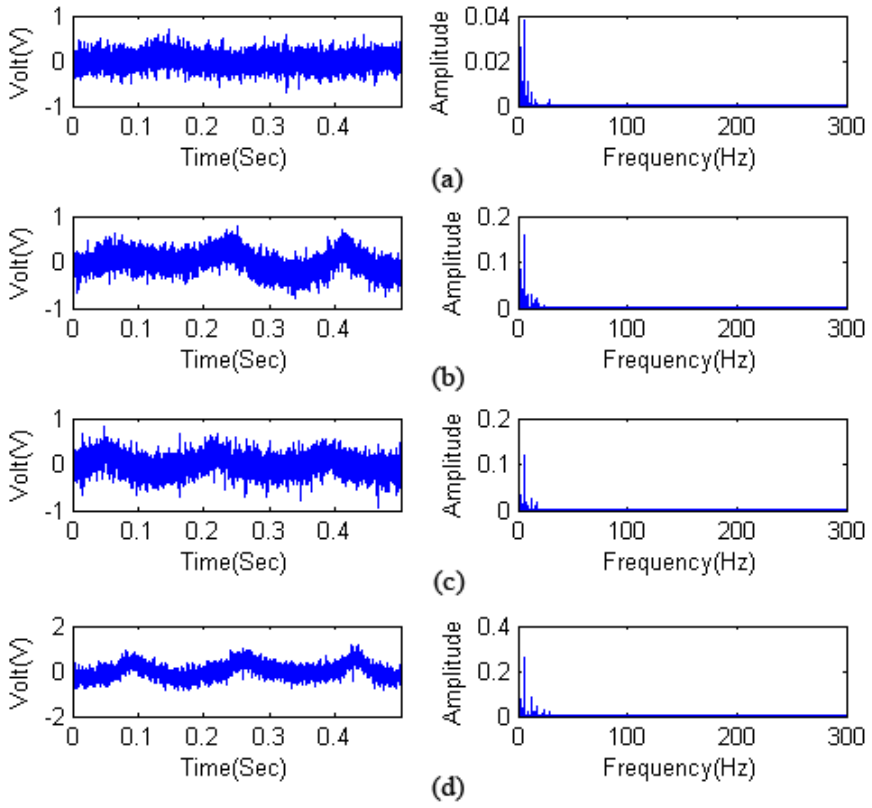

Figure 25. Sample raw PE strain sensor signals and their spectra at 50% output loading and 10Hz input shaft speed: (a)healthy, (b) sun gear fault, (c) planet gear fault, and (d) ring gear fault.

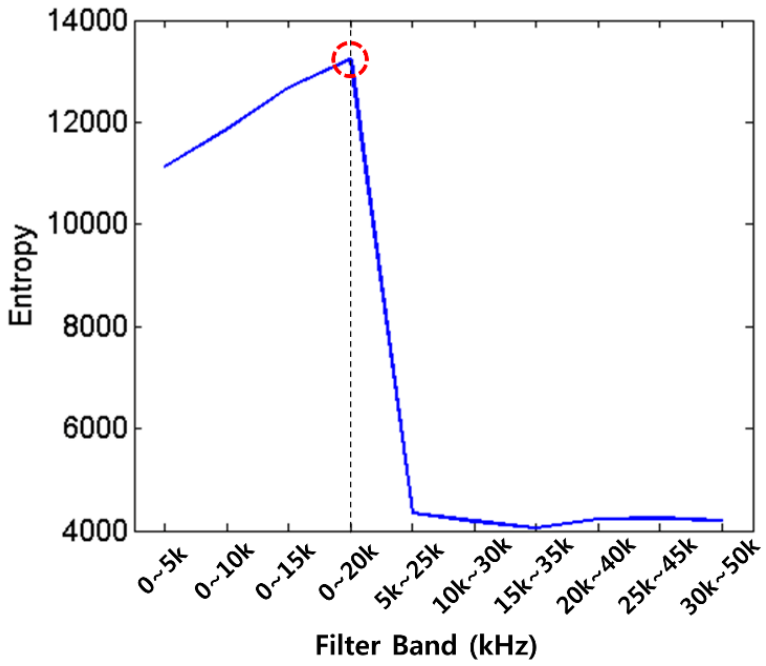

Figure 26. Entropy of band pass filtered healthy PGB signal at a shaft speed of 50Hz.

After the TSA signals were obtained, then all of the CIs described in Section A-2 were computed. Among the computed CIs, four of them were found effective: TSA RMS, TSA P2P, residual RMS, and residual P2P. Figure 27shows the TSA RMS plots for different gearbox health conditions at different shaft speeds and loading conditions. As one can see from the figure, by using TSA RMS alone, the three gear faults can be clearly separated. As the loading increases, the separation of the gear faults gets better. Also, by using TSA RMS alone, all the three gear faults can be clearly separated from the healthy condition. The detectability of the gear faults gets better as the loading increases. For all of the four gearbox conditions, TSA RMS remains relatively stationary within the same loading condition regardless the change of the shaft speed. This also shows that the TSA RMS is heavily correlated to the torque level of the gearbox. The vertical bar for each data point shown in Figure 27 represents a 95% confidence interval from the TSA RMS statistics.

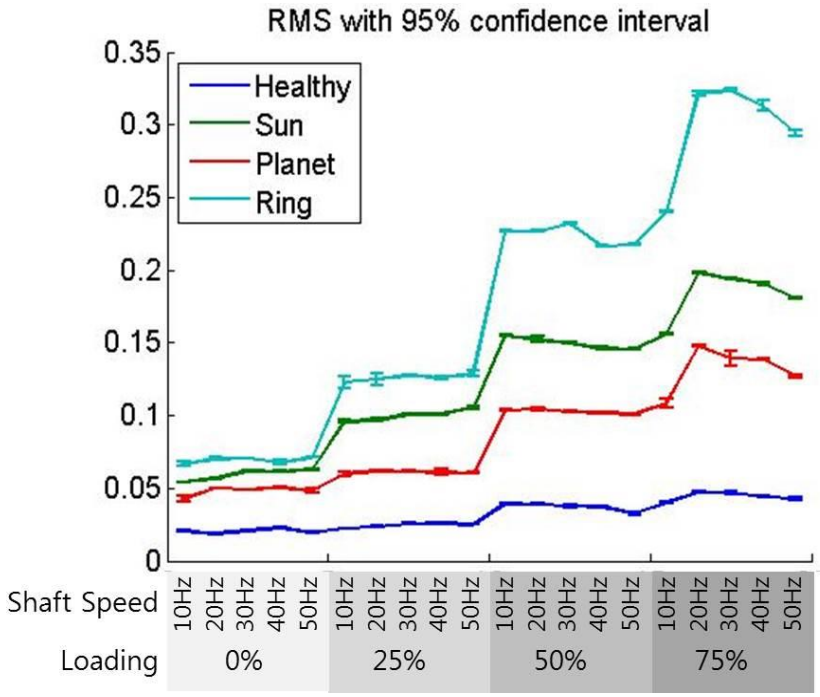

Figure 27. TSA RMS plot.

In order to check the statistical significance of the gear fault separation using TSA RMS, an analysis of variance (ANOVA) test was conducted using the TSA RMS data. In this test, it was assumed that the shaft speed has no effect on TSA RMS within a loading condition. The following hypotheses were established based on aforementioned assumptions:

$$\begin{gathered} \mathrm{H}_0: \mu_1 = \mu_2 = \mu_3 = \mu_4 \\ \mathrm{H}_1: \text{at least one} \mu_i \neq \mu_j \\ (\text{for } i, j = 1,2,3, \text{and } 4;\ i \neq j) \end{gathered} \tag{34}$$

where μ_i is mean CI value of the i^{th} gear health condition at a fixed loading condition, i = 1, 2, 3, and 4 represents healthy gearbox, sun gear fault, planet gear fault, and ring gear fault, respectively. Displayed in

TABLE **XVII** is the summary of ANOVA results with a 99% confidence level.

TABLE XVII

SUMMARY OF ANOVA RESULTS FOR TSA RMS

Loading	Source	DF	SS	MS	*F*	*P*
0%	Factor	3	0.0334141	0.0111380	1605.12	0.000
	Error	96	0.0006662	0.0000069		
	Total	99	0.0340802			
25%	Factor	3	0.1481272	0.0493757	8261.04	0.000
	Error	96	0.0005738	0.0000060		
	Total	99	0.1487010			
50%	Factor	3	0.4641124	0.1547041	10614.42	0.000
	Error	96	0.0013992	0.0000146		
	Total	99	0.4655116			
75%	Factor	3	0.845794	0.281931	781.55	0.000
	Error	96	0.034630	0.000361		
	Total	99	0.880424			

Note that in

TABLE **XVII**, notations *DF, SS, MS, F,* and *P* refer to the degree of freedom, the sum of squares, the mean square, the *F*-test value, and the *p*-value, respectively. These notations will be used in the remaining tables in related to ANOVA test. From the table, the *P*-values for all loading conditions are 0.000. With a 99% confidence level, the null hypotheses should be rejected ($\alpha = 0.01 > 0$). Therefore, it is safe to say that the separation of all the gear faults tested using TSA RMS is statistically significant at all loading conditions.

The results for the other three CIs: TSA P2P, residual RMS, and residual P2P are presented in the same way as TSA RMS in the following. Their associated plots of the CIs are provided in Figure 28 to Figure 30 and the ANOVA results in TABLE XVIII to TABLE XX, respectively. Similar results like TSA RMS can be observed for the other two CIs: TSA P2P and residual RMS. However, the diagnostic performance of these two CIs at the 0% loading condition is not as good as TSA RMS. A clear diagnosis of the gear faults can be observed at 25%, 50%, and 75% loading conditions. When the loading level reaches 25% or above, TSA P2P and residual RMS can be ranked like TSA RMS as the following order: ring gear fault → planet gear fault → sun gear fault → healthy gear. For residual P2P, a clear diagnosis of the gear faults can be observed only when the loading level reaches to 50% or above.Note that in TABLE XVIII to TABLE XX, even under the low loading conditions, the null hypothesis in (25) is rejected. This is because all the faulty CIs are significantly different from the healthy CIs even though the difference among the faulty CIs is not statistically significant. Also, note that for the four effective CIs, some of them have shown less sensitive to the change of the speed under the same loading condition, for example, TSA RMS. Others may have shown more sensitive to the change of the speed under the same loading condition, for example, Residual P2P. However, all those CIs increase their values as the loading level increases.

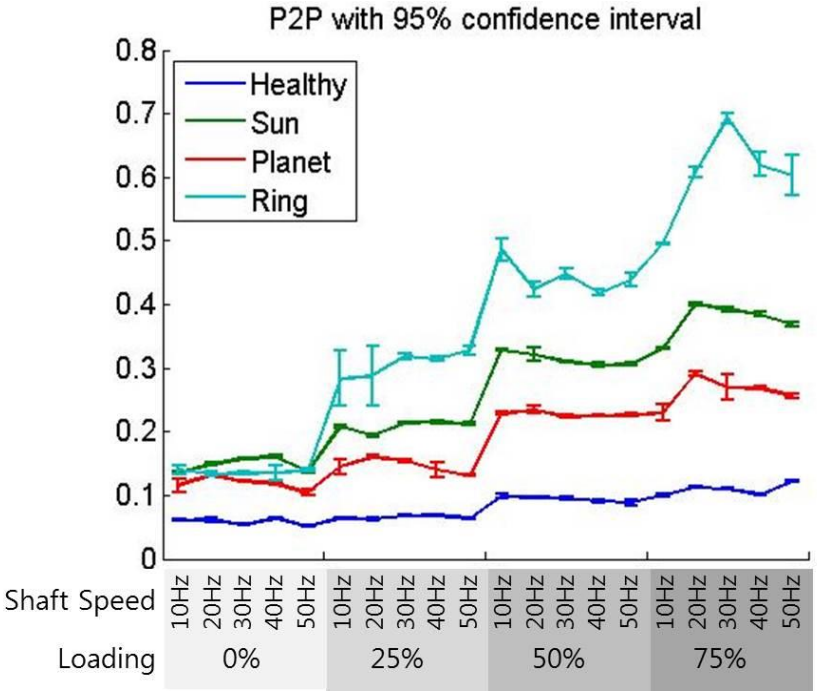

Figure 28. TSA P2P plot.

TABLE XVIII

SUMMARY OF ANOVA RESULTS FOR TSA P2P

Loading	Source	DF	SS	MS	*F*	*P*
0%	Factor	3	0.1199638	0.0399879	611.06	0.000
	Error	96	0.0062822	0.0000654		
	Total	99	0.1262461			
25%	Factor	3	0.775791	0.258597	1065.47	0.000
	Error	96	0.023300	0.000243		
	Total	99	0.799091			
50%	Factor	3	1.615071	0.538357	2682.91	0.000
	Error	96	0.019264	0.000201		
	Total	99	1.634335			
75%	Factor	3	3.25105	1.08368	787.88	0.000
	Error	96	0.13204	0.00138		
	Total	99	3.38309			

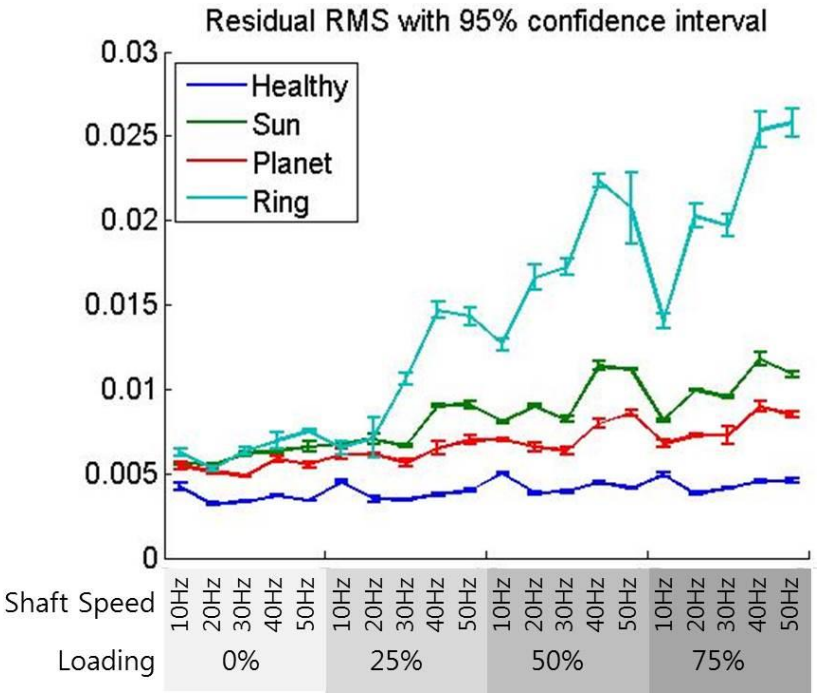

Figure 29. Residual RMS plot.

TABLE XIX

SUMMARY OF ANOVA RESULTS FOR RESIDUAL RMS

Loading	Source	DF	SS	MS	*F*	*P*
0%	Factor	3	0.0001227	0.0000409	147.50	0.000
	Error	96	0.0000266	0.0000003		
	Total	99	0.0001493			
25%	Factor	3	0.0006061	0.0002020	56.46	0.000
	Error	96	0.0003436	0.0000036		
	Total	99	0.0009497			
50%	Factor	3	0.0025676	0.0008559	219.08	0.000
	Error	96	0.0003750	0.0000039		
	Total	99	0.0029427			
75%	Factor	3	0.0038871	0.0012957	233.04	0.000
	Error	96	0.0005337	0.0000056		
	Total	99	0.0044208			

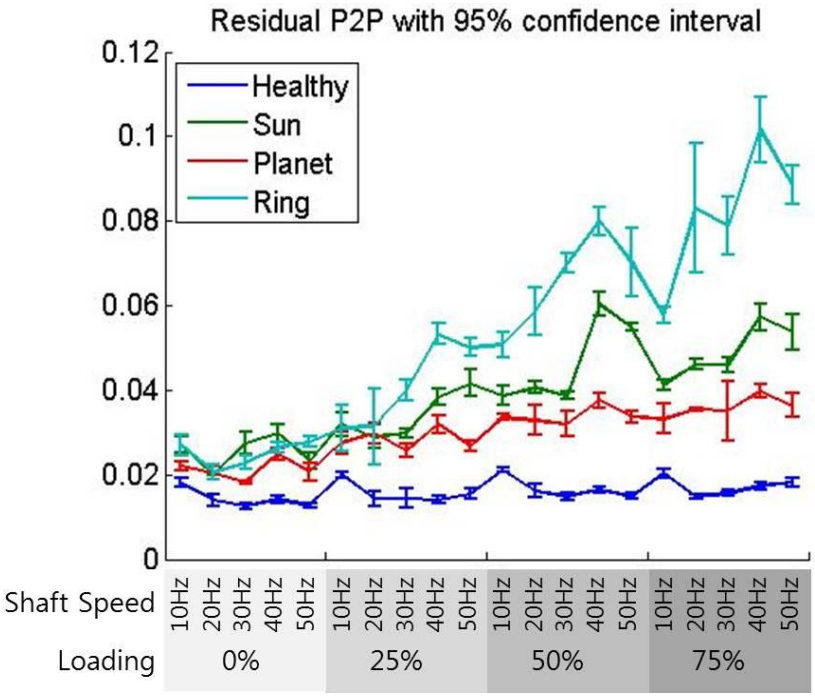

Figure 30. Residual P2P plot.

TABLE XX

SUMMARY OF ANOVA RESULTS FOR RESIDUAL P2P

Loading	Source	DF	SS	MS	*F*	*P*
0%	Factor	3	0.0019954	0.0006651	76.63	0.000
	Error	96	0.0008333	0.0000087		
	Total	99	0.0028287			
25%	Factor	3	0.0087545	0.0029182	79.85	0.000
	Error	96	0.0035084	0.0000365		
	Total	99	0.0122630			
50%	Factor	3	0.0323371	0.0107790	193.51	0.000
	Error	96	0.0053475	0.0000557		
	Total	99	0.0376846			
75%	Factor	3	0.0557005	0.0185668	239.39	0.000
	Error	96	0.0074456	0.0000776		
	Total	99	0.0631462			

D. Conclusions

In this Chapter, a new PE strain sensor based wind turbine PGB fault diagnostic methodology is presented. The presented method was accomplished through a combination of low pass filtering, TSA, and CIs to extract diagnostic features for PGB diagnosis. First, the PE strain sensor signal is low-pass filtered to retain the information related to the gear conditions. Then, the TSA signal is computed to obtain the periodically repeated waveform while white noise is suppressed. The presented method was validated using data collected from seeded fault tests conducted on a planetary gearbox test rig in a laboratory. The validation results have shown that by utilizing the TSA based PE strain sensor signal processing approach, fully separable diagnostic CIs towards all PGB fault types were captured regardless of shaft speed and output shaft loading condition. In summary, the four CIs extracted from PE strain sensor signals: TSA RMS, TSA P2P, residual RMS, and residual P2P effectively differentiate the localized faults such as gear tooth crack and breakage from all gears: sun gear, planetary gear, and ring gear, which has not been presented in the literature. The current PGB diagnostic methods mainly rely on vibration signal analysis. They provide limited fault diagnosis for PGB due to time varying vibration transfer paths. The PE strain sensor based diagnostic technique presented in this Chapter provides an attractive alternative to the current vibration analysis based approach.

VII. COMPARATIVE STUDY

PGB fault diagnosis has been done mostly through vibration analysis over the past years. However, the recent literature reported that there exist alternative diagnostic methods for PGB fault diagnosis which potentially be less sensitive to the vibratory AM effect caused by time variant vibration transfer paths. This Chapter presents a comparative study for PGB fault diagnostics with seeded localized faults using vibration, AE, and PE strain measurements. This is the first known attempt comparing the PGB fault diagnostic performance of all those three sensor analyses. First, the vibration signals were analyzed using the conventional signal processing methods of TSA, SA, enveloping, and etc. The vibration analysis with the Welch's spectral averaging was obtained followed by. Then, the AE analysis was conducted using the heterodyne technique based AE DAQ system, in which AE sampling rate become at a rate compatible to vibration analysis. Lastly, the PE strain analysis method was constructed using the fact that strain sensor signals is closely correlated to torsional vibration, which is insensitive to the vibratory AM effect caused by rotating planet gears and its career. Each sensor signal was further fault feature extracted using the CIs for the drivetrain diagnostic methods, currently used in the wind industry. Machine learning methods were further applied upon necessity. Results have shown that the AE sensor based analysis could give slightly improved results from the accuracy and the reliability stand points. Also, the PE strain analysis based diagnosis could be advantageous than vibration and AE in that it could isolate the faulty components without using any machine learning techniques.

A. Methodology

In addition to the currently available vibration based machinery fault diagnostic methods such as low-pass filtering, TSA, enveloping, and their combinational methods, herein, Welch's SA

based PGB fault diagnostic methods for vibratory analysis, AE sensor, and PE strain sensor based PGB fault diagnostic methods are investigated in a comparative study manner. Validation of the fault diagnostic methods was conducted from the seeded fault tests on a PGB test rig in the laboratory. Before the results are presented, each of the diagnostic methods are reviewed in this section. The overview of each PGB diagnostic methods are diagrammed in Figure 31 through Figure 33.

1. Vibration Based PGB Diagnosis

Although VS method is one of the well-established vibration analysis technique for PGB, VS could not be applicable to this study with the following reasons. First, sun gear fault cannot be detected by the PGB geometry as described in Samuel *et al.* (2004).Second, the vibration sample size is not big enough to apply VS technique. Therefore, in this Chapter, vibration signals were processed for the following four different methods (shown in Figure 31): (a) TSA, (b) enveloping then TSA, (c) TSR followed by Welch's method (*i.e.* SA), (d) TSR, enveloping, then Welch's method. First two methods of (a) and (b) are widely used vibration analysis methods and chosen for comparative results among vibration analyses. The Fast kurtogram was applied to find a universal filter band for each vibration sensor. The presented methods of (c) and (d) combine TSR, enveloping, SA for rotating machinery, fast kurtogram, computation of CIs, or implementation of PGB fault diagnostic classifiers. The details of the implementation can be found in Chapter IV. The overview of the vibration based PGB diagnostic method is diagrammed in Figure 31.

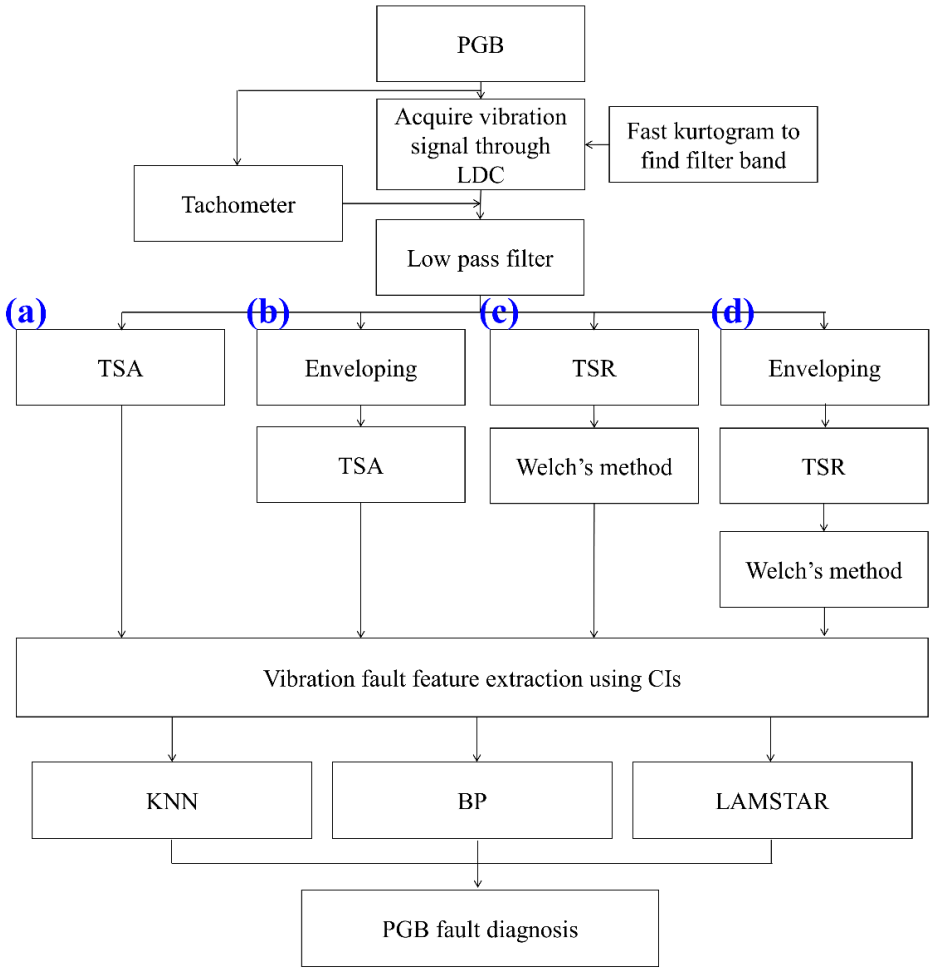

Figure 31. Overview of vibration based PGB fault diagnosis.

2. AE Based PGB Diagnosis

A new AE sensor based PGB fault diagnostic method was presented in the previous Chapters. The presented method comprises a heterodyne based AE DAQ system, EMD based rotating machinery fault diagnostic method, computation of CIs, and data mining based PGB fault classifiers. The details of the implementation can be found in Chapter V. The overview of the AE based PGB diagnostic methods is diagrammed in Figure 32.

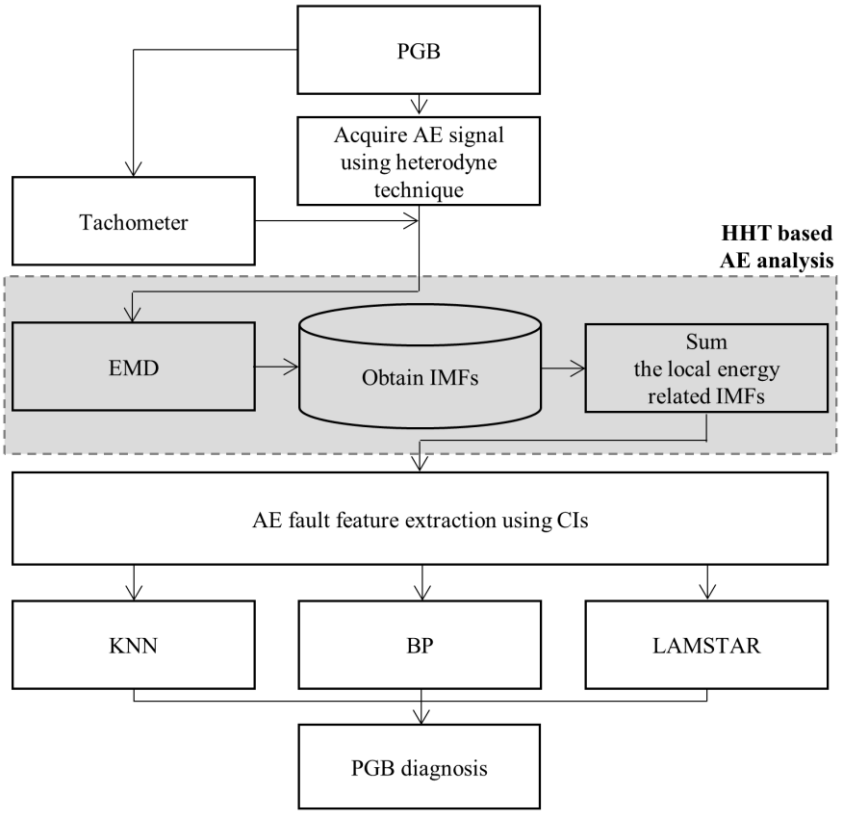

Figure 32. Overview of AE based PGB fault diagnosis.

3. PE Strain Sensor Based PGB Diagnosis

A new PE strain sensor based PGB fault diagnostic method was presented in the previous Chapters. The presented method comprises a PE strain sensor attached on the outside of the gearbox housing, low-pass filtering, TSA, and computation of CIs. Although the background idea of the methodology is same as that shown in Chapter VI, the cutoff frequency for the low-pass filter was slightly modified in this Chapter. By adapting the similar filter-band optimization procedure from the Chapter V, a new filter-band was selected for the new PE strain sensor data with 2-second duration because the highest level of entropy was observed with the use of a 0 ~ 5 kHz for all the filter bands and shaft speed investigate. The overview of the updated PE strain sensor based PGB diagnostic method is diagrammed in Figure 33.

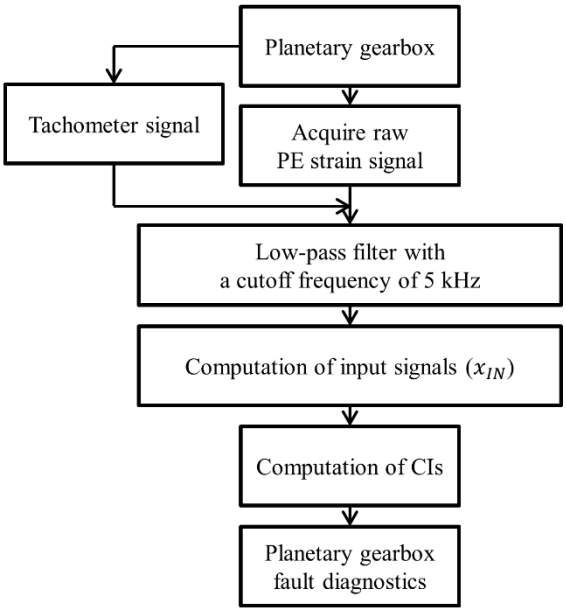

Figure 33.Overview of PE strain sensor based PGB fault diagnosis.

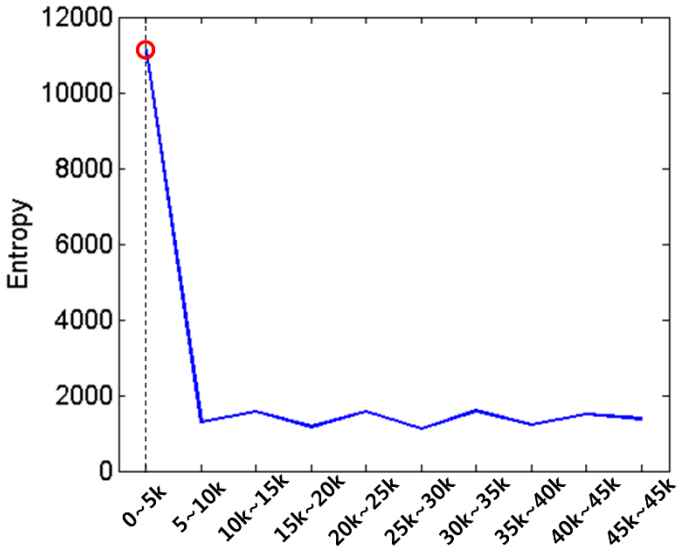

Figure 34. Entropy of band pass filtered healthy PGB signal at a shaft speed of 50Hz.

4. Fault Feature Extraction for Comparative Study

The six basis measurements were chosen: root mean square (*RMS*), peak to peak (*P2P*), skewness (*SK*), kurtosis (*KT*), crest factor (*CF*), and Shannon entropy (*SEnt*). CIs were computed using those basis measurements over varied input signals: Raw AE signals (TSA for PE strain sensor), energy operator (EO), narrow band (NB), amplitude modulation (AM), frequency modulation (FM), spectral averaging (SA) via Welch's method (Welch), and EO of the Welch. FM0 is obtained as an effective CI for distributed gear faults wear and multiple tooth cracks. FM0 is calculated from the formula below:

$$FM0 = \frac{P2P}{\sum A_k} \tag{35}$$

whereA_k is the sum of the gear mesh harmonics. Gear distributed fault (GDF) is used as an effective CI for distributed gear faults wear and multiple tooth cracks. GDF is calculated from the formula below:

$$GDF = \frac{\text{StdDev(residual signal)}}{\text{StdDev(original signal)}} \tag{36}$$

The EO in Teager (1992) is defined as the residual of the autocorrelation function as following:

$$x_{EO,i} = x_{IN,i}^2 - x_{IN,i-1} \cdot x_{IN,i+1}, \quad (\text{for } i = 2, 3, \dots, N-1) \tag{37}$$

where$x_{EO,i}$ is the i^{th} element of EO data; $x_{IN,i}$ is the i^{th} element of the input datax_{IN}. The NB filtered signal, x_{NB}, could be obtained by filtering out all tones except those of the gear mesh and the characteristic frequencies. In this Chapter, the characteristic frequencies are the sun gear fault frequency, planet gear fault frequency, and ring gear fault frequency, respectively. Finally, AM

and FM CIs are obtained by AM analysis and FM analysis ofx_{NB}. AM and FM signals are the absolute value and the derivative of the angle of the Hilbert transform of x_{NB}, respectively.

The SA based vibration fault features were obtained as below:

$$x_{Welch} = |\mathcal{F}^{-1}(|\mathcal{F}(x)|^2)| \tag{38}$$

where $\mathcal{F}$ and $\mathcal{F}^{-1}$ represent Fourier transform and inverse Fourier transform, respectively; $|\mathcal{F}(x)|^2$ originally refers to the power spectral density (PSD) of x and is replaced with the PSD estimate with Welch's method. The terminology "Welch" refers to the SA obtained by the Welch's PSD estimate hereafter. TABLE XXI provides the new definitions of the CIs investigated for PGB fault diagnosis. Once the CIs are computed, they will be used train the PGB fault classifiers using three supervised learning algorithms upon necessity.

TABLE XXI
THE DEFINITIONS OF THE CIS FOR THECOMPARATIVE STUDY

	Input Signal (x_{IN})								
CI	Formula	**Raw or TSA:** (x_{Raw} or x_{TSA})	**Residual:** Signal with primary meshing and shaft components removed (x_{RES})	**EO:** residual of the autocorrelation function (x_{EO})	**NB:** Narrow band pass filtered (x_{NB})	**AM:** Amplitude modulation of NB filtered signal ($AM(x_{NB})$)	**FM:** Frequency modulation of NB filtered signal ($FM(x_{NB})$)	**Welch:** Welch windowed spectral averaging (x_{Welch})	**Welch EO:** Energy operator of Welch $[(x_{Welch})_{EO}]$
RMS	$RMS(x_{IN}) = \sqrt{1/N \sum_{i=1}^{N} x_i^2}$	$RMS(x_{IN})$:measures the energy evolution of a signal.							
P2P	$P2P(x_{IN}) = \frac{(\max_{1\le i\le N}(x_i) - \min_{1\le i\le N}(x_i))}{2}$	$P2P(x_{IN})$:measures the maximum difference within the data range.							
SK	$SK(x_{IN}) = \frac{1/N \sum_{i=1}^{N}(x_i - \bar{x})^3}{\left[\sqrt{1/N \sum_{i=1}^{N}(x_i - \bar{x})^2}\right]^3}$	$SK(x_{IN})$:measures the asymmetry of the data about its mean value. A negative *SK* value and positive *SK* value imply the data have a longer or fatter left tail and the data have a longer or fatter right tail, respectively.							
KT	$KT(x_{IN}) = \frac{N \sum_{i=1}^{N}(x_i - \bar{x})^4}{\left[\sum_{i=1}^{N}(x_i - \bar{x})^2\right]^2}$	$KT(x_{IN})$:measures the peakedness, smoothness, and the heaviness of tail in a data set.							
CF	$CF(x_{IN}) = \frac{P2P(x_{IN})}{RMS(x_{IN})}$	$CF(x_{IN})$:measures the ratio between $P2P(x_{IN})$ and $RMS(x_{IN})$ to describe how extreme the peaks are in a waveform.							
SEnt	$SEnt(x_{in}) = -\sum_i x_i^2 \log(x_i^2)$	$SEnt(x_{in})$measures the Shannon entropy of an input signal.							

Note: x_i is i^{th} element of the input datax_{IN}; N is the length of the input datax_{IN}; max(·) returns the maximal element of input datax_{IN}; min(·) returns the minimal element of input datax_{IN}; $\bar{x}$ is a mean value of the input datax_{IN} defined as $\sum_{i=1}^{N} x_i / N$.

B. Experimental Setup

This section covers the experimental setup used to compare the performance of the vibration, AE sensor, PE strain sensor based PGB fault diagnostic methodology.

1. The PGB Test Rig

The PGB test rig comprises four main parts: (1) the DAQ systems, (2) the driving motor, (3) the PGB gearbox, (4) the load generator. The DAQ system captures vibration, AE, and PE strain data. The driving motor is a 3-phase 10 HP induction motor with a motor controller. A Hall effect sensor and a toothed wheel were mounted on the driving shaft and utilized to records the real-time shaft rotating remarks. For the PGB, a commercially available single stage PGB with a 5:1 speed reduction ratio was used. Then, the output end of the PGB was connected to a generator and a grid tie to serve as a load generator. The compositional structure of the PGB test rig is similar to those used in the residential wind turbines. The front view of the PGB test rig is provided in Figure 35.

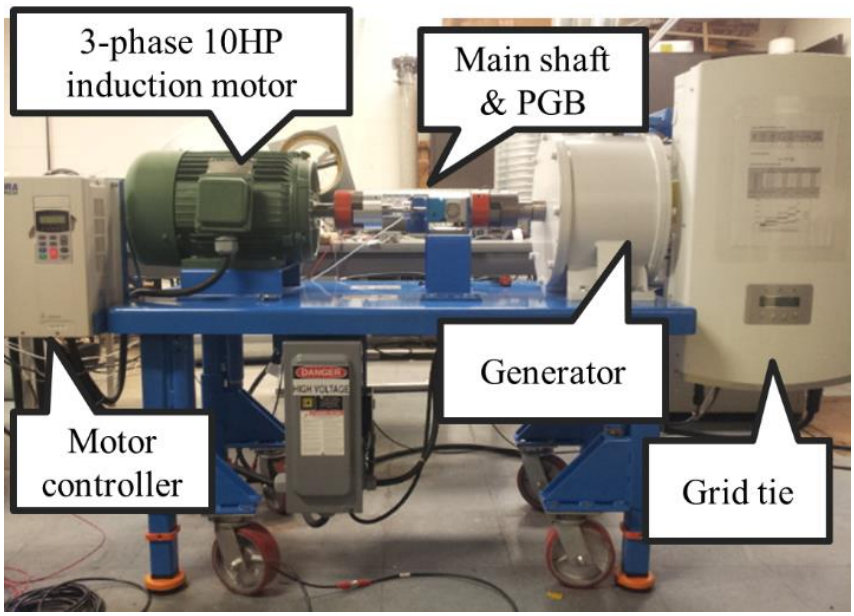

Figure 35. The front view of the PGB test rig.

Provided in Figure 36 is the schematic setup of the DAQ system. First, the vibration data were recorded using a commercially available vibratory wind turbine condition monitoring system from Renewable NRG Systems. The DAQ system comprises two high speed accelerators and a tachometer. Because the typical choice of sampling frequency of vibration data is under 20 kHz, vibration sensor 1 and vibration sensor 2 were sampled at rates of 24,414 Hz and 6,104 Hz, respectively. Second, the AE and PE strain sensor data were recorded using a National Instrument (NI)'s DAQ board with a maximum analog input sampling rate of 1.25MHz. Because there were no similar study of PGB fault diagnosis using AE and PE strain analyses, the sampling rate were identically chosen as 100 kHz. For the composition of AE DAQ, a wideband differential AE sensor, pre-amplifier (20db/40db/60db), demodulation board, and carrier frequency generator were utilized. Since the natural frequencies of AE lie in a higher frequency range (*e.g.* 1 kHz ~ 1 MHz), a high sampling rate between 2 to 10 MHz has been a typical choice of for AE analysis. However, the AE signals used in this study were sampled at 100 kHz, which is a rate compatible to vibration analysis, with an aid of hardware-implemented heterodyne technique. On the other hand, the PE strain sensor DAQ was comprised of a piezoelectric strain sensor and a signal conditioner. The PE strain sensor used in this study has a response frequency range from 0.5 to 100 kHz. In order to get the most of information, a sample rate of 100 kHz was used for the PE strain sensor because the maximum allowable sampling rate for the used sensor is 100 kHz. The details of the vibratory DAQ settings and the AE and PE strain DAQ settings are provided in TABLE XXII.

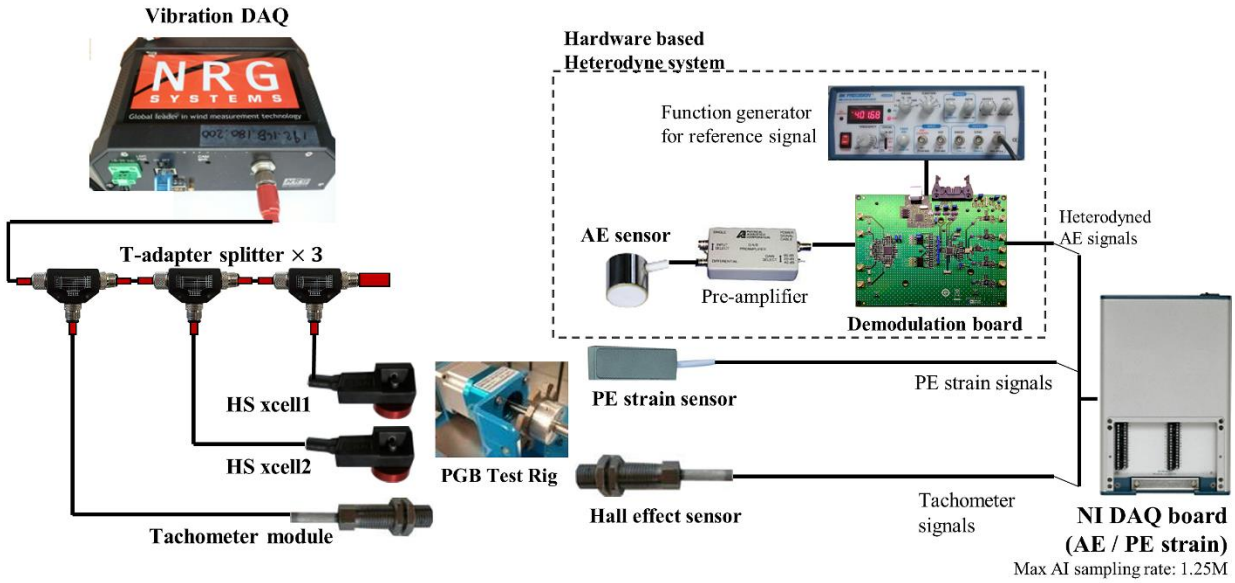

Figure 36. Schematic setup of the DAQ system.

TABLE XXII

DAQ SETTING FOR COMPARATIVE STUDY.

Sensor	Sensor type	Manufacturer	Sampling rate (Hz)	Recording time (sec)
Vibration sensor 1 for TSA, enveloping	High speed accelerometer	NRG systems	6104	40
Vibration sensor 1 for Welch's SA	High speed accelerometer	NRG systems	6104	4
Vibration sensor 2 for TSA, enveloping	High speed accelerometer	NRG systems	24414	20
Vibration sensor 2 for Welch's SA	High speed accelerometer	NRG systems	24414	2
Vibration Tachometer	Hall effect sensor	NRG systems (Sensoronix)	1000	-
AE sensor	Wideband differential AE sensor	Physical Acoustics	100k	2
PE strain sensor	Piezoelectric strain sensor	PCB Piezotronics	100k	2
AE/PE strain tachometer	Hall effect sensor	Sensoronix	100k	-

2. The Seeded Gear Faults

Similarly to the previous chapters, three types of PGB faults were created: sun gear tooth fault, planet gear tooth fault, and ring gear tooth fault. Each type of the gear fault was created by artificially damaging a tooth on a sun gear, planetary gear, and ring gear, respectively (see Figure 37).

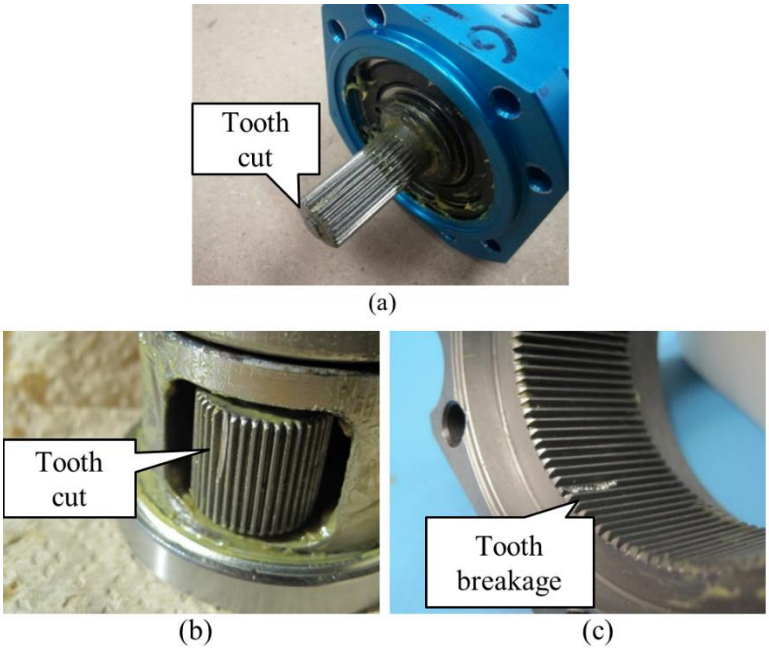

Figure 37. Seeded faults: (a) sun gear fault, (b) planet gear fault, (c) ring gear fault.

During the seeded fault tests, the tachometer signals were simultaneously recorded along with the vibration, AE, and PE strain signals to get revolution stamps. Both the healthy gearbox and the fault seeded gearboxes were tested at five different input shaft speeds: 10 Hz, 20 Hz, 30 Hz, 40 Hz, and 50 Hz. In addition to the shaft speed variation, varying loading conditions were applied at the output shaft of the gearbox: no loading, 25%, 50%, and 75% of the rated torque of the PGB. In each experimentation, the sensors were carefully mounted at the same location to prevent any uncontrolled environmental parameters.

C. Comparative Results

The comparative results for the vibration, AE, and PE strain sensors conducted on the PGB test rig are provided in this section. Provided in TABLE XXIII is the summary of the statistically separable CIs using all vibration, AE sensor, and PE strain sensor methods.

TABLE XXIII implies that the conventional signal processing techniques – method (a) and (b)– barely differentiate the faulty PGBs from the healthy ones. On the other hand, the Welch's SA based vibratory analysis methods (c) and (d) include CIs which isolate PGB fault from the healthy ones; those CIs include FM0 for the sun gear fault above 90%, Res RMS and WEO RMS for the planet gear fault 100%, and GDF for the ring gear fault 100%. Because the most separable CIs were obtained when the vibration sensor 2 was analyzed with the method (c), Welch's SA method would be utilized in this comparative study. Those resulting CIs were further utilized to diagnose the fault locations using three fault classifiers: KNN, BP, and LAMSTAR.

TABLE XXIII

STATISTICAL SEPARATION OF EACH CIS FOR PGB FAULT ISOLATION

		Accelerometer 1 (*fs* = 6104)		
		Sun fault	Planet fault	Ring
Vib. Method	(a) TSA	-	≥80%: P2P	-
	(b) Env-TSA	-	≥80%: P2P	≥80%: RMS, P2P
	(c) Welch	≥80%: Res RMS, Res P2P, WEO P2P	≥ **90**%: RMS, Res RMS ≥80%: P2P, Res P2P, EO P2P, W RMS, WEO P2P	≥80%: Res RMS, Res CF, EO P2P, W RMS, W KT, WEO RMS
	(d) Env-Welch	≥80%: Res RMS, EO RMS, WEO P2P	≥80%: P2P, Res RMS, EO RMS, EO P2P, W P2P, WEO P2P	≥80%: Res RMS, EO RMS, WEO RMS, WEO P2P
		Accelerometer 2 (*fs* = 24414)		
		Sun fault	Sun fault	Sun fault
Vib. Method	(a) TSA	≥80%: Res RMS, Res P2P, GDF	-	≥90%: GDF
	(b) Env-TSA	≥80%: Res RMS, Res P2P, GDF	≥80%: RMS, Res RMS, Res P2P	-
	(c) Welch	**≥90%**: FM0 ≥80%: Res RMS, Res KT, GDF	**≥100%**: Res RMS, WEO RMS **≥90%**: P2P, Res P2P, EO RMS, EO P2P, W P2P, WEO P2P ≥80%: RMS, W KT, W SK	**≥100%**: GDF **≥90%**: FM0, W RMS, WEO KT, WEO SK ≥80%: W KT, W CF, W SK, WEO RMS
	(d) Env-Welch	≥80%: Res RMS, EO RMS, WEO P2P	≥80%: P2P, Res RMS, EO RMS, EO P2P, W P2P, WEO P2P	≥80%: Res RMS, EO RMS, WEO RMS, WEO P2P
		AE sensor (*fs* = 100k)		
		Sun fault	Sun fault	Sun fault
AE Method		**≥90%:** FM0 ≥80%: KT, CF,EO P2P, EO KT, EO SK, and W CF	**≥100%**: RMS **≥90%:** FM0, NB RMS, NB P2P, WEO RMS, and WEO P2P ≥80%: KT, AM RMS, AM P2P, W RMS, W KT, W P2P, W CF, and W SK	**≥100%**: W CF, WEO KT, and WEO SK **≥90%:** W RMS, W KT, and W SK ≥80%: P2P, WEO RMS, WEO P2P, and WEO CF
		PE strain sensor (*fs* = 100k)		
		Sun fault	Sun fault	Sun fault
PE Strain Method		**≥100%:** TSA RMS, TSA SEnt **≥90%:**Res RMS, Res SEnt, W RMS, W P2P, W SEnt		

As shown from TABLE VII, none of the single CI provides acceptable diagnostic performance for all three fault classifiers although each CI can isolate faults from at least one or more PGB fault types. Also shown in TABLE VIII, two combinations of CIs were tested. From the fault diagnostic results, KNN achieved the overall minimal error rate of 3.63% when the first CI combination were used. LAMSTAR network, however, achieved the similar diagnostic error rate of 3.98% along with the lowest standard deviation. That is, LAMSTAR network could be equally desired as KNN from the reliability perspective.

In Chapter V, PGB fault diagnostic method using AE analysis were presented. The method combines the hardware-implemented heterodyne AE DAQ system, EMD method, computation of CIs, and implementation of PGB fault diagnostic classifiers. Provided in Table XXIII is the summary of the statistically separable CIs results from all AE methods. Among all of the CIs, FM0 showed 95% statistical separation for the sun gear fault, RMS displayed 100% statistical separation for the planet gear fault, and Welch CF, Welch EO KT, and Welch EO SK showed 100% statistical separation for the ring gear fault, respectively. Those effective CIs were further utilized to classify the faults (*e.g.* sun, planet, ring, or healthy) using the three classifiers: KNN, BP, and LAMSTAR. Provided in TABLE XIII and TABLE XIV are the diagnostic results using the three classifiers with both the individual CIs and the combinational CIs. As one can see from TABLE XIII, for all three classifiers, none of the individual CIs achieved acceptable level of fault diagnostic performance although those CIs display statistical separablability for at least one fault type. from TABLE XIV, it can be seen that LAMSTAR network achieved the lowest diagnostic error rate of $\leq$1% when the first combination of CIs were used while KNN achieved 7% error rate when the second CI combination was used. For the comparative study, the result from the LAMSTAR network will be utilized for AE analysis.

Lastly, from Chapter VI, PGB fault diagnostic method using PE strain analysis is were presented. However, the sample recording time was reduced to two second for fair comparison with vibration analysis and AE analysis. The method combines the low pass filtering with the cutoff frequency of 5 kHz, TSA, and computation of CIs. After the PE strain signals were low pass filtered, CIs described in Section A-3 were computed. Among the computed CIs, a few CIs were newly found effective: TSA RMS, TSA Shannon entropy (SEnt), Residual RMS, Residual SEnt, W RMS, and W P2P. Figure 38 shows those effective CIs for different gearbox health conditions at varying shaft speeds and loading conditions.

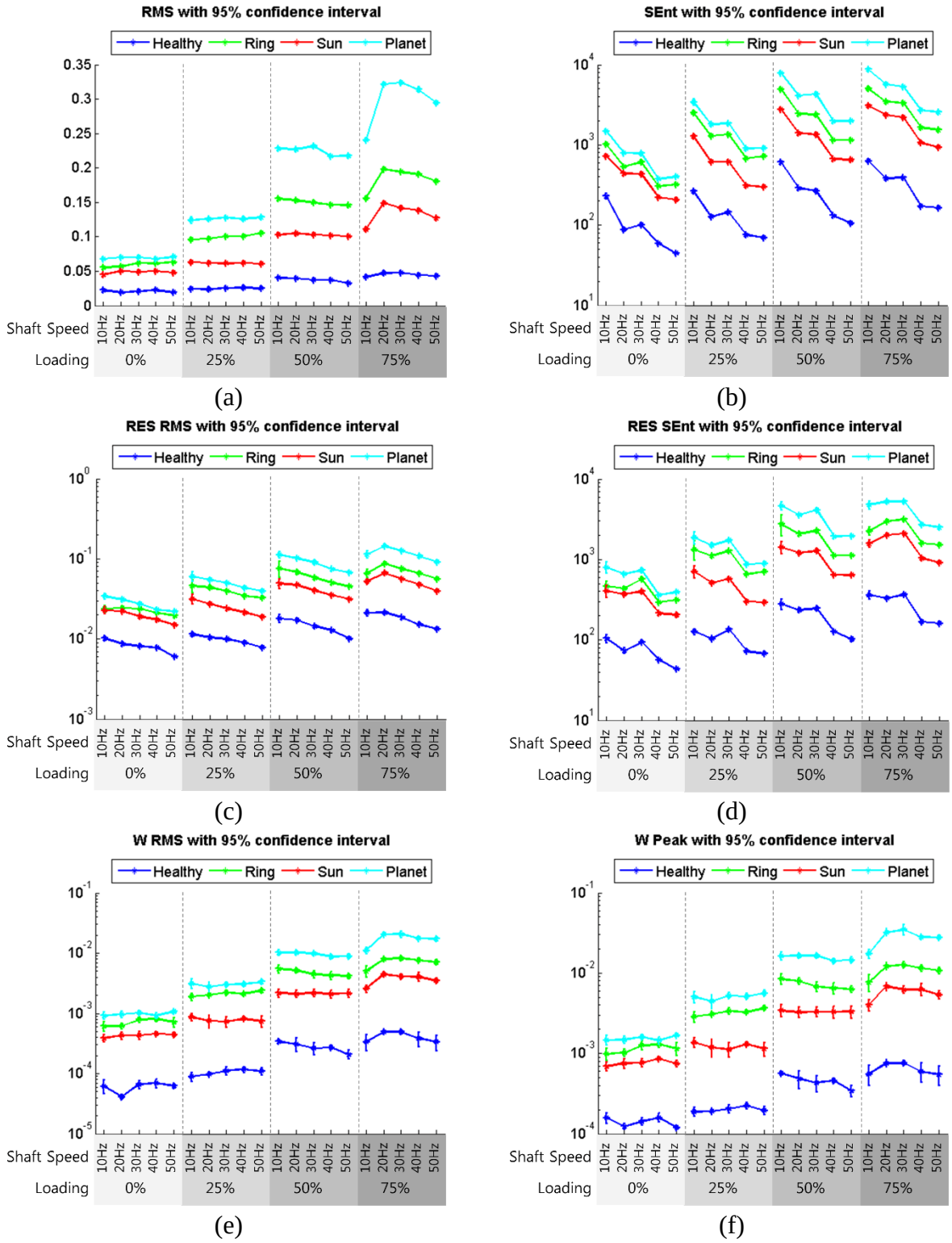

Figure 38. PGB fault diagnostic CIs from PE strain analysis: (a) TSA RMS, (b) TSA Shannon Entropy, (c) Residual RMS, (d) Residual SEnt, (e) Welch RMS, and (f) Welch P2P.

As one can see from Figure 38, by using TSA RMS, Welch RMS, and Welch P2P, the CIs remained relatively stationary within the same loading condition regardless the change of the shaft speed. Those CIs also showed that the PE strain sensor based CIs are heavily affected by the torque level of the gearbox. The vertical bars for each data point represent 95% confidence intervals.

Provided in TABLE XXIV is the comparative summary of the PGB fault diagnostic methods.

TABLE XXIV

COMPARATIVE SUMMARY OF THE PGB FAULT DIAGNOSTIC METHODS

	Vibration	AE	PE strain
Analysis method	Welch's SA	Heterodyne AE, EMD	TSA
Sampling frequency (Hz)	24414	100k	100k
Sample recording time (sec)	2	2	2
Fault detecting CIs for particular gear faults	O	O	O
Fault diagnosable CIs for all gear faults	×	×	O
Fault diagnostic ability using machine learning	O	O	Not required
Fault diagnostic error rate	~3% (w/ both KNN, and LAMSTAR)	$< 1\%$ (w/ LAMSTAR)	-

VIII. CONCLUSIONS

In this dissertation, effective and efficient PGB fault diagnostic methods and tools were developed and validated on a set of seeded localized faults on all gears: sun gear, planetary gear, and ring gear. Specifically, to overcome the PGB's known issue of the AM effect, caused by rotating vibration transfer path, new PGB fault diagnostic methods were developed using: vibration analysis with Welch's spectral averaging; alternative sensors of AE and PE strain sensors and their associated analysis methods.

In Chapter IV, the spectral averaging (SA) based PGB fault diagnostic method using a vibration sensor was presented. The proposed method is comprised of the TSR, SA for rotating machinery, computation of CIs, and implementation of PGB diagnostic systems. The presented method was validated with a set of seeded fault tests performed on a PGB test rig in a laboratory. First, the digitized accelerometer signals were processed by TSR and SA technique to compute Cis and to extract PGB fault features. The effective CIs were grouped into two combination sets according to the level of statistical separation followed by training three machine learning algorithms: KNN, BP network, and LAMSTAR network. The validation results have shown: (1) the minimal error rate of 3.63% was achieved using KNN with the chosen CI combination; (2) An average diagnostic error rate of 8.94% was achieved using the BP algorithm. Meanwhile, the local minima convergence was observed at a rate of 12~16% out of all occurrences; (3) LAMSTAR network displayed a similar level of diagnostic error rate of 3.98% as KNN. But LAMSTAR network achieved the minimal standard deviation and it is a desired aspect from the reliability perspective. In summary, the presented method effectively differentiated the localized faults on all gears: sun gear, planetary gear, and ring gear, which has not been presented in the literature.

In Chapter V, a new AE sensor based PGB fault diagnostic method was presented. The presented method comprises a heterodyne based AE DAQ system, EMD based rotating machinery fault diagnostic method, computation of CIs, and data mining based PGB fault classifiers. By applying the heterodyne technique, the AE response frequency could be downshifted from several hundred kHz to below 10s of kHz. Besides, the AE signals could be demodulated to remove non-vital high frequency components while the fault characteristic components are maintained. As a result, the AE signals could be sampled at a rate comparable to that of vibration analysis. The presented AE method was validated with a set of seeded fault tests performed on a PGB test rig in a laboratory. First, the sampled AE signals were signal processed using EMD to extract PGB fault features and compute CIs. Those CIs were then grouped into two combination sets according to the level of statistical separation followed by training three supervised learning algorithms (*i.e.* classifier): KNN, BP, and LAMSTAR. The results have shown the followings: (1) An error rate of 7% was achieved using KNN; (2) An average diagnostic error rate of 7% was achieved using the BP algorithm. However, a local minima convergence was observed at a rate of 12~16%; (3) The LAMSTAR network displayed less sensitivity to the local minima issue. The best overall diagnostic error rate of about 0.5% was achieved using LAMSTAR network.

In Chapter VI, a new piezoelectric strain sensor based PGB fault diagnostic methodology was presented. The presented method was accomplished through a combination of low pass filtering, TSA, and CIs to extract diagnostic fault features for PGB. Since there was no similar study available in the literature, a filter-band optimization procedure was performed to apply the low-pass filter. Then, the varied input signals and CIS were computed which are widely used in real applications such as health and usage monitoring systems (HUMS) installed in helicopters and the condition monitoring systems in wind turbines. The presented method was further validated

using data collected from seeded fault tests conducted on a PGB test rig in a laboratory. The validation results have shown that fully separable diagnostic CIs towards all PGB fault types were captured regardless of shaft speeds and loading conditions. A total of four CIs were extracted from PE strain sensor signals: TSA RMS, TSA P2P, residual RMS, and residual P2P which effectively differentiate the localized faults on all gears: sun gear, planetary gear, and ring gear, which has not been presented in the literature. The PE strain sensor based PGB fault diagnostic technique presented in this chapter provides an attractive alternative to the current vibration analysis based approach.

The comparative results for the vibration, AE, and PE strain sensors conducted on the PGB test rig are provided in Chapter VII. From the conventional signal processing techniques for machinery fault diagnostics such as TSA, enveloping, VS and etc. were investigated. Then those developed in the previous Chapters were utilized to provide a comparative study from the PGB diagnostic feasibility stand point. The following conclusion could be drawn:

- The conventional analysis techniques such as TSA, enveloping, VS barely shown any differential results for the faulty PGBs from the healthy PGBs.
- The Welch's SA based vibratory analysis was able to diagnose two types of localized PGB faults with an aid of machine learning techniques; the minimal error rate around 3~4% was achieved using KNN and LAMSTAR, however, LAMSTAR network achieved the minimal standard deviation and it is a desired aspect from the reliability perspective.
- The AE based analysis was more accurate than the Welch's SA based vibratory analysis for the PGB fault diagnostic method; the best diagnostic error rate of ~0.5% was achieved using LAMSTAR network.

- The PE strain sensor based analysis was desirable in that any machine learning was not required in PGB diagnosis. The following CIs were found effective: TSA RMS, TSA Shannon entropy (SEnt), Residual RMS, Residual SEnt, W RMS, and W P2P. Assume that the output loading is a known parameter using power-torque equation from the generator. For those effective CIs, some of them have shown less sensitive to the change of the speed under the same loading condition, for example, TSA RMS. It can be observed that the CI level of TSA RMS almost linearly increased when loading condition increased. Therefore, in the varying loading scenario, this CI can be used by setting thresholds (or formulating threshold equation) for the known loading condition. In addition to that, other CIs may have shown more sensitive to the change of the speed under the same loading condition, for example, SEnt. Under the varying shaft speed scenario, the CI level of SEnt almost linearly decreased when shaft speed increased.

REFERENCES

Al-Balushi K. R., and Samanta B.: Gear fault diagnosis using energy-based features of acoustic emission signals, ProcInstnMechEngrs Vol 216 Part I, 216(3):249-263, 2002.

Al-Ghamd A. M., and Mba D.: A comparative experimental study on the use of AE and vibration analysis for bearing defect identification and estimation of defect size", Mech. Syst. Signal Pr., 20(7):1537-1571, 2006.

Al-Ghamd, A. M. and Mba, D.: A comparative experimental study on the use of ae and vibration analysis for bearing defect identification and estimation of defect size, Mech. Syst. Signal Pr., 20(7):1537-1571, 2006.

Altman, N. S.: An introduction to kernel and nearest-neighbor nonparametric regression, Am. Stat., 46(3):175-185, 1992.

Antoni, J.: Fast computation of the kurtogram for the detection of transient faults, Mech. Syst. Signal Pr., 32(1):108-124, 2007.

Astridge, D. G.: Helicopter transmissions – design for safety and reliability, J. Aerospace Eng., 203(2):123-138, 1989.

Banaszak, D.: Comparison of piezoelectric strain sensors with strain gages, Proc. Annu. Meeting Am. Stat. Asso., Aug. 5 – 9, Atlanta, GA, 2001.

Barszcza, T., and Randall, R.B.: Application of spectral kurtosis for detection of a tooth crack in the planetary gear of a wind turbine, Mech. Syst. Signal Pr., 23(1):1352-1365, 2009.

Bartelmus, W., and Zimroz, R.: A new feature for monitoring the condition of gearboxes in non-stationary operation conditions, MechSyst Sig Process, 23(5), 1528-1534, 2009b.

Bartelmus, W., and Zimroz, R.: Vibration condition monitoring of planetary gearbox under varying external load, MechSyst Sig Process, 23(1):246-257, 2009a.

Bartelmus, W., and Zimroz, R.: Vibration spectra characteristic frequencies for condition monitoring of mining machinery compound and complex gearboxes, Sci. P. Inst. Min. Conf., 133(40):17-34, 2011.

Bechhoefer, E. and Kingsley, M.: A review of time synchronous average algorithm, Annu. Conf. PHM Soc., Sep 27 – Oct 1, San Diego, CA, 2009.

Bechhoefer, E., Qu, Y., Zhu, J., and He, D.: Signal processing technique to improve an acoustic emission sensors, Proc. Annu. Conf. PHM Soc., Oct. 14 – 17, New Orleans, LA, USA, 2013b.

Bechhoefer, E., Van Hecke, B., and He, D.: Processing for improved spectral analysis, Proc. Annu. Conf. PHM Soc., Oct. 14 – 17, New Orleans, LA, USA, 2013a.

Braun, S.:The extraction of periodic waveforms by time domain averaging,Acustica, 32(1):69-77, 1975.

Cusido, J., Romeral, L., Ortega, J.A., Rosero, J.A., and Garcia Espinosa, A.: Fault detection in induction machines using power spectral density in wavelet decomposition, IEEE Trans. Ind. Electron., 55(2):633-643, 2008.

Eftekharnejad, B., Carrasco, M.R., Charnley, B., and Mba, D.: The application of spectral kurtosis on acoustic emission and vibrations from a defective bearing", Mech. Syst. Signal Pr., 25(1):266-284, 2011.

Eurocopter, https://www.youtube.com/watch?v=oD4jKBOIBwc, 2015.

Feng, Z., and Liang, M.: Complex signal analysis for wind turbine planetary gearbox fault diagnosis via iterative atomic decomposition thresholding, J. Sound Vib., 333(20):5196-5211, 2014.

Feng, Z., and Liang, M.: Fault diagnosis of wind turbine planetary gearbox under nonstationary conditions via adaptive optimal kernel time frequency analysis, Renew. Energ., 66:468-477, 2014a.

Feng, Z., and Zuo, M.J.: Fault diagnosis of planetary gearboxes via torsional vibration signal analysis, Mech. Syst. Signal Pr., 36(2):401-421, 2013.

Feng, Z., and Zuo, M.J.: Vibration signal models for fault diagnosis of planetary gearbox, J. Sound Vib., 331(22):4919-4939, 2012.

Feng, Z., Chen, X., and Liang, M.: Iterative generalized synchrosqueezing transform for fault diagnosis of wind turbine planetary gearbox under nonstationary conditions, Mech. Syst. Signal Pr., 52–53:360-375, 2015.

Feng, Z., Zuo, M. J., Qu, J., Tian, T., and Liu, Z.: Joint amplitude and frequency demodulation analysis based on local mean decomposition for fault diagnosis of planetary gearboxes, Mech. Syst. Signal Pr., 40(1):56-75, 2013.

Fessenden, R.A.: Wireless signaling, U.S. 706,740A, 28 Sep 1902; 4 pp, 12 Aug 1902.

Flsmidth: [online] http://www.flsmidth.com/en-US/Industries/Categories/Products/Material+Handling/Stockyard+Equipment/Gear+Units+for+Bucket+Wheel+Excavators/MAAG+KPB+transmission+gear+unit, 2015.

Freire, N.M.A., Estima, J.O., and Marques Cardoso, A.J.: Open-circuit fault diagnosis in PMSG drives for wind turbine applications, IEEE Trans. Ind. Electron., 60(9):3957-3967, 2013.

GE Drivetrain Technologies: [online] http://gedrivetrain.com/assets/PDFs/GE_DrivetrainTechnologies_Gearboxes_broch.pdf, 2014.

Gong, X., and Qiao, W.: Bearing fault diagnosis for direct-drive wind turbines via current-demodulated signals, IEEE Trans. Ind. Electron., 60(8):3419-3428, 2013.

Google Patents: http://www.google.com/patents/US5920852, 2015.

Graupe, D. (GraNNet Corporation): Large memory storage and retrieval (LAMSTAR) network, U.S. 5,920,852A (Cl. G06F 15/18; 706/26), Appl. 08/846,577, 30 Apr 1997; 51 pp, 6 Jul 1999.

Graupe, D., Kordylewski, H.: A large memory storage and retrieval neural network for adaptive retrieval and diagnosis, Int. J. Softw. Eng. Know., 8(1):115-138, 1998.

Graupe, D.: Principles of Artificial Neural Networks, 3rd edition, World Scientific Publishing, Singapore, 2013.

Hawman, M.W., and Galinaitis, W.S.: Acoustic emission monitoring of rolling element bearings, IEEE Ultrason. Symp. Proc., Oct. 2-5, Chicago, IL, 1988.

He, D., Li, R., Zhu, J., and Zade, M.: Data mining based full ceramic bearing fault diagnostic system using AE sensors, IEEE Trans. Neural Networ., 22(12):2022-2031, 2011.

He, D., Li, R., and Zhu, J.: bearing fault diagnosis based on a two-step data mining approach, IEEE Trans. Ind. Electron., 60(8): 3429-3440, 2013.

Howard, I.M.: Epicyclic transmission fault detection by vibration analysis, Australian Vib. Noise Conf., Melbourne, Australia, 1990.

Huang, N., Shen, Z., Long, S., Wu, M., Shih, H, Zheng, Q., Yen, N., Tung, C., and Liu, H.: The empirical mode decomposition and the Hilbert spectrum for nonlinear and non-stationary time series analysis, Proc. R. Soc. London, Ser. A, 454:903-995, 1998.

Jiang, X., Kim, K., Zhang, S., Johnson, J., and Salazar, G.: High-temperature piezoelectric sensing, Sensors, 14(1):144-169, 2013.

Karimi, S., Gaillard, A., Poure, P., and Saadate, S.: FPGA-based real-time power converter failure diagnosis for wind energy conversion systems, IEEE Trans. Ind. Electron., 55(12):4299-4308, 2008.

Kiddy, J.S., Samuel, P.D., Lewicki, D.G., LaBerge, K.E., Ehinger, R.T., and Fetty, J.: Fiber optic strain sensor for planetary gear diagnostics, NASA Technical Report (NASA/TM-2011-217123), NASA Glenn Research Center, Cleveland, OH, 2011.

Kohonen, T.: Self-Organization and Associative Memory, Springer-Verlag, Berlin, 1984.

Kon, S., Oldham, K., and Horowitz, R.: Piezoresistive and piezoelectric MEMS strain sensors for vibration detection, Proc. SPIE, 6529:1– 11, 2007.

Kordylewski, H., Graupe, D., and Liu, K.: A novel large-memory neural network as an aid in medical diagnosis applications, IEEE Trans. Inf. Technol. B., 5(3):202-209, 2001.

Lee C.K. and O'Sullivan, T.: Piezoelectric strain rate gages, J. Acoust. Soc. Am., 90(2):945-953, 1991.

Lei, Y., Han, D., Lin, J., and He, Z.: Planetary gearbox fault diagnosis using an adaptive stochastic resonance method, Mech. Syst. Signal Pr., 38(1):113-124, 2013.

Lei, Y., Lin, J., Zuo, M.J., and He, Z.: Condition monitoring and fault diagnosis of planetary gearboxes: A review, Measurement, 48:292-305, 2014.

Lewicki, D.G., Laberge, K.E., Ehinger, R.T., and Fetty, J.: Planetary gearbox fault detection using vibration separation technique, NASA Tech. Rep. (NASA/TM-2011-217127), NASA Glenn Research Center, Cleveland, OH, 2011.

Liu, B., Riemenschneider, S., and Xu, Y.: Gearbox fault diagnosis using empirical mode decomposition and Hilbert spectrum, Mech. Syst. Signal Pr., 20:718-734, 2006.

Loutas T.H., Roulias D., Pauly E., and Kostopoulos V., The Combined Use of Vibration, AE and Oil Debris On-line Monitoring Towards A More Effective Condition Monitoring of Rotating Machinery, Mech. Syst. Signal Pr., 25(4):1339-1352, 2011.

Lucas, M.: Condition monitoring: why acoustic emission represents the next generation of vibration, Monthly Archives of Kittiwake, Feb. 2012, [online]: http://www.kittiwake.com/news/2012/02/

Luo, H., Hatch, C., Hanna, J., Kalb, M., Weiss, A., Winterton, J., Inalpolat, M., and Dannehy, C.: Amplitude modulations in planetary gears, Wind Energy, 17:505–517, 2014.

Mathews, J.R.: Acoustic Emission, Gordon and Breach Science Publishers Inc., New York, NY, USA, 1983.

Mathworks, [online]: http://www.mathworks.com/machine-learning/index.html, (2014).

McFadden, P.D., and Howard, I.M.: The detection of seeded faults in an epicyclic gearbox by signal averaging of the vibration, Aeronautical Research Laboratory (AD-A230 403), Melbourne, Victoria, Australia, 1990.

McFadden, P.D.: A revised model for the extraction of periodic waveforms by time domain averaging, Mech. Syst. Signal Pr., 1(1):83-95, 1987.

McFadden, P.D.: A technique for calculating the time domain averages of the vibration of the individual planet gears and the sun gear in an epicyclic gearbox, J. Sound Vib., 144(1):163-172, 1991.

McFadden, P.D.: Window functions for the calculation of the time domain averages of the vibration of the individual planet gears and sun gear in an epicyclic gearbox, J. Vib. Acoust., 116(2):179-187, 1994.

Patrick, R., Orchard, M.E., Zhang, B., and Koelemay, M.D.: An integrated approach to helicopter planetary gear fault diagnosis and failure prognosis, Proc. IEEE AUTOTESTCON, Baltimore, MD, 2007.

Qu, Y., He, D., Bechhoefer, E., and Zhu, J.: A new acoustic emission sensor based gear fault detection approach, Int. J. PHM, 4(Special Issue on Wind Turbine PHM):1-14, 2013a.

Qu, Y., He, D., Yoon, J., Van Hecke, B., Bechhoefer, E., and Zhu, J.: Gearbox tooth cut fault diagnostics using acoustic emission and vibration sensors – a comparative study, Sensors, 14(1):1372-1393, 2014.

Qu, Y., VanHecke, B., He, D., Yoon, J., Bechhoefer, E., and Zhu, J.: Gearbox fault diagnosis using AE sensors with low sampling rate, J. Acoust. Emiss., 31(1):67-90, 2013b.

Rojas, R.: Neural Networks - A Systematic Introduction, Springer-Verlag, Berlin, 1996.

Rumelhart, D.E., Hinton, G.E., and Williams, R.J.: Learning representations by back-propagating errors, Nature, 323(6088):533-536, 1986.

Samuel, P.D., Conroy, J. K., and Pines, D. J. Planetary transmission diagnostics, NASA Technical Report(NASA/CR-2004-213068), NASA Glenn Research Center, Cleveland, OH, 2004.

Scheer, C., Reimche, W., and Bach, F.W.: Early fault detection at gear units by acoustic emission and wavelet analysis, J. Acoust. Emission, 25(1):331-340, 2007.

Sheng, S., Link, H., LaCava, W., van Dam, J., McNiff, B., Veers, P., Keller, J., Butterfield, S., and Oyague, F.: Wind turbine drivetrain condition monitoring during GRC phase 1 and phase 2 testing, NREL Technical Report (NREL/TP-5000-52748), 2011.

Sheng, S.: Gearbox reliability database: yesterday, today, and tomorrow, NREL Technical Report (No. PR-5000-63106), 2014.

Sheng, S.: Wind turbine gearbox condition monitoring round robin study – vibration analysis, NREL technical report (NREL/TP-5000-54530), Denver, CO, 2012.

Sirohi J., and Chopra, I.: Fundamental understanding of piezoelectric strain sensors, J. Intel. Mat. Syst. Str., 11(4):246-257, 2000.

Tandon, N. and Mata, S.: Detection of defects in gears by acoustic emission measurements, J. Acoust. Emiss., 19:23-27, 1999.

Teager, H.M., and Teager S.M.: Evidence for nonlinear sound production mechanisms in the vocal tract, In: Speech Production and Speech Modeling Symposium, Time Frequency and Time-Scale Analysis, eds. Hardcastle, W.J. and Marchal, A., pp. 345 – 348. Netherlands, Springer, 1992.

Tomoya, M., Katsumi, I., and Masana, K.: Acoustic emission during fatigue crack growth in carburized gear tooth, Trans. Jpn. Soc. Mech. Eng., Part C, 60(575):2456-2461, 1994.

Van Hecke, B., Qu, Y., He, D., and Bechhoefer, E.: A new spectral average-based bearing fault diagnostic approach, J Fail. Anal. andPreven., 14:354–362, 2014a.

Van Hecke, B., He, D., and Qu, Y.: On the use of spectral averaging of acoustic emission signals for bearing fault diagnostics, J. Vib. Acoust., 136(6):1-13, 2014b.

Vedreno-Santos, F., Riera-Guasp, M., Henao, H., Pineda-Sanchez, M., and Puche-Panadero, R.: Diagnosis of rotor and stator asymmetries in wound-rotor induction machines under

nonstationary operation through the instantaneous frequency, IEEE Trans. Ind. Electron., 61(9):4947-4959, 2014.

Wachel J.C., and Szenasi, F.R.: Analysis of torsional vibrations in rotating machinery, Proc. 22ndTurbomach. Symp., Texas A&M University, College Station, TX, 1993.

Welch, P.: The use of fast Fourier transform for the estimation of power spectra: a method based on time averaging over short, modified periodograms, IEEE Trans. Audio Electroacoust., 15(2):70-73, 1967.

Wu, B., Saxena, A., Khawaja, T. S., Patrick, R., Vachtsevanos, G., and Sparis, P.: An approach to fault diagnosis of helicopter planetary gears, Proc. IEEE AUTOTESTCON, San Antonio, TX., 2004.

Yan, R., and Gao, R.: Hilbert-Huang transform-based vibration signal analysis for machine health monitoring, IEEE Trans. Instrum. Meas., 55:2320-2329, 2006.

Yang, W., Tavner, P.J., Crabtree, C.J., and Wilkinson, M.: Cost-effective condition monitoring for wind turbines, IEEE Trans. Ind. Electron., 57(1), 263-271, 2010.

Yoon, J., He, D., and Qiu, B.: Full ceramic bearing fault diagnosis using LAMSTAR neural network, IEEE PHM Conf., Gaithersburg, MD, USA, Jun. 2013.

Yoon, J., He, D., and Van Hecke, B.: A PHM approach to additive manufacturing equipment health monitoring, fault diagnosis, and quality control, Annu. Conf. PHM Soc., Sep. 29 – Oct. 2, Fort Worth, TX, USA, 2014.

Yoon, J., He, D., Van Hecke, B., Nostrand., T., Zhu, J., and Bechhoefer, E..: 'Vibration based wind turbine planetary gearbox fault diagnosis using spectral averaging', AWEA Wind Power Conf., Orlando, FL, USA, May. 2015.

Yoshioka, T., and Fujiwara, T.: A New acoustic emission source locating system for the study of rolling contact fatigue, Wear, 81(1):183-186, 1982.

Yoshioka, T., and Fujiwara, T.: Application of acoustic emission technique to detection of rolling bearing failure, ASME Prod. Eng. Div., [Publ.] PED, 14(1):55-76, 1984.

Yoshioka, T.: Detection of rolling contact subsurface fatigue cracks using acoustic emission technique, Lubr. Eng., 49(4):303-308, 1992.

Zhu, J., Yoon, J., He, D., and Bechhoefer, E.: Online particle-contaminated lubrication oil condition monitoring and remaining useful life prediction for wind turbines, Wind Energy, 18(6):1131-1149, 2014.

Zimroz, R., and Bartkowiak, A.: Two simple multivariate procedures for monitoring planetary gearboxes in non-stationary operating conditions", MechSyst Sig Process, 38(1):237-247, 2013.

APPENDIX

(Accepted to appear, currently the manuscript is being formatted to make a publish version.)

IET Science, Measurement & Technology

Research Article

IET Journals
The Institution of Engineering and Technology

Planetary gearbox fault diagnostic method using acoustic emission sensors

ISSN 1751-8822
Received on 21st January 2015
Revised on 16th May 2015
Accepted on 12th June 2015
doi: 10.1049/iet-smt.2014.0375
www.ietdl.org

Jae Yoon, David He ✉

Department of Mechanical and Industrial Engineering, University of Illinois at Chicago, 842 W. Taylor Street, Chicago, IL, 60607, USA
✉ *E-mail: davidhe@uic.edu*

Abstract: In this study, a new acoustic emission (AE) sensor-based planetary gearbox (PGB) fault diagnosis method is presented. The method includes a heterodyne-based AE data acquisition system, empirical mode decomposition (EMD)-based AE signal analysis method, and computation of condition indicators (CIs) for PGB fault diagnosis. The heterodyne technique is hardware-implemented to downshift the sampling frequency of AE signals at a rate compatible to vibration analysis. The sampled AE signals are processed using EMD to extract PGB fault features and compute the CIs. The CIs are input into supervised learning algorithms for PGB fault diagnosis. The method is validated on a set of seeded localised faults on all gears: sun gear, planetary gear, and ring gear. The validation results have shown a promising PGB fault diagnostic performance using the presented method.

9.1.6 ResearchGate: The IET classes ResearchGate as a social media site and as such authors are able to upload their accepted manuscript (reviewed, revised and typeset) but not the published PDF.

Any questions should be addressed to the editorial officer (journals@theiet.org).
Back to the top

10. Copyright and Open Access License

10.1. Right to publish

An author submitting a paper should ensure that he or she has the right to publish the paper and that it contains nothing defamatory. The IET will assume that all co-authors have agreed to the submission of any paper received.

10.2. Copyright Form for Subscription Access

Authors who choose to publish through the subscription access model will be required to fill in the online copyright form in the ScholarOne Manuscripts Author Centre. The submitting author should sign on behalf of all co-authors.

Unless the paper is either 'United Kingdom Crown copyright' or 'a work of the US Government and in the Public Domain', the Bylaws of the IET require that copyright should belong to the IET.

10.3. Open Access: Creative Commons Licences

Authors who choose to publish their papers open access in the IET Research Journals will be asked to sign a Creative Commons Licence as opposed to a copyright form. All Creative Commons Licence types will incur an Article Processing Charge of $1,450 USD. These licences allow the author to retains the copyright to their work. As we offer a number of different licence options for authors it is advised that authors take some time to consider which licence they would like to use when they submit their paper so as not to delay the publication of the paper on acceptance. Authors whose work is funded by the Wellcome Trust or Research Councils UK must sign the Creative Commons Attribution (CC BY). Other licences available are: Attribution-NoDerivs (CC BY-ND), Attribution-NonCommercial (CC BY-NC) and Attribution-NonCommercial-NoDerivs (CC BY-NC-ND). For more information on these options please see below.

Creative Commons Attribution (CC BY) This licence lets others distribute, remix, tweak, and build upon your work, even commercially, as long as they credit you for the original creation. This is the most accommodating of licences offered. Recommended for maximum dissemination and use of licenced materials. (If your work is funded by The Wellcome Trust or Research Councils UK you must use this licence.)

Preview licence

Creative Commons Attribution-NoDerivs (CC BY-ND) This licence allows for redistribution, commercial and non-commercial, as long as it is passed along unchanged and in whole, with credit to you.
Preview licence

Creative Commons Attribution-NonCommercial (CC BY-NC) This licence lets others remix, tweak, and build upon your work non-commercially, and although their new works must also acknowledge you and be non-commercial, they don't have to licence their derivative works on the same terms.
Preview licence

Creative Commons Attribution-NonCommercial-NoDerivs (CC BY-NC-ND) This licence is the most restrictive licence we offer, only allowing others to download your works and share them with others as long as they credit you, but they can't change them in any way or use them commercially.
Preview licence

10.4 Permissions to reproduce

10.4.1 If you wish to make use of previously published illustrations, diagrams or photographs in your paper, whether for commercial or non-commercial purposes, you must obtain the written permission of the editorial office.

10.4.2 The IET will not make a charge where the work is being reproduced for non-commercial purposes, e.g. teaching, research presentations, etc.

10.4.3 Charges apply where IET copyrighted material is being reproduced for commercial purposes, e.g. book chapters, review articles.

10.4.4 The source of the material must also be acknowledged in full.

10.4.5 Please note, all authors have to obtain their own permissions for re-used text, figures and tables which do not belong to the IET in their submitted papers.
Back to the top

VITA

NAME: Jae Myung Yoon

EDUCATION:

Ph.D. in Industrial Engineering and Operation Research, University of Illinois at Chicago, IL, USA, 2015

M.S. in Mechanical Engineering (Thesis based), University of Florida, Gainesville, FL, USA, 2012

B.E. in Control and Instrumentation, Kwangwoon University, Seoul, South Korea , 2006

PROFESSIONAL EXPERIENCE:

Job Title: Senior Application Engineer *Date:* 05/2015-Present

Employer: The DEI Group *Location:* Millersville, MD, USA

Job Description: Modeling of machinery life cycle sustainment; Identification, design, and implementation of analytic methods and techniques using vibration monitoring and on-line fluid analysis technologies within Predictive Machinery Analyzer (PreMA) solutions including:

- Application Engineering for PreMA based projects

- Establishing internal core competency for developing PreMA applications related to rotating machinery using vibration analysis technologies

- Identifying and supporting the implementation of equipment failure mode analysis technologies and life cycle decision management approaches into the continued PreMA product enhancements

- Development of new tools for risk modeling of rotating machinery

Job Title: Research & Teaching Assistant *Date:* 08/2012-05/2015

Employer: University of Illinois at Chicago *Location:* Chicago, IL, USA

Job Description: Development of rotational machinery (e.g., gearbox and bearing) health monitoring, diagnostic and prognostic systems using vibration, AE, and PE strain sensor analysis; Development of water/particle contaminated lubrication oil degradation models and diagnostic and prognostic systems; Investigation of efficient prognostic estimators; Participation in the validation of the industrial wind turbine test rig, local data collector (LDC), and evaluation of commercial vibration/AE sensors from industrial companies.

Job Title: Product Engineer *Date:* 2006-2008

Employer: Samsung Electronics Co. LTD., Semiconductor Business *Location:* Hwasung-Si, South Korea

Job Description: Involved in a machine development project of a high accuracy bonding for wafer stacked package (WSP).Within the project, worked on the bonding surface copying system, ultra-thin wafer (15um-40um) handling, and gold bump formation. Contributed to the development of the world first 16-layer DDR2 WSP working samples by operating the newly developed bonding equipment and process. Machine set-up for gold wire coating machine and materials, stress-free stealth-laser dicing machine. Received extensive training in the semiconductor assembly process.

JOURNAL PUBLICATION:

Papers Published:

Yoon, J., and He, D., (Accepted to appear) "A new planetary gearbox fault diagnostic method using acoustic emission sensors," *IET Science, Measurement and Technology*.

Yoon, J., He, D., and Van Hecke, B. (2015) "On the use a single piezoelectric strain sensor for wind turbine planetary gearbox fault diagnosis," *IEEE transactions on Industrial Electronics*, DOI: 10.1109/TIE.2015.2442216.

Yoon, J. and He, D. (2015). "Development of an efficient prognostic estimator," *Journal of Failure Analysis and Prevention*. Vol. 15, No. 1, pp. 129-138.

Zhu, J., Yoon, J., He, D., and Bechhoefer, E. (2014). "Online particle contaminated lubrication oil condition monitoring and remaining useful life prediction for wind turbines," *Wind Energy*, DOI: 10.1002/we.1746.

Qu, Y., He, D., Yoon, J., Van Hecke, B., Bechhoefer, E., and Zhu, J. (2014). "Gearbox tooth cut fault diagnostics using acoustic emission and vibration sensors - a comparative study," *Sensors*, Vol. 14, No. 1, pp. 1372 - 1393.

Qu, Y., Van Hecke, B., He, D., Yoon, J., Bechhoefer, E., and Zhu, J. (2013). "Gearbox fault diagnosis using AE sensors with low sampling rate," *Journal of Acoustic Emission*, Vol. 31, No. 1, pp. 67 – 90.

Zhu, J., Yoon, J., He, D., Qu, Y., and Bechhoefer, E. (2013). "Lubrication oil condition monitoring and remaining useful life prediction with particle filtering," *International Journal of Prognostics and Health Management (PHM)*, Vol. 4, Special Issue on Wind Turbine PHM, pp. 1 – 15.

Papers Submitted:

Yoon, J., He, D., Van Hecke, B., Nostrand, T., Zhu, J., Bechhoefer, E., (2015) "Vibration based wind turbine planetary gearbox fault diagnosis using spectral averaging," *Wind Energy*.

Van Hecke, B., Yoon, J., and He, D., "Low speed bearing fault diagnosis using acoustic emission

sensors," *Journal of Applied Acoustics.*

Yoon, J., He, D., and Van Hecke, B., "A PHM approach to additive manufacturing equipment health monitoring," fault diagnosis, and quality control, *Journal of 3D Printing and Additive Manufacturing*.

CONFERENCE PUBLICATION/PRESENTATION:

Yoon, J., He, D., Van Hecke, B., Nostrand, T., Zhu, J., Bechhoefer, E., (2015) "Vibration based wind turbine planetary gearbox fault diagnosis using spectral averaging," *AWEA Wind Power 2015 Conference*, May 18-21, Orlando, FL, USA.

Yoon, J.,Van Hecke, B., He, D.,(2015) "Planetary gearbox fault detection using an acoustic emission sensor," *Joint Conference: MFPT 2015 and ISA's 61st International Instrumentation Symposium*, May 12 – 14, Huntsville, AL, USA.

Van Hecke, B., Yoon, J., and He, D., 2015, "On the use of acoustic emission sensors with low sampling rate for low speed bearing fault diagnostics", *Joint Conference: MFPT 2015 and ISA's 61st International Instrumentation Symposium*, May 12 – 14, Huntsville, AL.

Yoon, J., He, D., and Van Hecke, B. (2014). "A PHM approach to additive manufacturing equipment health monitoring, fault diagnosis, and quality control," *Annual Conference of the PHM society*, Sep 29 – Oct 2, Fort Worth, TX, USA.

Yoon, J., He, D., Van Hecke, B., Nostrand, T., Zhu, J., and Bechhoefer, E. (2014). "Planetary gearbox fault diagnosis using a single piezoelectric strain sensor," *Annual Conference of the PHM society*, Sep 29 – Oct 2, Fort Worth, TX, USA.

Yoon, J., He, D., and Dempsey, P. (2014). "An efficient prognostic estimator," *MFPT Conference*, May 20 – 22, Virginia Beach, VA, USA.

Qu, Y., Van Hecke, B., He, D., and Yoon, J., (2014). "A study on comparing acoustic emission and vibration sensors for gearbox fault diagnostics," *MFPT Conference*, May 20 – 22, Virginia Beach, VA, USA.

Yoon, J., He, D, and Qiu, B. (2013). "Full ceramic bearing fault diagnosis using LAMSTAR neural network," *IEEE International Conference on PHM 2013*, June 24 – 27, Gaithersburg, MD, USA.

Zhu, J., Yoon, J., Qiu, B., He, D., and Bechhoefer, E.(2013), "Online condition monitoring and remaining useful life prediction of particle contaminated lubrication oil," *IEEE International Conference on PHM 2013*, June 24 – 27, Gaithersburg, MD, USA.

OTHER PUBLICATION:

Yoon, J., (2012), "A comparative study of adaptive MCMC based particle filtering methods," *Master Thesis*, University of Florida.

AWARDS, VOLUNTEER AND ACTIVITIES

- Paper reviewer for the following journals and conferences: *Journal of Intelligent Manufacturing*, *International Journal of PHM*, *Science and Technology of Nuclear Installations*, *PHM Society Conference.* 2012 - present
- Runner-up student paper award by British Institute Non-Destructive Testing (BI-NDT), *Joint Conference: 69th MFPT and ISA's 61st International Instrumentation Symposium.* 2015
- IEEE 2014 technical symposium planning staff, Chicago section. 2013 – 2014
- Selected for 6th annual doctoral symposium of PHM society. 2014
- Best student paper award (co-authored) by Saab Defense Security USA, *the 68th MFPT conference.* 2014
- Faydor Litvin graduate scholarship award, University of Illinois-Chicago. 2012
- LGenius Members fellowship award, LG display Co., LTD. 2011 - 2012
- College of Engineering achievement award, University of Florida 2010
- 3rd Prize, Samsung Electronics research performance and presentation competition, Samsung Research Center, Hwasung-si, South Korea. 2006
- 2nd Prize, Capstone design award, Kwangwoon University, Seoul, South Korea. 2005